DOCTOR OF PHILOSOPHY

Mechanical properties and internal mechanisms characterization of calcined clay geopolymer concrete

Shinkafi, Aminu Bature

Award date:
2020

Awarding institution:
Coventry University

Mechanical Properties and Internal Mechanisms Characterization of Calcined Clay Geopolymer Concrete

By

Aminu Bature Shinkafi

PhD

October 2020

Mechanical Properties and Internal Mechanisms Characterization of Calcined Clay Geopolymer Concrete

By

Aminu Bature Shinkafi

PhD

October 2020

A thesis submitted in partial fulfilment of the University's requirement for the degree of Doctor of Philosophy

Certificate of Ethical Approval

Applicant:

Aminu Shinkafi

Project Title:

RHEOLOGY AND SELECTED DURABILITY OF CALCINED CLAY AND GGBS ALKALI ACTIVATED STRUCTURAL CONCRETE

This is to certify that the above named applicant has completed the Coventry University Ethical Approval process and their project has been confirmed and approved as Low Risk

Date of approval:

02 October 2018

Project Reference Number:

P76199

DECLARATION

This is to declare that all the original work produced in this thesis is mine. Any other external material used in the thesis has been duly acknowledged.

Signed: Aminu Shinkafi

Date: 04/10/2020

List of Publications:

Journal papers:

A. S. Bature[a], M. Khorami[a], E. Ganjian[a] and M. Tyrer[a] (Accepted) Influence of alkali activator type and proportion on strength performance of calcined clay geopolymer mortar. *Construction and Building Materials* (**CONBUILDMAT-D-19-06616R1)**

A. S. Bature[a], M. Khorami[a], E. Ganjian[a] and M. Tyrer[a] (under review) Mechanical properties and microstructural characterization of calcined clay geopolymer concrete.

Published journal paper:

Bature, A.S., Khorami, M. and Lawan, A. (2020) effects of ground granulated blast furnace slag and pulverized fuel ash on rheology of concrete. *Nigerian Journal of Technology*, *39*(1), pp.97-104.

Edited book:

Ganjian, E., Claisse, P., Limbachiya, M. and Shinkafi, A. B. (ed.) (2019) Fifth International Conference on Sustainable Construction Materials and Technologies (SCMT5): In Honour of Professor Tim Ibell, 38 p. Available from https://www.amazon.co.uk/International-Conference-Sustainable-Construction-Technologies/dp/1078201684/ref=sr_1_4?keywords=scmt5&qid=1563464421&s=gateway&sr=8-4

Conference papers:

Bature, A. S., Khorami, M., Ganjian, E. and Tyrer, M. (2019) 'Effects of Sodium Silicate Proportion on Strength Development of Calcined Clay Geopolymer Mortar'. in Ball, R, Dams, B, Ferrandiz-Mas, V, Ke, X, Paine, K, Tyrer, M & Walker, P. (ed.) *39th Cement and Concrete Science Conference 2019*. [online] held 2019. University of Bath, UK, 148–152. available from https://purehost.bath.ac.uk/ws/portalfiles/portal/197842011/39th_Cement_and_Concrete_Science_Conference_2019.pdf

Bature, A. S., Khorami, M., Ganjian, E. and Tyrer, M. (2019) Effect of the nature of chemical activator on the compressive strength of calcined clay geopolymer mortar, in: *5th International Conference of Sustainable Construction Materials Technology* (*SCMT5): Volume 3 (SCMT Conferences)* . Ganjian, E., Claisse, P., Limbachiya, M. & Goyal, A. (eds.). International Committee of the SCMT conferences, Vol. 3. p. 17-28 11 p. 5132

Bature, A. S., Khorami, M., Ganjian, E. and Tyrer, M. (2018) 'Influence of Alkali Solution on Compressive Strength of Calcined Clay and GGBS Alkali Activated Mortar'. in Tyrer, M., Ganjian, E. and West, A. (ed.) *38th Cement and Concrete Science Conference*. held 2018. Paper No. 16

Bature, A. S. (2019) Micrsotructural characterzation of calcined lithomarge geopolymer mortar. *11th Geopolymer Camp, Campus Universitaire de Saint-Quentin, University of Picardie, Saint-Quentin, France*. Available on https://geopolymer.org/fichiers/?dir=gpcamp-

2019

Internal conferences:

Bature, A. S. and Khorami, M. (2019) Mixture optimization on compressive strength of red geopolymer mortar. Presented at *Doctoral capability and development conference (DCAD19)*. Available on http://recap.coventry.domains/DCAD/dcad19-programme/

Bature, A. S., Khorami, M., Ganjian, E. and Tyrer, M. (2018) Effect of NaOH Proportion and Concentration on Compressive Strength of Alkali Activated Slag Mortar. *Engineering, Environment and Computing reseacrh symposium.* Coventry University.

ABSTRACT

Calcined clay is presently receiving attention as a promising aluminosilicate source that has the potential of extending the application of geopolymers because of its global abundance and low-embodied energy. However, rheological, mechanical and durability performances of calcined clay based geopolymers depend substantially on the calcination process, mineralogy of the clay, type and proportion of chemical activator, *etc*. Until recently, lateritic clay was considered to be an unsuitable precursor for geopolymers due to its large iron composition. Specifically, the limited research and development interest in the past into this globally available geological material, was due to the reported harmful action of some ferrous compounds (Fe^{++}) that blocked the development of the geopolymeric reaction. Other reasons are the dubious role of iron oxide goethite (FeO(OH)) reported in the scientific literature, and the limitation of some analytical techniques (such as Nuclear Magnetic Resonance spectroscopy (NMR)) in analysing the geopolymeric molecular structures caused by the large iron composition of the lateritic clay. It is against this backdrop that this research focused on studying the technical viability of utilizing flash calcined lateritic clay to produce sealed cured geopolymer concrete. This was achieved by determining the peak strength formulation based on a mass and molar oxide compositional ratios range that produced structural grade concrete using four types of liquid activators. Specifically, the effect of variation in selected mix proportion parameters (activator dosage, paste volume, molar oxide composition and free water content) on performance of the calcined clay geopolymers was studied. The study also involved benchmarking the behaviour of the calcined clay geopolymer mortar against that of alkali activated slag and conventional Portland cement mortars, to determine the similarities and differences between these binder systems. This data laid the foundations for the development of the mix design for the low purity kaolin geopolymer concrete. The study further explored the viability of using the calcined lateritic clay as the main pozzolan for a ternary, semi-dry hydraulically bounded mixture to substitute the scarce GGBS used for that application

The rheological behaviour and mechanical properties of the calcined clay based geopolymer concretes were studied. Other properties of the calcined clay geopolymer concrete that had been studied were: setting times, consistency, chloride permeability, and freeze-thaw resistance; as well as internal mechanism analysis that included X-Ray Diffraction (XRD), Scan Electron Microscopy (SEM) and Fourier Transform Infrared Spectroscopy (FTIR). The results showed that structural grade concrete obtained by activating the calcined clay with 45% potassium silicate solution achieved a peak strength of 40 MPa after three days and had the

best workability. The results further showed that the binding phase of the peak strength concrete was poly ferro-sialate (-Fe-Si-O-Al), and sealed curing was found to enhance the performance of the calcined lateritic clay based geopolymer concrete by preventing atmospheric carbonation. Likewise, the XRD revealed albite and sanidine mineral frameworks for the geopolymer concretes. These are the geopolymeric frameworks that have Si:Al of 3 and are similar to Na-Poly(sialate-disiloxo) and K-Poly(sialate-disiloxo) respectively. Furthermore, the ternary binder composition – Calcined Clay (CC 40%) / Basic Oxide Slag (BOS 50%) / By-Pass Dust (BPD 10%) activated with 15% water content satisfied the strength requirement for Hydraulic Road Binder HRB10 (the 28 days compressive strength of standardized mortars higher than 10 MPa). Additionally, the geopolymer concrete also exhibited excellent freeze-thaw resistance: such that the mass and compressive strength of the samples were greater than 70% of the 28 days old specimens after 300 freezing and defrosting cycles in an aqueous environment.

Keywords: Calcined clay, geopolymer, mechanical properties, freeze-thaw resistance, microstructure, phase characterization, FTIR spectroscopy, life cycle analysis (LCA)

Acknowledgement

All praise and thanks are due to Almighty Allah the lord of the universe. May His peace and blessings be upon his noble messenger and his household, Ameen. Indeed, the Phd journey has been an intense one, and only the support of my kith and kins kept me going.

Firstly, I wish to express my profound gratitude to the sponsors of this PhD programme, the Petroleum Technology Development Fund (PTDF) Nigeria.

Special thanks goes to my Director of study, Dr Morteza Khorami for guiding me through this journey and for always taking extra steps to ensure that I get every resource I need for the research. My sincere appreciation goes to my second supervisor, Prof Essie Ganjian who has been very generous to me with his time and experience throughout the program. The support and mentoring I received from my third supervisor and the Director of Centre for Built and Natural Environment Coventry University, Prof Mark Tyrer will always be cherished by me.

I can only say Jazakumullahu khair to my parents and siblings for their care, support and prayers to me. Indeed, only Allah can reward you for been there for me all my life.

I owe a lot of thanks and gratitude to my darling wife, Hajara Adamu for her love, compassion and empathy to me throughout our married life. Certainly, no words can describe her contribution to this PhD by 'holding up at the Homefront' and for her words of encouragement when things get tough. To my daughters, Aisha and Safiya, who endured little attention from me including weekends because of the demanding nature of the programme, I say to them - Baba loves you.

I also have to thank my friends, colleagues and all the members of Nigeria Muslim Forum Coventry Chapter for the brotherly support they offered me and my family. Your company made my stay in Coventry a memorable one.

Finally, I wish to thank the management and staff of Sokoto Energy Research Centre for the support they have rendered me over the past 3 years while I have been on study leave. May Allah reward everyone with the best of rewards, Ameen.

Table of Contents

LIST OF FIGURES

LIST OF TABLES

ABBREVIATIONS

Al^{3+}	Aluminium ion
Si^{4+}	Silicon ion
Fe^{++}	Iron compound
3 – D	Three dimensional
A-S-H	Alumina Silicate Hydrate
R-A-S-H	Sodium or Potassium Alumina Silicate Hydrate
C-A-S-H	Calcium Alumina Silicate Hydrate
C-S-H	Hydrate of Calcium Silicate
Fe-Si-O-Al	Ferro-sialate
Si-Al	Silicate aluminate
$H_2O:Al_2O_3$	Water to aluminate ratio
Na_2O/Al_2O_3	Sodium oxide to aluminate ratio
SiO_2/Al_2O_3	Silicate to Aluminate ratio
A:B	Aggregate to Binder ratio
C:S	Calcium to Silicate ratio
L:B	Liquid to Binder ratio
L:S	Liquid to Solid ratio
W:S	Water to Solid ratio
Al_2O_3	Aluminate
AAC	Alkali Activated Concrete
AAS	Alkali Activated Slag
AAM	Alkali Activated Materials
BOS	Basic Oxide Slag
BPD	By-Pass Dust
BRE	Building Research Establishment
C	Calcium Oxide
Ca	Calcium
CC	Calcined Clay
CEM I	Portland cement
CLSM	Controlled Low Strength Material
CO_2	Carbon dioxide
DoE	Design of experiment

FeO(OH)	Goethite
Fe	Iron
FTIR	Fourier Transform Infrared spectroscopy
GGBS	Ground Granulated Blast Furnace Slag
GHG	Green House Gases
GC/K-RM	Potassium silicate activated geopolymer concrete based on modified Rangan guidelines (70% aggregate content)
GC/Na-R	Sodium silicate activated geopolymer Concrete based on Rangan guidelines (75% aggregate content)
GC/Na-M-RM	Blended activator (mixture of sodium silicate and sodium hydroxide in the ratio of 2.5) geopolymer concrete based on modified Rangan guidelines (70% aggregate content)
GC/Na-RM	Sodium silicate activated geopolymer Concrete based on Modified Rangan guidelines (70% aggregate content)
GWP	Global Warming Potential
HRB	Hydraulic Road Binder
ICAR	International Centre for Aggregate Research
IR	Infrared
K_2SiO_3	Potassium Silicate
K	Potassium
kWh/t	Kilowatt hour per tonne
LC^3	Limestone Calcined Clay Cement
LCA	Life Cycle Analysis
M	Molarity
MK	Metakaolin
MR	Molecular Ratio
MPa	Mega Pascal
Na	Sodium
NaOH	Sodium Hydroxide
Na_2O	Sodium Oxide
Na_2SiO_3	Sodium Silicate
$Na_2SiO_3.5H_2O$	Sodium Silicate Pentahydrate
NMR	Nuclear Magnetic Resonance spectroscopy
PC	Portland Cement

PFA	Pulverised Fuel Ash
RCPT	Rapid chloride permeability test
RH	Relative Humidity
RHA	Rice Husk Ash
SiO_2	Silicate
S	Silicon Oxide
SAI	Strength Activity Index
SCM	Supplementary Cementitious Materials
SEM	Scan Electron Microscopy
SH	Sodium Hydroxide
SS	Sodium Silicate
SSP	Sodium Silicate Pentahydrate
UPV	Ultrasonic Pulse Velocity
WMK	White metakolin
XRD	X-ray Diffraction Analysis
XRF	X-ray Fluorescence Analysis

CHAPTER 1 INTRODUCTION

1.0 Background

Concrete is the second most-consumed product by societies after water all over the world (IEA WBCSD - World Business Council for Sustainable Development, 2009). It is a basic building construction material that has Portland cement (PC) classified as CEM I to V as its dominant constituent. In 2016, 4.2 billion metric tonnes of PC was produced globally (Ober, 2017), and the production is predicted to rise to more than 5 billion metric tonnes by 2030 due to increasing demand for infrastructure and rapid urbanization especially in developing countries (Müller and Harnisch , 2008). Around 50% of the world's PC was used to produce around 11 billion metric tonnes of concrete in 2011 (Imbabi, Carrigan and McKenna, 2012).

However, cement production and use are associated with tremendous energy and environmental impact resulting from high energy cost and high rate of CO_2 emissions in their manufacturing processes, as well as relatively poor durability performance such as weak acid and sulphate resistance (Duxson *et al.*, 2007). According to Davidovits (1994), the manufacturing process of cement produced a billion tons of CO_2 worldwide in 1989 which accounts for about 5% of the total greenhouse gases (GHGs) produced that year. Equally, Cement Sustainability Initiative (2014) reported that the cement industry produced approximately 5% of current global man–made CO_2 emission in 2013.

Consequently, remarkable progress has been made in the past decades to improve PC production through technological advances that include energy-efficient production, low carbon production methods, blended cement, carbon capture storage and utilization, development of alternative binders based on Alkali-Activated Materials (AAM), *etc*.

AAM have continued to receive attention as construction materials with lower CO_2 emissions that will further improve sustainability in the construction industry (Scrivener, John and Gartner, 2018). The most promising precursors for AAM are Ground Granulated Blast Furnace Slag (GGBS) and Pulverized Fuel Ash (PFA) of adequate quality (Provis, 2018). However, the global supply of these materials is dwindling due to rapid decommissioning of coal thermal power plants in developed nations that generate PFA as a by-product and massive utilization of GGBS as Supplementary Cementitious Material (SCM) for Portland cement. According to Scrivener, John and Gartner (2018), calcined clay is presently the material with substantial potential to extend the availability of suitable minerals for AAM.

Previous studies focused on the utilization of metakaolin as an aluminosilicate source, but competing demand by different industries for high purity kaolin clay, high-cost, and the intensive purification process are some of the factors limiting its availability to be used as either SCM or precursor for alkali activation (Zhou *et al.*, 2017). Calcined clays are presently considered as cost-effective alternatives to high purity metakaolin clay, and offer greater supply sustainability due to availability of vast clay reserves globally supplemented by clay waste generated by the ceramics industries and construction projects (Lopez, 2009).

Iron-rich clays are abundantly available across the globe and were formerly considered unsuitable precursors for geopolymers until recently when research proved the viability of red (calcined lateritic clays) geopolymer cement (Davidovits, 2012). The iron content of kaolin clay is classified based on target application. In ceramic whiteware production, iron content of more than 0.9% is considered high and require intensive purification process. However, iron content of lateritic clay that can be used as precursor is considered high when it is more than 15% (Stoops and Marcelino, 2018). The clay used in this study has goethite and kaolinite content of 24.3% and 70.1% respectively prior to calcination.

Alkali activation involves the release of the alumina (Al^{3+}) and silica (Si^{4+}) ions from an aluminosilicate source by reacting with the alkali metal source to produce a hydrate of alumina silicates gel (R-A-S-H, where R=Na or K) that forms a solid mass when hardened and used as binder (Brough, A. R. and Atkinson, 2002). The binding phase of calcined clay is almost exclusively aluminosilicate that forms a highly coordinated 3-dimensional Si-O-Al polymeric network through a polycondensation reaction typical of a geopolymer binder (Provis *et al*., 2014a). According to Davidovits (2015), the binding phase for iron-rich calcined clay geopolymers is poly ferro-sialate (Fe–Si–O–Al). Meanwhile, the reaction product obtained from high calcium content aluminosilicate sources such as GGBS is an aluminium substituted hydrate of calcium silicate gel (C-A-S-H). This gel is similar to the C-S-H formed by PC, but has a lower calcium to silicate (C:S) ratio; determined in part by the nature of activator used for the reaction (Bernal *et al.*, 2011). This low C:S increases the strength of the binding phase due to its high silicate content and is enhanced by the use of silicate-based alkali solutions (Passuello *et al*., 2017a).

The focus precursor utilized in this study has the potential of satisfying the current and future demands of aluminosilicate sources in the United Kingdom (UK). Kwasny *et al*., (2018) studied the strength performance of rotary calcined lithomarge activated with a proprietary

activator – waste derived potassium silicate solution, to produce geopolymer mortar. However, the difference in the calcination process and the type of activators used in this study have provided a different perspective. Moreover, presently, there is serious research interest globally that seeks to understand the role of iron (Fe) in the geopolymerisation phase of calcined lateritic clay (Shi, Qu and Provis, 2019; Davidovits and Davidovits, 2020). This challenge is partly due to the limitation of nuclear magnetic resonance spectroscopy (NMR) in analysing the geopolymeric molecular structure caused by the large iron content of the lateritic clay. Considering the impracticality of prescriptive recipe-based standard for geopolymers due to its ability to utilize the ever-growing range of materials, it becomes necessary to characterize the strength performance of this precursor considering different variables. The variables considered in this present work by the author were studied in four stages:

First stage: geopolymer mortar formulation based on mass ratios derived from water demand of the precursor using three types of activators.

Second stage: geopolymer mortar formulations based on the prescribed molar oxide ratios compositional range, which enabled the determination of the ratios that produced the peak strength for this precursor.

Third stage: geopolymer concrete formulation using four types of chemical activators based on the molar oxide ratios obtained for the peak strength mortar and constant water to solid ratio of 0.48.

Fourth stage: ternary, semi-dry mixture with the calcined lateritic clay as the main pozzolan for hydraulically road binder application.

In summary, the effects of different types, dosage and concentration of activators (sodium metasilicate pentahydrate, sodium hydroxide, potassium silicate and sodium silicate solutions), on the fresh behaviour, mechanical properties and microstructural characteristics of calcined clay geopolymer mortar and GGBS alkali-activated mortars cured by air and sealed conditions were studied and reported. The molar oxide compositional ratios obtained from the peak strength calcined clay geopolymer mortars were used to design four geopolymer concrete mixes based on four types of chemical activators. Afterwards, the rheological behaviour, mechanical properties, durability performance, and internal mechanisms of the produced geopolymer concretes were evaluated and reported.

1.1 Significance of Calcined lateritic clay

In recent years, there has been tremendous research effort dedicated towards use of GGBS, PFA or pure metakaolin into development of cement free binders and concretes (Provis, 2018). These alternatives being explored seek to overcome the shortcomings and lower the carbon footprint of PC concrete. However, supply of these precursors cannot be secured especially in the Europe due to rapid decline in their production or competing demand by other industries (Heath et. al., 2014). According to Scrivener et al. (2016), the global supply of calcined clay is 6000 Mt/year against 330 Mt/year of GGBS and 900 Mt/year of PFA (out of which only a third are suitable quality). Also, the carbon emission associated with production of calcined clay is 70 kgCO_2/tonne, 67 kgCO_2/tonne for GGBS and 800 kgCO_2/tonne for PC (Ding et. al., 2016). Consequently, calcined lateritic clay has emerged as the precursor that can ensure wide adoption of geopolymers because of its global availability and low embodied carbon associated with its calcination (Davidovits and Davidovits, 2020).

1.2. Aim and objectives

1.2.1 Aim of the Study

The aim of this study is to determine the appropriate mix proportion of iron-rich, flash-calcined clay-based geopolymer concrete that is activated with various types of alkali metal sources, as well as viability of using the precursor as the main pozzolan for hydraulically bound mixture .

1.2.2 Objectives of the Study

The specific objectives of this study are:

I. To study the effects of mass and molar oxide compositional ratios on fresh behaviour, mechanical properties and mechanisms of calcined clay geopolymer mortar cured under sealed conditions
II. To investigate the selected durability performance of the calcined clay geopolymer concrete and compare with that of Portland cement concrete.
III. To develop a ternary mixture of the calcined clay and other waste pozzolans for the production of semi-dry hydraulically bounded binder for road base foundation To evaluate the environmental footprint of the calcined clay geopolymer concrete and estimate the carbon savings in relation to Portland cement concrete.

1.3 Research Questions

The experiments undertaken and reported in this report provide answers to the following research questions:

What will be the performance of a geopolymer binder produced by activating the calcined lateritic clay with a range of alkali metal sources under sealed conditions?

How will the various mix design variables influence the fresh behaviour and mechanical properties of the calcined clay geopolymer binder?

Can the calcined lateritic clay be used as the main pozzolan in a ternary binder system for a hydraulically bound mixtures?

1.4 Research Program

The study undertaken are grouped under the following tasks:

Task 1: Material Characterization of the GGBS and calcined clay through analytical techniques that include laser particle size analysis, X-ray fluorescence analysis (XRF), XRD, fineness, specific gravity, and strength activity index test (SAI).

Task 2: Mix designs and preliminary tests to determine the strength performance of the calcined clay and GGBS mortars activated with (a) various proportion of $Na_2SiO_3.5H_2O$ dissolved under normal atmospheric conditions, (b) different concentration of NaOH solution, and (c) commercially sourced Na_2SiO_3 and K_2SiO_3 solutions, which are cured either in air or under sealed conditions. Evaluation of the internal mechanisms that include SEM, XRD and FTIR for the various calcined clay geopolymer mortars.

Task 3: Testing of fresh and hardened properties of the peak strength calcined clay geopolymer mortar which includes slump, density, Ultrasonic Pulse Velocity (UPV) and compressive strength development. Testing of the setting times and rheological properties of the calcined clay geopolymer grout formulated with various water to geopolymer solid ratios.

Task 4: Calcined clay geopolymer concrete mixes designed based on molar oxide compositional ratios obtained from the peak strength mortar using different types of chemical activators. Testing of the calcined clay geopolymer concretes which include slump, stress-growth, and flow curve tests using concrete rheometer, density, UPV, compressive strength development, freeze-thaw resistance and permeability tests.

Task 5: Semi-dry, ternary mix design and strength development tests for the calcined clay for controlled low strength application.

Task 6: Analysis and discussion of the results obtained from the various tests. LCA of the iron-rich flash-calcined clay geopolymer concrete and carbon saving estimation in comparison to the Portland cement concrete.

1.5 Thesis layout

Chapter 1: This is the introduction to the research chapter that provided background to the study and justification for carrying out the research. The chapter also outlined the significance of the research, as well as the objectives that were followed to achieve the research aim.
Chapter 2: This chapter covered review of relevant literature which provided insight into the current state-of-art and identified the research gaps that form the basis of the research questions developed for this research.
Chapter 3: This chapter described the methods through which the research was designed and carried out. It highlighted the justification for adopting the research approach and method of data collection.
Chapter 4: The details of the materials used in this study, the testing and experimental methods were featured in this chapter. Also, mix designs and the molar oxide calculations have been covered in this chapter.
Chapter 5: This is the chapter that contained the results obtained from the various experiments undertaken in this research. The presented results were analysed and discussed in the context of relevant literature.
Chapter 6: The details of the life cycle analysis of the calcined clay geopolymer concrete were presented in this chapter. The computed environmental impacts were compared with that of Portland cement concrete.
Chapter 7: This is the chapter that outlined the various conclusion drawn from the discussed results. The limitation of the research, as well as, programme for future work were highlighted in this chapter.

CHAPTER 2 LITERATURE REVIEW

2.0 Alkali Activated and Geopolymer Cement

Alkali activation refers to the reaction of alkalis or alkali earth ions with finely divided inorganic materials to release their latent cementitious properties. This reaction is analogous to the concept of the synthesis of natural alkali/alkaline earth-aluminosilicate minerals that dominate much of the Earth's crust. This analogy stimulated an early interest in alkali-activated materials and, subsequently, geopolymers. Xu and Van Deventer, (2000) concluded that although natural Al–Si minerals are the source material for Al^{3+} and Si^{4+} ions in the geopolymer binding system, it is still impossible to predict quantitatively the specific Si-Al mineral that is suitable for geopolymerisation.

Subsequently, Fletcher *et al*., (2005) showed that the alkali-activated products formed within the compositional range of $1< Si/Al < 5$ are suitable for general construction applications. In contrast, products outside that range (i.e. Si/Al less than one or greater than five) are characterised as low-strength and thermally unstable with generally poor chemical resistance and tendency to dissolve in water, and therefore not suitable to be used as a construction material.

Interestingly, geopolymer as a binder is different from alkali-activated aluminosilicate, but many researchers preferred the term 'geopolymer' to refer to all the alkali-activated aluminosilicate binders (Arham, 2009). Alkali-activated binders and geopolymer cement are both derived from the reaction between the aluminosilicate source and alkali solution but have different reaction products, reaction mechanisms, and structure. Some of these differences are summarized in table 2.1.

Table 2 1 Some differences between alkali-activated and geopolymer binders

Alkali-activated binder	Geopolymer cement
Produced from both low- and high- Ca aluminosilicate sources such as calcined clay, GGBS, *etc*.	Produced mainly from Ca free, or low Ca aluminosilicate sources.

	High Ca aluminosilicate sources such as GGBS require the addition of a specific amount of low Ca aluminosilicate sources such as metakaolin to produce geopolymer binder.
Reaction is governed by dissolution of aluminosilicate sources and formation of R-A-S-H where R is an alkali metal; commonly Na or K	Reaction is governed by dissolution of aluminosilicate sources, coagulation, polycondensation, and gelation
The synthesis is not sensitive to molar oxide composition	The synthesis is very sensitive to molar oxide composition and the recommended range are: Na:Al =0.8 – 1.2; Si:Al = 3 -5.5; H_2O:Na_2O = 12 – 18
The reaction process is limited to hydration and produces a gel similar to that of PC, but with a low C:S	The reaction is governed by polymerization reaction and polycondensation M[-(Si-O_2)z-Al-O)]n.wH_2O where M is the alkaline element, n is the degree of polymerization and w is the amount of binding water
The binding phase may not necessarily be exclusively aluminosilicate and has chains characteristic of C-S-H gel.	The binding phase is highly coordinated aluminosilicate that forms a pseudo-zeolitic network structure
Less stable structure with the presence of free end positive charge alkalis outside the structure	Highly stable 3-D polymeric network structure

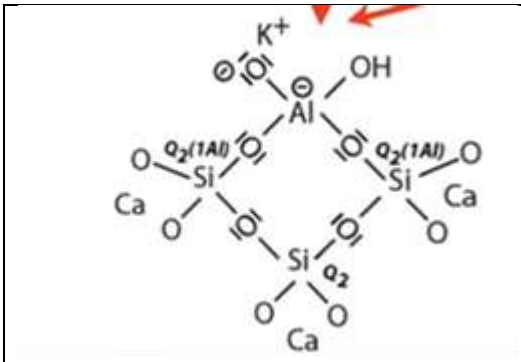	
Concrete produced from alkali activation is often associated with high compressive strength and mixed durability performance resulting from a less stable structure.	Concrete produced from geopolymerization and polycondensation is often associated with lower compressive strength and better durability performance resulting from its highly stable structure.

Accordingly, this study focused on developing geopolymers from iron-rich, flash calcined, low purity kaolin clay sourced from Northern Ireland. Because of the impracticality of prescriptive recipe-based standard for geopolymers due to its ability to utilize ever growing range of materials, it became necessary to characterize the engineering properties of geopolymer formulated from this precursor considering different variables. These properties were benchmarked against alkali activated slag and Portland cement mortars or concrete.

2.1 Alkali-Activated Materials

AAM refer to any binder system obtained from the reaction of aluminosilicate source material with an alkali metal source (Shi, Krivenko and Roy, 2006). These materials could be minerals or industrial by-products that primarily constitute of silicates, aluminates and calcium. Aluminosilicate sources occur abundantly in the Earth's crust and are rich in alumina (Al_2O_3) and silica (SiO_2) compounds, constituting more than 70% of the total composition in a reactive amorphous phase (Liew *et al*., 2016).

AAM are generally associated with lower CO_2 emissions compared to PC, and are considered to be one of the important options that could reduce the global CO_2 emissions associated with the construction industry. The most promising aluminosilicate source materials for large scale

applications of AAM are GGBS and PFA of adequate quality (Provis, 2018). However, availability of these precursors is limited globally. Clay is another aluminosilicate material rich in Al_2O_3 and SiO_2 with both compounds constituting between 70% and 90% of its total composition. Presently, calcined clays are considered to have substantial potential to extend the availability of suitable minerals that can be used as AAM (Scrivener, John, and Gartner, 2018).

One important classification of AAM is based on the composition of hydration products. According to Shi, Krivenko and Roy, (2006), the two classes of AAM are:

I. Alkaline Alumino Silicate Hydrate (R-A-S-H where R = alkali metal, commonly Na or K) system. This category is referred to as "geocement" due to the similarity of their formation process to the geological process of natural zeolites. However, if the reaction is a polycondensation rather than hydration, they are referred to as a "geopolymer" that yields the bond $M[-(Si-O_2)z-Al-O)]n.wH_2O$ (where M is the alkaline element, n is the degree of polymerization and w is the amount of binding water).
II. The alkaline – alkaline earth systems (R-C-A-S-H) that has a hydration products of Calcium Silicate Hydrate (C-S-H) gel with low Calcium to Silicate (C: S) ratio.

Another classification of AAM is based on their mineral content as presented in Fig. 2.1.

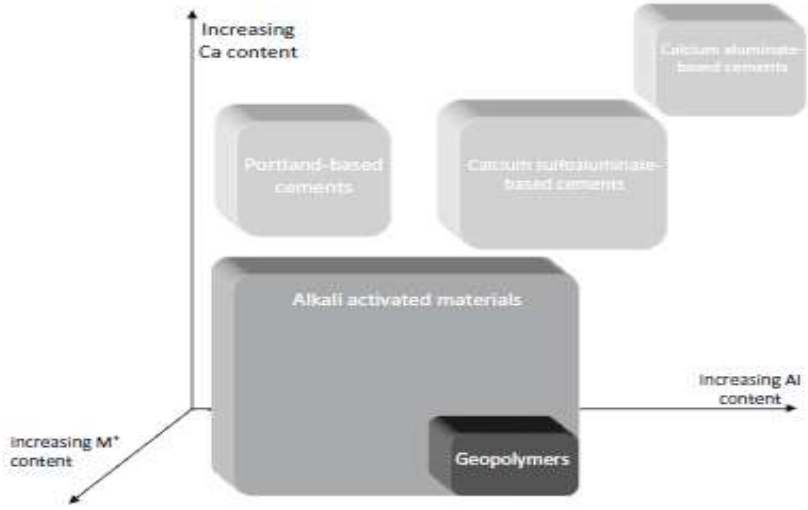

Fig. 2.1 Classification of AAM compared to PC and other binders (Provis *et al*., 2014a)

2.1.1 GGBS

GGBS is a finely ground non-crystalline slag processed by applying high-pressure jets of water to rapidly quench molten slag; which is a by-product of pig iron blast furnace production

(shown in Fig 2.2) and is predominantly composed of non-metallic residue such as quicklime, silica and alumina (Lukowski and Salih, 2015). This is the type of slag that is suitable for use as a cementitious material, while the other crystalline slags which do not possess hydraulic properties can only be used as aggregate, road base material, or dispose of as waste product (Davidovits, 1994). The granulation processing of GGBS prevents recrystallization of some of its phases that would have occurred during slow- or air-cooling, lending itself to alkali activation.

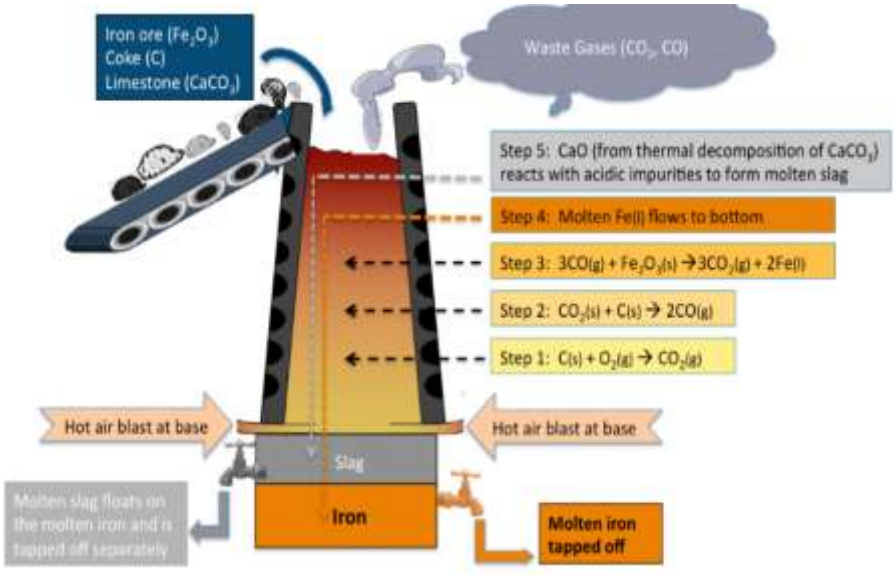

Fig. 2.2 Blast furnace production of pig iron (Secondaryscience4all, 2014)

GGBS is the preferred AAM that can be used to produce AAC at room temperature. The amount of GGBS available globally is around 330Mt/year and over 90% of it is being used by the cement industry for blending with the clinker (shown in Fig 2.3). The GGBS available for cement production is only 8% in 2014, decreasing from the 17% that was available in 1980 (Scrivener, John and Gartner, 2018).

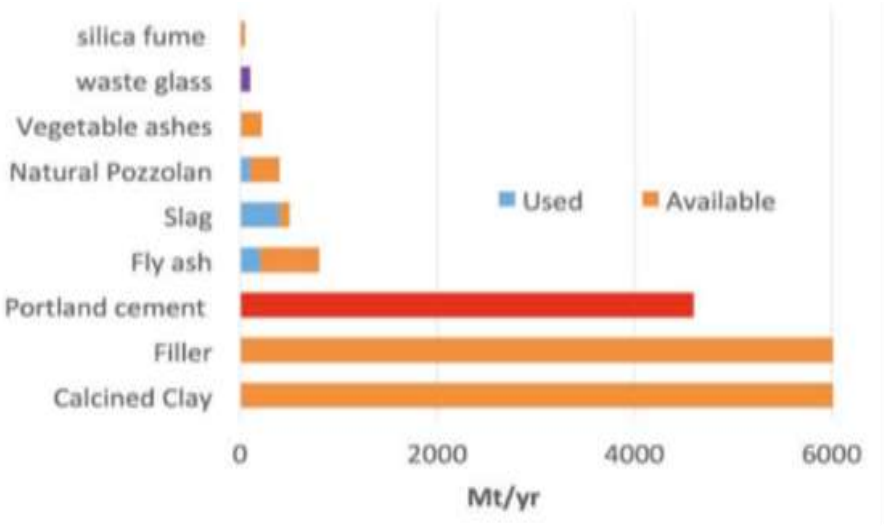

Fig. 2.3 Use and estimated availability of selected supplementary cementitious materials (SCM)(Scrivener, John and Gartner, 2018)

GGBS is a glassy product with latent hydraulic property that hydrate very slowly when it reacts with water. Likewise, its hydration products form a thin Si-rich layer on the surface of the slag grain that eventually prevents further hydration (Thomas, 2013). However, when mixed with PC, the GGBS is activated by slaked lime and other alkalis released by the hydrating cement without depleting them (Claisse, 2016). Alkali contents of GGBS range between 0.3 and 2.6% Na_2O_e, and most of it is bound in the glass phase, while the water-soluble alkali contents is typically less than 0.1% Na_2O_e (Thomas, 1996).

Rafeet *et al*., (2017) showed that increasing the GGBS content of any AAC mix results in compressive strength gain (especially early-age strength), lowers the consistency of the concrete, and shortens its initial setting time. The faster setting caused by the GGBS may be undesirable, and the chemical admixtures presently used as retarders are incompatible with an alkali-activated system. Detrimental effects on compressive strength are associated with the use of retarders in AAC (Puertas, Palacios and Provis, 2014).

The dense angular shape of GGBS particles (shown in Fig 2.4) and the accelerated reaction of its calcium content are largely responsible for the quick setting associated with the introduction of GGBS into a concrete mix (Deb, Nath and Sarker, 2014). Specifically, Claisse (2016) associates the angular shape of the GGBS with the fast setting, reduced flowability and increased water demand to wet its surface.

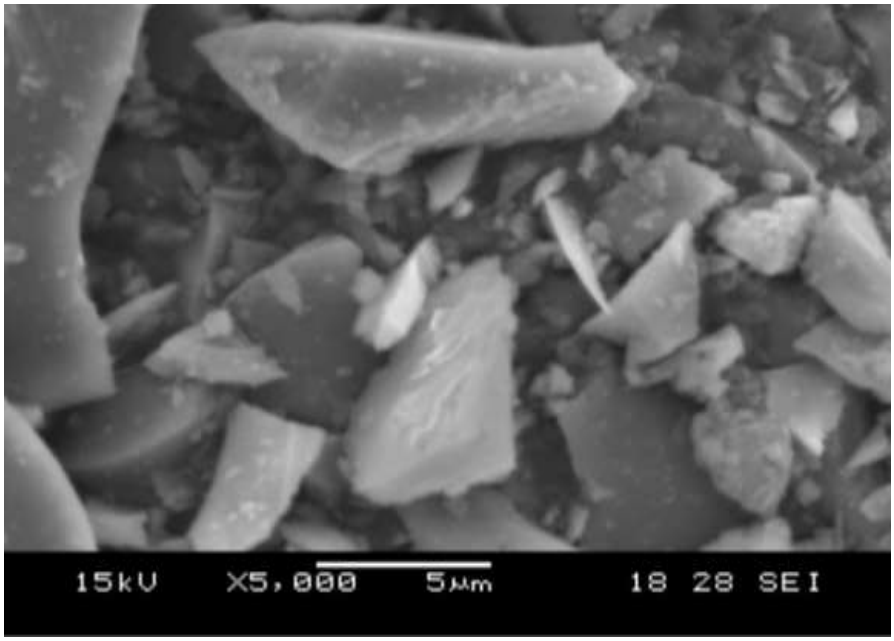

Fig. 2.4 Morphology of angular-shaped GGBS particles (Zhou, 2016)

2.1.2 The Clay

Clay is defined by different disciplines based on its grain size, plasticity, and hardening properties. Guggenheim and Martin (1995) referred to clay as a naturally occurring material composed primarily of fine-grained minerals that is generally plastic at appropriate water contents and hardened when dried or fired. Clay minerals are hydrous aluminosilicate that constitute over 50% of any clay and are grouped into illite, montmorillonite and kaolinite mineral groups. The kaolinites are the simplest clay mineral with layers held together by fairly weak bonds, whereas the bonding in illite and montmorillonite is strong due to the presence of positively charged metal ions: potassium in the case of illite, and calcium and sodium in the case of montmorillonite (Brigatti, Galan and Theng, 2006). The kaolinite clay mineral group is the most reactive, followed by montmorillonite. While the illite clay mineral group is the least reactive (Sabir, Wild and Bai, 2001). The kaolinite has a 1:1 neutral dioctahedral layered structure that comprises of gibbsite ($Al(OH)_3$ and $(Si_2O_5)_n^{2-}$) sheets stacked and held together by weak bonds (as shown in Fig. 2.5). The layered structure and small surface area of kaolinite allows minimum dissolution of the Al^{3+} and Si^{4+} by the alkali solution resulting in a low strength binder (Li*ew et al*., 2016).

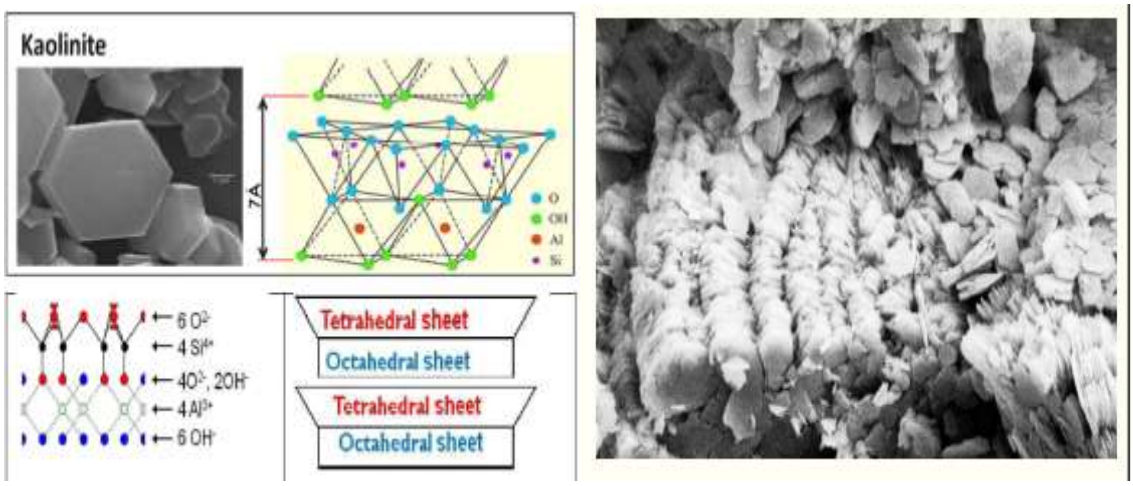

Fig. 2.5 Kaolinite $Al_2Si_2O_5(OH)_4$ (Liew *et al*., 2016)

Large deposits of pure kaolin are rare globally and this limit their wide use for the production of concrete. Also, processing kaolin from the abundant natural clay that mostly contains other clay minerals and impurities such as quartz and feldspar is highly energy intensive and expensive; and produces a significant amount of clay as waste (Zhou, *et al.* 2017).

Meanwhile, clay reserves are abundantly available across the world as shown in Fig. 2.6. Countries with an established ceramic industry (such as India and China) produce substantial clay as a waste material (Scrivener, John and Gartner, 2018). Also, major civil infrastructure projects across the globe generate large volumes of clay as waste. For instance, the new east–west London rail line generated more than 7 million tonnes of tunnelling waste that predominantly consists of London clay (Crossrail, 2017).

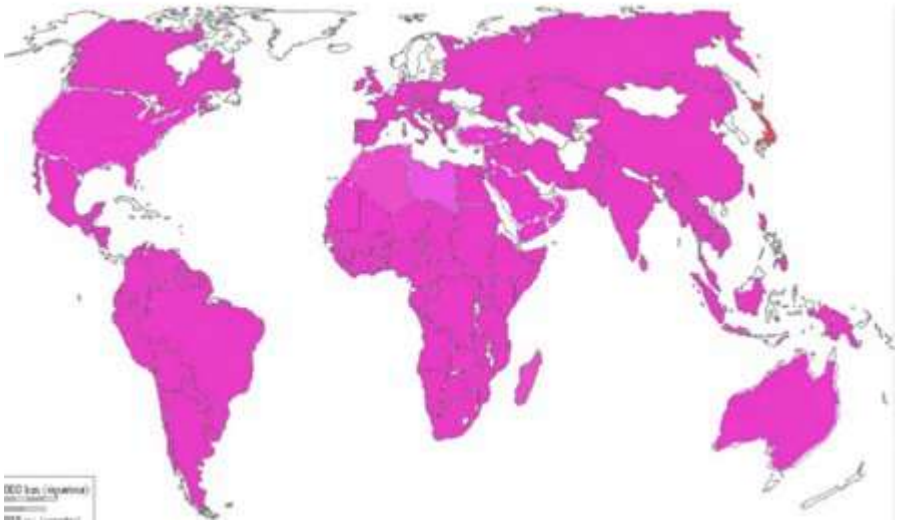

Fig. 2.6 World distribution (availability) of iron-rich clay (Davidovits, 2019)

2.1.3 Clay Calcination

The properties of clay-based geopolymers largely depend on its pre-treatments such as mechanochemical treatment, chemical treatment in either an acidic or alkaline medium, and thermal treatment. However, thermally treated clays always produce geopolymers with the best mechanical and durability properties compared to any other treatment (Xu and Van Deventer, 2000). This thermal treatment (also known as the calcination of clay) is a process of heating clay minerals at temperatures between 600 and 1000°C for a period of between 2 – 24 hrs. This breaks its lattice crystal structure by mainly losing its octahedral hydroxyl ion, thereby forming a transition phase with a high amorphous reactivity phase and increased surface area. However, excessive heating of clay results in over-calcination that transforms the reactive amorphous phase into mullite crystalline phases that are not reactive, thereby decreasing its pozzolanic and geopolymeric reactivity.

Various optimum calcining temperatures and durations have been reported for various clays (Li*ew et al*., 2016). According to Zhou *et al.*, (2017), experiment-based optimization is necessary for the development of reactive natural clay due to the variability of its mineral content between locations. To determine the optimum calcining temperature of any clay that will be used as a precursor for alkali activation, it is, therefore, necessary to understand how each crystalline phase would respond – chemically and structurally – to increased heating.

The reactivity of calcined clay is not only determined by the temperature and duration of the calcination process, but also dependant on the type and quantity of clay minerals, impurities present, amorphous phase content, particle size, and surface area of the grounded calcined clay. High non-clay impurities (such as quartz and feldspar) have an unfavourable effect on the reactivity of calcined clay, and the technology required for their purification is complex and expensive (Zhou, 2016).

The predominant factor that ensures a satisfactory strength development of a calcined clay alkali-activated binder is the ratio of the reactive SiO_2/Al_2O_3 in the aluminosilicate source. Ruiz-Santaquiteria *et al*., (2013) showed that the SiO_2/Al_2O_3 ratio in the N–A–S–H gel has a more significant effect on the compressive strength than the amount of the gel formed.

The two common clay calcination methods are flash and rotary calcination. Fig. 2.7 illustrates the stages involved in these two methods that are used for the production of calcined clays by Banah UK (McIntosh *et al*., 2015).

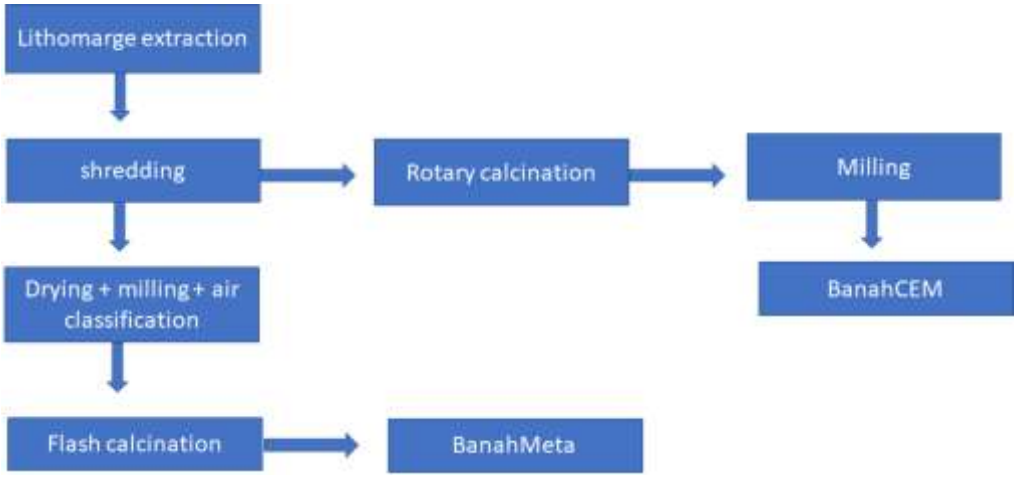

Fig. 2.7 Stages involved in flash and rotary calcination of lithomarge

2.1.3.1 Flash Calcination

The flash calcination of kaolinite is a process that exposes the dry clay powders to desired high temperatures for short periods (residence times of 0.2–1 s). The flash calcined clays are characterized by lower density and show structural changes (internal voids) caused by the rapid release of water vapour. A typical flash calcination set-up is shown in Fig. 2.8. Some of the advantages of flash calcination include:

- Quick attainment of a target temperature.
- An efficient dehydroxylation through the precise control of temperature.
- Limited energy consumption of between 400 to 800 kWh/t.
- The production of a very fine metakaolin (pre-milling).

However, some of the drawbacks associated with the flash calcination of clays are:

- A complex operational system.
- A relatively high-cost of investment compared to rotary calcination.
- A dried and milled clay needed as feed.

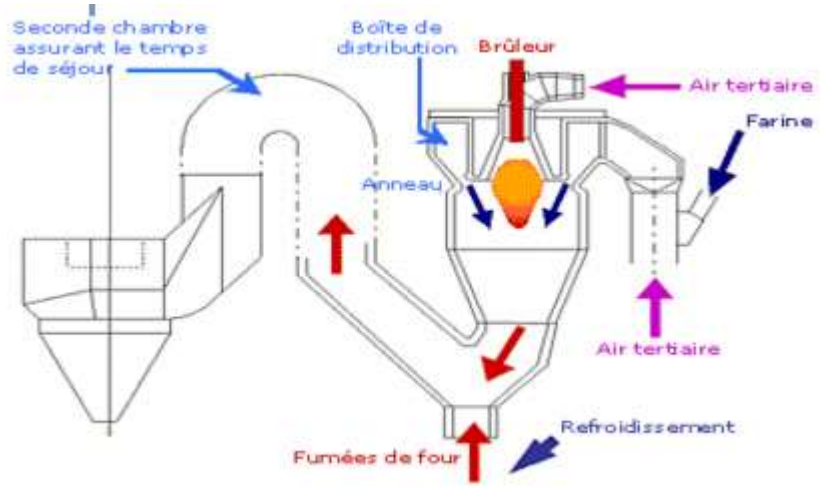

Fig. 2.8 Schematic of a typical flash calcination plant (Soleil-Raynaut, 2019)

2.1.3.2 Rotary Calcination

The rotary calcination of clay is a process of heating clay under controlled temperatures and in a controlled environment using a rotary kiln. This pyroprocessing device raises the clay to the desired high temperature through a continuous process. The rotary kiln is a cylindrical vessel inclined at an angle to the horizontal and is slowly rotated along its longitudinal axis. The ground clay is fed into the upper end of the cylinder. As the kiln rotates, the heated clay gradually flows down toward the lower end. Hot gases are generated in the process and pass along the kiln in the same direction as the process material that is referred to as the co-current, (Hot gases going in the opposite direction referred to as counter-current). The hot gases may also be generated in an external furnace or by a flame inside the kiln. The flame is projected from a burner-pipe. The fuel for the rotary kiln may be gas, low-pour fuel oil, pulverized petroleum coke or pulverized coal. A typical rotary kiln set up is shown in Fig. 2.9. Some of the advantages of rotary calcination are:

- The technology is reliable and robust (similar to a cement plant).
- Efficient energy consumption of between 800-1200 kWh/t.
- A good throughput rate of 10-12 tonnes/h.

On the contrary, some of the drawbacks associated with rotary calcination are:

- The control of dehydroxylation after heating requires a good knowledge of the process.
- temperature gradient in the pellet since the feed material has the same shape with the pellets.
- The calcined clay has to be milled after the calcination.

- The kiln has to be run continuously so there is a need for a certain volume or combination of other materials.

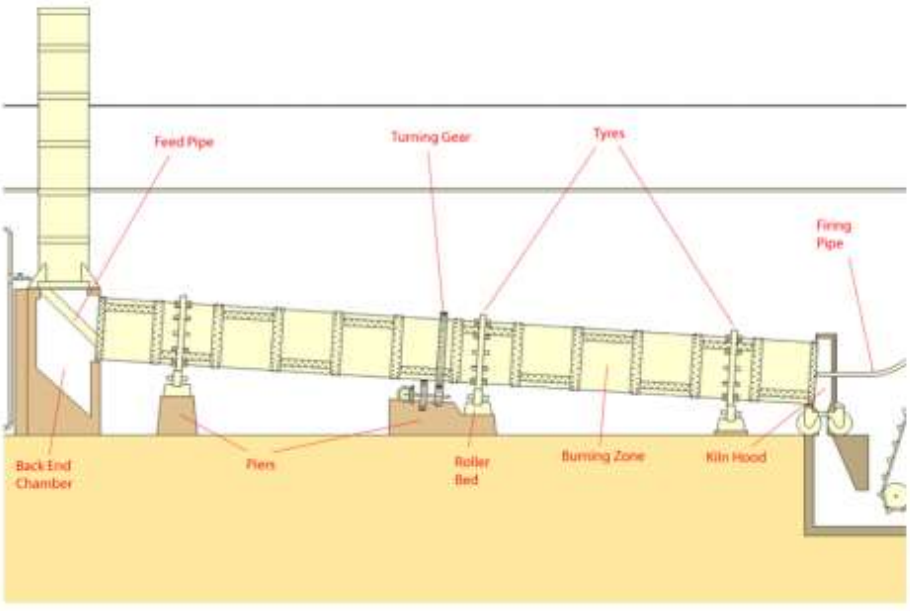

Fig. 2.9 Set up of a typical rotary kiln (Soleil-Raynaut, 2019)

2.1.4 Alkali Metal Source

The synthesis of AAM is limited to the alkaline medium. Meanwhile, geopolymers are synthesised in either alkaline mediums (Na^+, K^+, Li^+, Ca^{2+}, Cs^+ and the like) or acidic mediums (phosphoric acid, organic carboxylic acids from plant extracts (acetic, citric, oxalic, and humic acids)). However, the alkaline route is preferred for research and development as well as commercial applications.

A broad range of potential activators had been studied and reported in the scientific literature. Vinai and Soutsos (2019) noted that, among all the reported available options for activators (hydroxides, silicates, sulfates, carbonates, acidic solutions), the blending of an alkali hydroxide (either sodium or potassium) with an alkali silicate (either sodium or potassium) is favoured because it provides high compressive strengths when used with most known precursors.

Duxs*on, et al*. (2014) recommend that the preferred activator for practical applications of AAM system should be one that:

- Can efficiently trigger and ensure a full reaction with the precursor within the desired time (low early-age strength may be caused by extended reaction times, while short reaction times may result in fast-setting problems).
- Is available at a low cost with an abundant supply.
- Enables simple and cost-effective use.
- Possesses a low environmental impact.

For geopolymer systems, Davidovits (2015) noted that user-friendly activators are necessary for practical applications and will serve as their commercial driver. Table 2.2 summarises the features of a user-friendly activator in comparison to hostile systems as defined by Davidovits (2011). The hostile activators are classified as corrosive, which are difficult to handle on-site because of their high alkalinity and therefore pose health and safety risks. Conversely, the user-friendly systems are classified as irritants and do not possess any significant hazards to its users.

Table 2 2 Difference between user-friendly and hostile activator (Davidovits, 2011)

Hostile	Friendly
CaO (quick lime)	$Ca(OH)_2$
NaOH	Portland cement
KOH	Iron slag
Sodium metasilicate $SiO_2:Na_2O = 1$	Slurry soluble silicate/kaolin MR $1.25<SiO_2:M_2O<1.65$
Any soluble silicate MR $SiO_2:M_2O$ <1.65	Any soluble silicate MR $SiO_2:M_2O$ >1.65

It can, therefore, be argued that silicate-based activators of an appropriate molar ratio are preferred for geopolymer systems. The methods of production of silicate-based activators have far-reaching consequences on geopolymers with respect to the sustainability of the system. Waste derived silicates are presently studied extensively and reported in the scientific literature due to their enormous potential towards improving the sustainability of geopolymers (Passuello *et al.*, 2017). The two common methods of silicate production are the hydrothermal and furnace routes.

2.1.4.1 Hydrothermal Process

The industrial production of sodium silicates generally involves the dissolution of quartz sand with sodium hydroxide in a reactor. The energy requirements temperatures for this process are in the range of 1400 to 1500 °C. The melt, which solidifies on cooling, is then dissolved in water under pressure at an elevated temperature (Fawer, Concannon and Rieber, 1999). On the contrary, the hydrothermal process involves the fusion of quartz, hydroxide and water in a pressure reactor vessel that is then cooled and filtered to desired purity (as shown in Fig. 2.10).

However, since geopolymers do not require high purity silicate, hydrothermal processes have been widely adopted using waste such as glass cullet and Rice Husk Ash (RHA) as the silica source for the production of silicate solution in order to make geopolymers more economically and environmentally viable (Kouassi *et al.*, 2010). The reaction governing silicate production is given in equation 2.1.

$$2MOH + xSiO_2 \rightarrow M_2O.xSiO_2 + H_2O \quad where\ M = Na, K, Li \qquad (2.1)$$

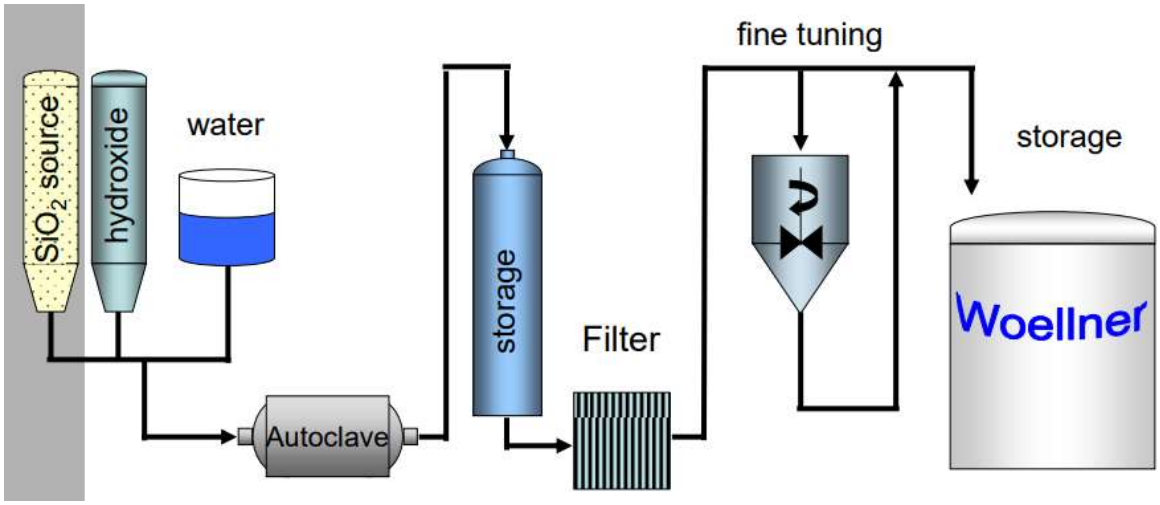

Fig. 2.10 Hydrothermal production of silicate solution (Wöllner, 2020)

2.1.4.2 Calcination and Solving Process

The calcination and solving process of sodium silicate production involves the dissolution of silica and its fusion into molten sodium carbonate whose melting points are 1713 °C and 851 °C respectively (Greenwood and Earnshaw, 1997). The reaction governing this process is given in equation 2.2, while a typical production layout for this method is shown in Fig. 2.11.

$$xNa_2CO_3 + SiO_2 \rightarrow (Na_2O)x.SiO_2 + CO_2 \qquad (2.2)$$

As can be seen, this calcination and fusion process releases large quantities of CO_2 in addition to its energy intensiveness, which makes it unattractive for silicate production due to cost and environmental concerns (Vinai and Soutsos, 2019).

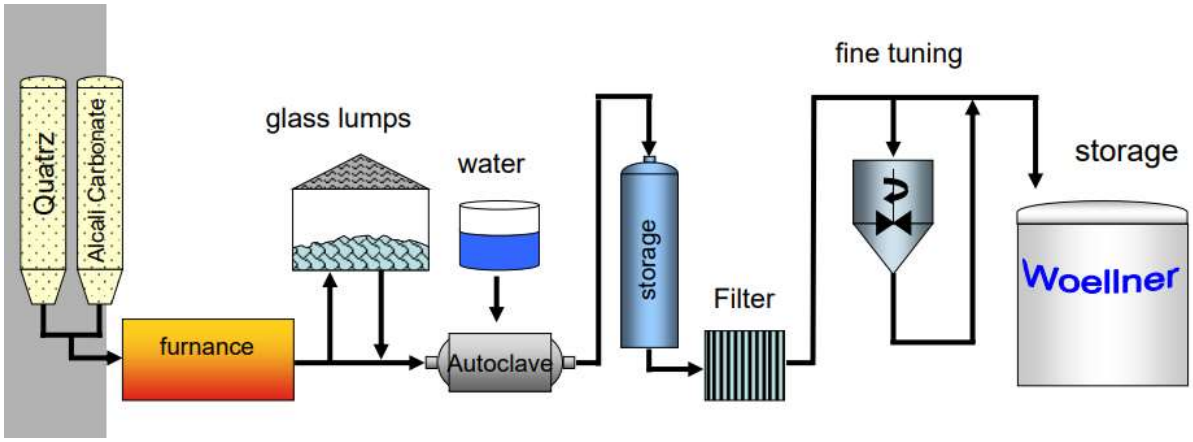

Fig. 2.11 Melting and solving process for silicate solution (Wöllner, 2020)

2.2 Alkali-activated Mortar

Alkali-activated mortars are produced with a broad range of precursors (e.g. calcined clay, GGBS, *etc),* alkali metal source (e.g. alkali hydroxides, alkali silicates, etc) and fine aggregates finer than a 5mm sieve size. In other words, an alkali-activated mortar is simply a concentration of fine aggregates in alkali activated paste and is used for various construction applications such as rendering, plastering, binder for stone and brick masonry, *etc*. The mix sequence of alkali-activated mortar is similar to that of PC mortar, and the trend in its engineering performance corroborates with that of AAC.

Workability, mechanical, and durability performance of alkali-activated mortars depends on the nature and concentration of the alkali metal source, the nature of the aluminosilicate source, the ratio of alkali solution to binder, and the aggregate to binder ratio (Alonso *et al*., 2017).

2.2.1 GGBS based Alkali-activated Mortar

Hydrated calcium aluminosilicate gel (C–A-S–H) is the main hydration product of a GGBS based alkali-activated mortar. The C:S ratio in the aluminium substituted C–S–H gel is generally similar to that of the unhydrated slag, but much lower compared to the C:S ratio in the C–S–H gel produced from the hydration of Portland cement (Chen and Brouwers, 2007). Taylor (1997) reported that, the C:S ratio found in alkali-activated slag (AAS) hydration gel is below 1.5, while that of Portland cement is approximately 2. Also, Brough and Atkinson (2002) examined the hydration product of AAS mortar and found that the inner product regions of the

hydrates contained C-S-H gel with a C:S ratio of around 0.9 mixed with a high Mg hydrotalcite, while the outer hydration product regions had a C:S ratio of around 0.7 and lower Mg hydrotalcite. This higher silicate content in the AAS gel is the cause of its increase strength compared to the OPC hydration gel. Moreover, the structure and composition of this gel-type are influenced by the type and nature of the activator used. For example, the reaction product with a more ordered C-A-S-H structure and higher C:S ratio are formed by NaOH activation of GGBS compared to the Na_2SiO_3 activated binder due to additional silicate induced into the pore solution of the silicate activated system (Bernal *et al*., 2014). Fernández-Jiménez, Palomo and Puerts (1999) concluded that sodium silicate solution produces the highest flexural and compressive strength of GGBS based alkali-activated mortar.

The pore structure of GGBS based alkali-activated mortar is also influenced by the type of activating solution. Smaller porosity is recorded for GGBS-based sodium silicate activated mortar compared to NaOH-activated mortar (Brough and Atkinson, 2002).

2.2.2 Calcined Clay Geopolymer Mortar

The most common clay minerals that have been used for alkali activation is the kaolinite that has a low surface area which limits the extent of its reactivity (Liew *et al*., 2016). Due to the kaolinite's small surface area, only minimum dissolution by alkali reactant is possible thereby producing weak structure and low strength mortar. According to Van Jaarsveld, Van Deventer and Lukey, (2002), the incorporation of a high volume kaolin clay in fly ash geopolymers decreases the strength of the mortar, because not all the kaolinite takes part in the geopolymerization reaction that forms the geopolymer network.

Meanwhile, calcined kaolin clay has a greater surface area and amorphous phase resulting from the thermal treatment. As such, increased compressive strength is achieved with the use of calcined kaolin clay as precursor for alkali-activated mortar due to the reactive amorphous phases that contribute active constituents, thereby eventually determining the ultimate strength of the geopolymer mortar.

2.3 Alkali-activated Concrete

The behaviour of an AAC based on various aluminosilicate sources has been extensively studied and has proven to have superior strength and durability performance compared to OPC concrete (Duxson *et al.*, 2006).

The alkali-activation process involves a breakdown of the Si–O chemical bonds in the glassy components of the aluminosilicate mineral binder to lend itself to reacting with the alkaline solution and subsequently form inorganic polymer comprising molecular chains and networks. The chemistry of this reaction is dependent on the composition of the aluminosilicate mineral binder (Andrew, Quillin and Kofi, 2011). The main reaction product of AAM and alkaline metal sources is alkaline alumina-silicate gel (R-A-S-H gel, where R = alkali metal). This gel is zeolitic in nature and has an entirely different structure in relation to the C-S-H gel produced by hydration reaction of PC (Provis, 2014).

The fresh and hardened properties of AAC are reported to be strongly influenced by the nature and concentration of the chemical activator, activator to binder ratio, nature of the precursor, curing condition, *etc*. Thermal curing is desirable for most AAC to achieve a relatively high early strength, as they are reported to not attain any strength at room temperature or when cured with water (Abdul Aleem and Arumailraj, 2012). Curing temperatures between 50 – 80°C are reported to have a significant influence on the mechanical and durability properties of AAC regardless of the precursors. According to Rangan (2008), AAC is characterized by a very flexible curing regime with regards to curing duration, temperature, sequence, *etc*. Abora *et al*. (2009) reported that the addition of components such as GGBS in an AAC mix produces concrete that sets and hardens at room temperature.

2.3.1 GGBS based AAC

GGBS is used on its own as a binder for AAC, or blended with other aluminosilicate sources such as fly ash, metakaolin, *etc*. to produce an AAC that can be cured at room temperature and possesses a high mechanical performance using relatively low dosage of activating solution (Rafeet *et al*., 2017). Chi (2012) noted that the main reaction product of a GGBS based AAC is a low crystalline hydrated calcium silicate similar to the C-S-H gel-type, but with a different gel phase and structure from that of OPC paste. Equally, Bernal *et al.* (2014) concluded that there is a consensus in studies on the reaction products of alkali-activated GGBS that, it is a C-A-S-H type gel with a disordered tobermorite-like C-S-H type structure and a secondary reaction product such as aluminoferrite mono (AFm), stratlingite, hydrotalcite phases.

When blending GGBS with other aluminosilicate sources to produce AAC, increasing the GGBS proportion of the concrete mix up to 30%, results in compressive strength gain by improving the microstructure of the geopolymer matrix to a more compact one and formation of additional C–A–S–H gel (Deb, Nath and Sarker, 2014).

2.3.2 Calcined Clay Geopolymer Concrete

Calcined clays are presently considered as cost-effective alternatives to high-purity metakaolin clay and offer greater supply sustainability due to the availability of vast clay reserves globally and tremendous clay waste generated by ceramic industries, construction projects, *etc*. (Lopez, 2009). Previous studies have mostly focused on the use of metakaolin as an aluminosilicate source for geopolymers. However, competing demand from different industries for high-purity kaolin clay, high cost and intensive purification process are some of the factors limiting its availability to be used as both supplementary cementitious material (SCM) and the precursor for alkali activation.

Metakaolin has often been associated with lowering the heat of hydration, enhanced workability, improving strength and increasing the durability of concrete (Siddique and Klaus, 2009). For instance, in 1992 Davidovits patented poly(sialate-siloxo) cement that is obtainable by blending metakaolin calcined at 750°C, alkali-disilicates (Na_2, K_2)(H_2SiO_4)$_2$, and GGBS. The cement was reported to harden rapidly at room temperature and provide compressive strength of about 20MPa within 4 hrs of placement and compressive strength between 70 – 100MPa (Davidovits, 1994) after 28 days. Meanwhile, in some instances where metakaolin is used as the sole aluminosilicate source, excessively high porosity in the binders was observed. This was due to the very high water demand of the metakaolin that is associated to its plate-like particle shape (Prov*is et al*., 2014a).

2.3.3 Alkali Solution as an Activating Agent for AAC

An alkali solution is required for the dissolution of aluminosilicate sources to release the SiO_4 and AlO_4 tetrahedral units for further reactions in any alkali-activated system (Yip, Lukey and Van Deventer, 2005). Alkali-hydroxide solutions, alkali-silicate solutions, alkali-carbonate solutions and alkali-aluminate solutions, as well as their combination, have been studied for different AAM and their performances are reported to vary from desirable to poor (Andrew, Quillin and Kofi, 2011). According to Provis (2014), soluble alkali-silicates are reported to be the most desirable activators of any AAC in terms of providing the best rheological, mechanical and durability properties. Equally, Passuello *et al*. (2017) noted that the use of soluble silicate in the alkali-activation of concrete yields a denser and more compact material with higher mechanical strength and a lower porosity compared to hydroxide-activated concrete. However, the most commonly used activator is a mixture of soluble alkali hydroxides (NaOH or KOH) and soluble alkali silicates (Na_2SiO_3 or K_2SiO_3) solutions (Rangan, 2008).

Moreover, according to Davidovits (2015), alkalination of aluminosilicates with only highly concentrated alkali hydroxides without an alkali silicate solution produces non-geopolymer products. These products are either crystalline zeolite-A type or hydroxysodalite that has a non-stable structure and also suffers leachate when they react with water because of the presence of free end positive charge alkalis outside their structure. Furthermore, Na-based alkali-activators are generally preferred for the alkalination of AAC rather than K-based alkali-activators mainly due to cost (Provis *et al*., 2014b).

Previous studies have shown that the mixture of alkali silicate and alkali hydroxide solutions as an activating agent produces a better microstructure and enhances strength properties through the inducement of certain amounts of soluble SiO_2 to form monomers, dimmers, and oligomers (Liew *et al.*, 2016).

2.4 Workability and Rheological Performance of AAC

Concrete workability is commonly determined using single-point tests such as slump, compacting factor, Vebe time, flow, *etc*. These tests are generally simple and rapid, that measures either time, horizontal or vertical distance. These variables only defines the consistency of concrete, but cannot measure yield stress and plastic viscosity which are fundamental rheological parameters. However, these parameters are effectively measured through multi-point tests using a rotational rheometer, slump rate machines, *etc*. (Koehler and Fowler, 2003). The International Centre for Aggregate Research's (ICAR) concrete rheometer enables measurement of flow curve and the performance of a stress growth test. It is reported to be appropriate for virtually all ranges of concrete workability from a slump of approximately 50mm to self-consolidating concrete.

Rheology measurements are based on stress, rate of strain, and time factors. According to Laskar and Bhattacharjee (2011), rheology provides more detailed quantitative measurements and characterises properties of fresh concrete such as workability loss, stability, compactibility and flow behaviour, and it has not been adequately studied for AAC. The rheology of any fresh concrete is summarised in Fig. 2.12:

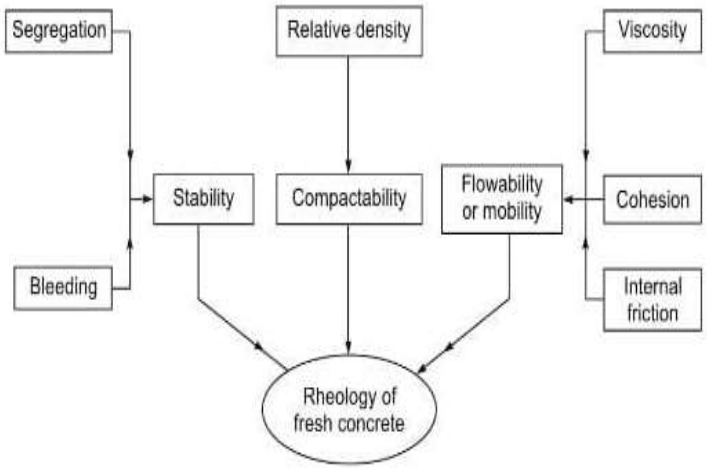

Fig. 2.12 Rheological parameters of fresh concrete (Arjun, 2017)

The characterisation of fresh concrete's rheological properties is complex, using various models for characterisation of the flow properties of fluids. These models are based on the relationship between shear stress and shear rate which is represented graphically by flow curves. The complexity is caused by the wide range of particle sizes in concrete, as well as the time-dependent nature of properties fresh of concrete (Koehler and Fowler, 2004). The flow curves for some of the common models that can be associated with the characterisation of fresh concrete over a range of shear stresses and shear rate are shown in Fig. 2.13.

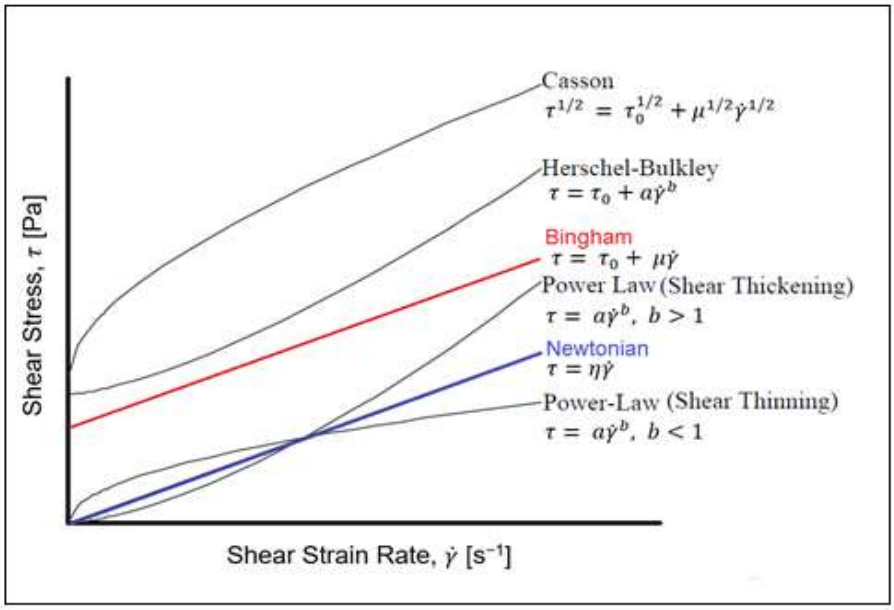

Fig. 2.13 Flow curves based on the constitutive relationship of concrete flow (Koehler and Fowler, 2004).

According to Laskar and Bhattacharjee (2013), fresh AAC is a suspension of aggregates bounded by alkali-activated mortar and can therefore be effectively described as fluid that follows the Bingham model. In this model, the concrete flow is defined by the yield stress and has linear relationship between the shear stress and shear rate as shown in Fig 2.13. However, Erdoğan *et al.* (2008) noted that concrete is not a perfect Bingham fluid because the relationship between its shear stress and shear strain rate is not always linear. Shear thickening (the increase in viscosity of concrete with shear rate) and shear thinning (decrease in viscosity of concrete with shear rate) are good examples of concrete behaving as a non–perfect Bingham fluid.

Nevertheless, Claisse, Lorimer and Omari (2001) concluded that concrete rheology can best be characterized by the Bingham model because of the simplicity of the model and reported appropriateness for most concrete mixes. The model flow curve shown in Fig. 2.14 indicates the relationship in terms of yield stress and plastic viscosity.

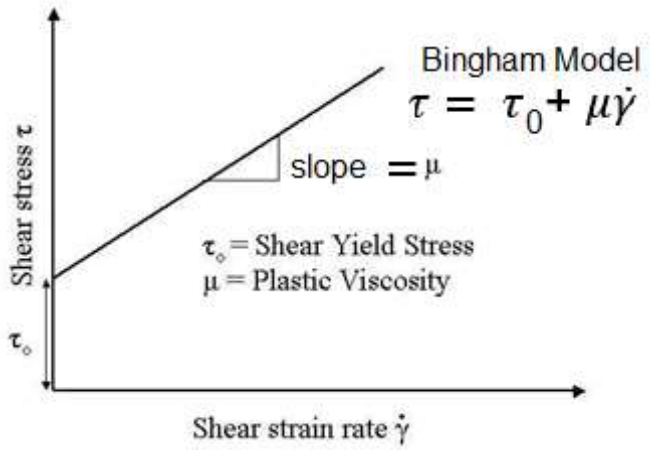

Fig. 2.14 Bingham rheological model (Koehler and Fowler 2004)

Many studies revealed that the rheological behaviour of AAC is sensitive to the nature of the aluminosilicate sources that include composition, particle size, surface activity, specific surface area and shape, alkali concentration and modulus of the alkali activator (Deb, Nath and Sarker, 2014).

2.4.1 GGBS based AAC

The workability, yield stress, and plastic viscosity of GGBS based AAC are sensitive to the nature and concentration of the alkaline activator, liquid to solid (L/S) ratio and the proportion of aggregate (aggregate to binder ratio) used in AAC mix formulations.

GGBS based AAC sets very quickly as expected of a high-calcium alkali-activated system, due to the formation of a primary C-S-H gel resulting from the reaction between the Ca^{2+} and the Si^{4+} ions in the GGBS and the silicate solution, respectively. This is in addition to its angular shape, which decreases its flowability, thereby affecting its workability (Torres-Carrasco and Puertas, 2017). Chi (2012) reported that due to the short-setting time of GGBS based AAC, its workability is difficult to measure without the introduction of a chemical admixture into the mix. However, chemical admixtures being used as retarders are associated with detrimental effects on the compressive strength of AAC (Rafeet *et al.*, 2017).

Deb, Nath and Sarker (2014) studied the effects of the proportion of GGBS on the workability of binary-mix geopolymer concrete and observed a decreasing trend in workability with an increase in slag content regardless of the alkali solution to binder ratio. The study also reported that as the ratio of Na_2SiO_3 to NaOH decreases the workability of the GGBS and PFA binary-mix geopolymer concrete showed a decreasing trend.

2.4.2 Calcined Clay Geopolymer Concrete

The workability of clay-based geopolymer concrete is influenced by the proportion and properties of the constituent materials that produce the geopolymer paste (Liew *et al.*, 2012). The layered structure of clay imposes interparticle friction that causes the mixture to be viscous and sticky, thereby decreasing the workability of calcined clay-based geopolymer concrete.

2.5 Compressive Strength Development of AAC

Compressive strength is a basic property of concrete that has a very strong correlation with other mechanical and durability properties of concrete. AACs are mostly reported to have low early strength and a high final strength gain at 28 days; depending on the precursors, alkali solution concentration, curing condition, *etc* (Provis 2018).

2.5.1 GGBS Based AAC

The compressive strength of GGBS based AAC increase with its age (similar to that of PC concrete). Chi (2012) observed that the compressive strength of GGBS sodium silicate activated concrete at the age of three days is 3.5–5 times higher than that of PC concrete, while their respective compressive strength development remained the same after three days. This rapid strength gain by the GGBS in a strong alkaline medium can be associated with the quick precipitation of the C-N-A-S-H gel, compared to the relatively slow precipitation of the C-S-

H gel by the PC hydration. Chi (2012) also noted that the highest compressive strength for GGBS based AAC was achieved when cured at 60°C and 80% relative humidity (RH). (Bernal *et al.*, 2011) also showed that the mechanical strength for the GGBS based AAC is higher than that of the PC concrete mix produced with a similar binder, water content and curing temperature. Fig. 2.15 presents the results from the BRE study on the effect of curing temperature on the compressive strength development of FA/GGBS based AAC.

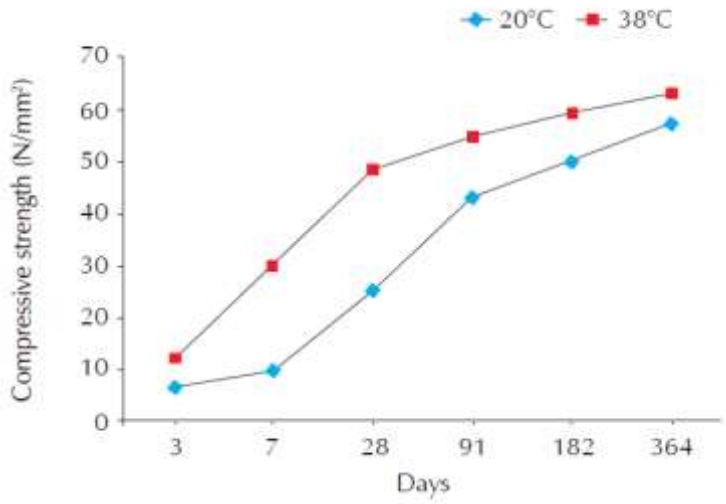

Fig. 2.15 Compressive strength development of AAC cured at room and elevated temperature (Andrew, Quillin and Kofi, 2011)

Al-Otaibi (2008) reported that the dosage and type of activator affect the strength of GGBS based AAC. This happened as increased dosage resulted in increased strength, while increasing the silicate modulus of the activator also increased the strength. On the contrary, Andrew, Quillin and Kofi (2011) reported that a decrease in the dosage of activating solution (low liquid : binder), resulted in an increase in the compressive strength of the concrete. Their study further reported that an increase in the sodium concentration of the activating solution increased the compressive strength of the PFA/GGBS based AAC, as shown in Fig. 2.16. Rafeet *et al.* (2017) balanced these contradicting opinions by showing that the strength increases with increasing alkali modulus until an optimum value is reached, above which there will be a drop-in strength due to the reduced amount of available silica required for the reaction. These optimum values are in the range of 0.95 and 1.25 for GGBS based AAC.

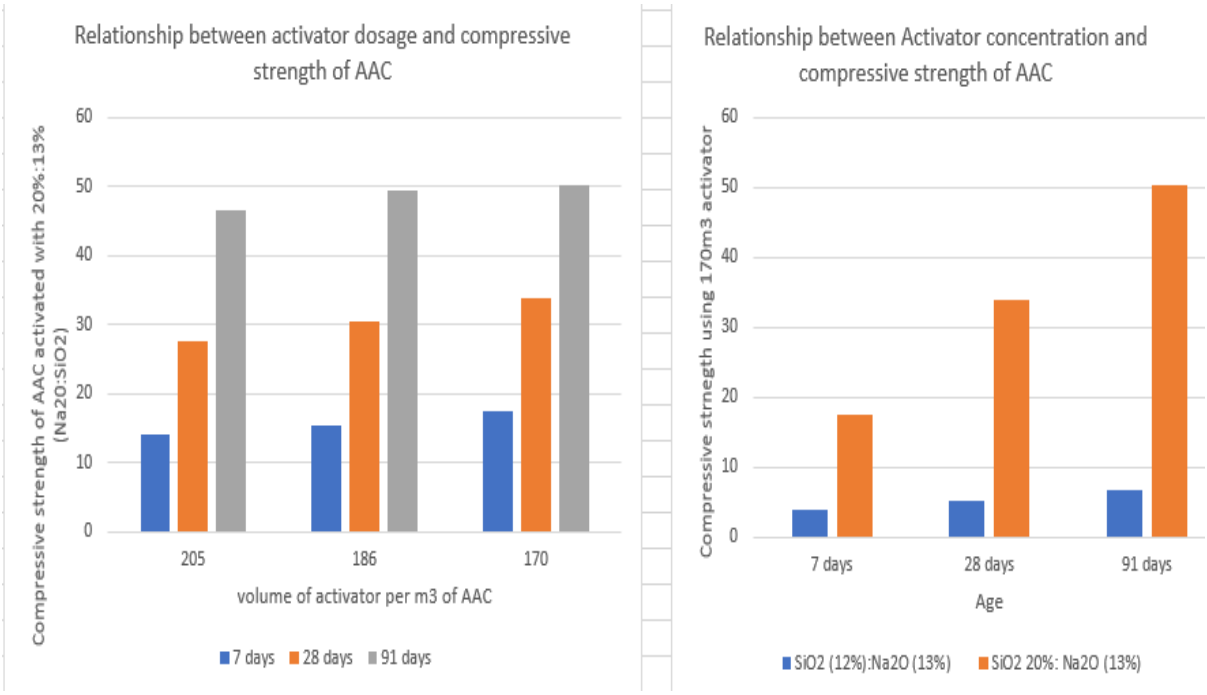

Fig. 2.16 The relationship between activator dosage, activator concentration, and compressive strength development of PFA/GGBS based AAC (Abora *et al.*, 2009)

2.5.2 Calcined Clay Geopolymer Concrete

Unlike PFA based geopolymers, the heat-curing of calcined clay based geopolymer concrete is not desirable because it is not found to influence the chemical reaction of the paste. Increasing the temperature and duration of curing does not result in compressive strength gain in the clay-based geopolymer concrete. However, the process that is proven to enhance the strength performance of calcined clay-based geopolymers is blending it with calcium from other sources such as slaked lime, GGBS, *etc*. This blending results in the formation of Ca-rich Al-substituted silicate hydrate (C-(A)-S-H) reaction product that will coexist with the aluminosilicate 'geopolymer' gel in the structure (Bernal *et al.*, 2011).

2.6 Durability Performance of AAC

The durability performance of concrete is basically studied in the context of sulphate attack, freeze-thaw resistance, alkali-silica reaction, fire resistance, leachate resistance, carbonation and corrosion of steel reinforcement. Carbonation and chloride ingress is the most significant processes that destroy the protective iron oxide film that passivates the steel in the strongly alkaline environment of concrete, which could result in corrosion of the steel and its accompanying spalling of the concrete (Claisse, 2016).

Accordingly, the main property of concrete that influences its durability performance is its permeability to the ingress of water, chlorides, carbon dioxides, sulphates and other deleterious substances. In other words, the permeability of concrete is the property that governs the rate of flow of fluid into the concrete and is not only a function of its porosity but depends on the size, distribution, shape, and continuity of the pores (Neville, 2011).

Presently, unlike PC concrete, there are few studies and a limited understanding of AAC degradation mechanisms (Abora *et al.*, 2014). For instance, according to Provis (2018) the corrosion of steel reported in AAC cannot just be predicted based on the alkalinity of the pore solution and therefore requires further study of the interaction between the binder and the embedded steel. Also, since the deterioration mechanism of AAC is different from that of PC concrete, the test parameters need to be different. For instance, the main difference between PC concrete and AAC degradation under sulphate attack is related to the formation of expansive calcium sulphate aluminate and decalcification of the C-S-H gel in the PC concrete. On the other hand, the low Ca content in AAC induces different degradation mechanisms that require modification of the test parameters to give a good representation of the likely in-service behaviour of AAC (Abora *et al.*, 2014).

2.6.1 Freeze-thaw Resistance of GGBS based AAC

Fu, Cai and Yonggen (2011) proved that GGBS based AAC had excellent freeze-thaw resistance. Their finding indicated the relative dynamic elasticity modulus to be about 90% after 300 freeze-thaw cycles. Their results further showed little mass loss and thin surface freeze-thaw damage layers that effectively restrained the freeze-thaw damage of the concrete from worsening.

The excellent freeze-thaw resistance of GGBS based AAC is attributed to its final hydration products which were mostly C–S–H with low C:S ratio, alkaline aluminosilicate and zeolite minerals. Because of the absence of $Ca(OH)_2$ and transition strip in the GGBS based AAC system, water penetration becomes difficult due to its symmetrical and compact structure (Fu, Cai, and Yonggen 2011). This makes it difficult for the concrete to become frozen and saturated. Another reason advanced for the good freeze-thaw resistance of GGBS based AAC is its improved ability to restrain interface damage due to its high compressive strength features (Jianguo, C., Jinyu, L. and Li 1999).

2.6.2 Freeze-thaw Resistance of Calcined Clay Geopolymer Concrete

In many parts of the world, particularly colder regions, freeze-thaw resistance is an issue of significant interest. This concern is due to the reported rapid deterioration of PC under freeze-thaw cycling; especially in highway applications where de-icer salts are often applied to the concrete surfaces. Škvára, Jílek and Kopecký (2005) noted that geopolymer materials have excellent frost resistance such that even after 150 freezing and defrosting cycles in an aqueous environment, the mass of the sample was constant and the compressive strength drop was not significant. The improved frost resistance of the geopolymer can be attributed to its binding phase (Na/K – Al – Si), which is not a hydrate unlike Portland cement concrete, and therefore does not suffer increased pore pressure due to freezing and thawing. Meanwhile, (Alanazi *et al.*, 2017) compared the frost resistance of metakaolin geopolymer and Portland cement concrete containing 5% air-entraining agent (a treatment for enhance frost resistance). Their findings showed that the geopolymer concrete did not exhibit superior freeze-thaw resistance. They further noted that the geopolymer concrete performance depended on the water to solid ratio and molar oxide ratios of the geopolymer mix.

2.6.3 Chloride Permeability of GGBS based AAC

The mass transport properties of GGBS based AAC is essential in determining its durability since it characterises the flow of aggressive external species into the concrete that deplete the alkalinity of the pore solution and cause corrosion of the embedded steel. Permeability analysis and testing of GGBS based AAC is widely adopted in studying its durability performance (Bernal *et al.*, 2014). Different permeability testing methods measure different variable to characterize the permeability of AAC.

According to Bernal, De Gutiérrez and Provis (2012), GGBS based AAC has low water permeability compared to both OPC concrete and GGBS blended concrete due to the lower filling capacity of the N-A-S-(H) type of gel compared to that of C-A-S-H gels. In other words, the dense structure of the N-A-S-H type gel produced in alkali activated system can be attributed to its low permeability of external species compared to the calcium based gel system.

2.6.4 Chloride Permeability of Calcined Clay Geopolymer Concrete

The transport properties of calcined clay AAC under pressure gradient which is characterised by its permeability depends primarily on the structure of the geopolymerized paste. According to Neville (2011), permeability tests of concrete including calcined clay AAC has not been

standardised thereby making it difficult to compare the measured variables obtained from different studies. Nevertheless, the coefficient of water permeability of calcined clay AAC can be accurately calculated using Darcy's law, presented in equation 2.3.

$$Kf = \rho g L Q / P A \quad (2.3)$$

Where: Kf = coefficient of water permeability of the specimen (m/s)
ρ = density of water (kg/m3)
L= length of specimen (m)
g = gravitational acceleration (m/s2) Q = flow rate (m3/s)
A = area is the cross-sectional area of the specimen (m2)
P = pressure is the water pressure (MPa)

According to Pacheco-Torgal *et al.* (2012), metakaolin based AAC is generally reported to show better permeability resistance to external species compared to Portland cement system.

2.7 Microstructural Characterisation of AAC

Microstructural analysis is becoming an increasingly indispensable tool for understanding the engineering performance of concrete by providing insight into the density, porosity, and fineness of its structure. The microstructure of any concrete has a strong correlation with its durability, which significantly determines its service life. The microstructure of AAC is reported to be denser and more compact when correctly formulated, cured, and placed than that of PC concrete (Andrew, Quillin and Kofi, 2011). The microstructure of AAC depends on the type of precursor, type of alkali metal source, curing conditions, *etc*.

2.7.1 GGBS Based AAC

Song *et al.* (2000) studied the microstructure of the GGBS based AAC using SEM and showed that the microstructure was a smooth, homogeneous and interconnected-solid. Some of the pores between the grains appeared isolated from others and generally looked tortuous; irrespective of the concentration of the activator used. Brough and Atkinson (2002) also showed that the microstructure of alkali-activated GGBS gel consists of a homogeneous gel and micro-cracking against the aggregate interface after early hydration. Moreover, this degree of shrinkage and cracking which is caused by drying reduces upon completion of full hydration.

2.7.2 Calcined Clay Geopolymer Concrete

The strength and durability of clay-based geopolymer concrete are closely related to the density and porosity of the concrete microstructure. Low porosity, high density, and fine-grained

microstructures are characteristics of high-strength geopolymer concrete. This structure is achieved with a mixture using high-alkali and low-water contents: such as Na_2O/Al_2O_3 = 1.2 and H_2O/Al_2O_3 = 12 respectively. A high SiO_2/Al_2O_3 of between 3.5 and 3.8 also produces this structure, but there is a maximum above which the strength deteriorates (Steveson and Sagoe-Crentsil, 2005). Metakaolin based geopolymer concrete shows only homogenous geopolymer phase while blending it with GGBS reveals two distinct phases of the geopolymer matrix and C-S-H gel as shown in Fig. 2.17.

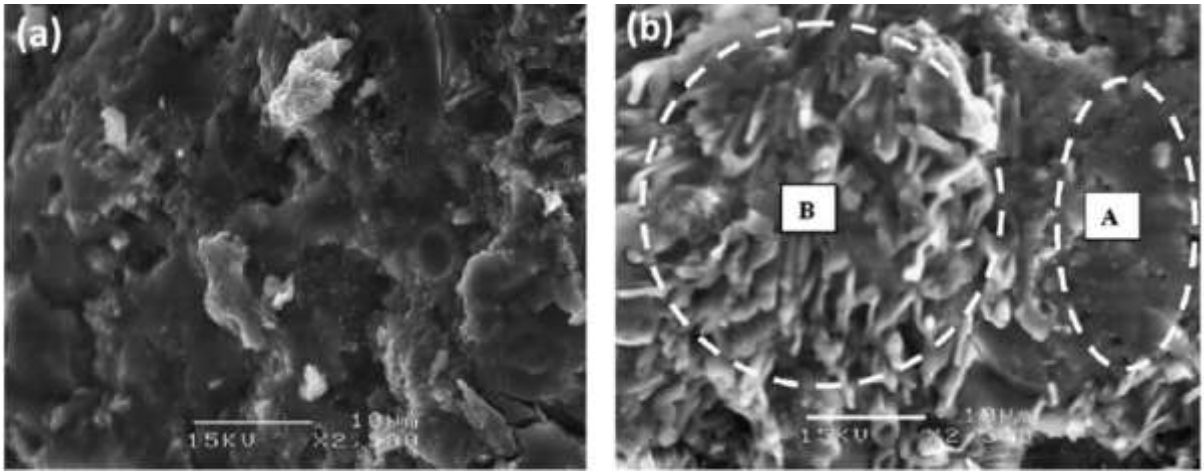

Fig. 2.17 Microstructure of (a) Metakaolin geopolymer (b) Metakaolin geopolymer blended with 50% GGBS (A – geopolymer matrix; B- C-S-H gel) (Yunsheng *et al.*, 2007)

(Davidovits (2015) concluded that the microstructure of metakaolin geopolymer concrete is not compact and remained a layered structure after geopolymerization reaction due to the reaction occurring at the surface.

2.8 Mineralogical Phase Characterisation of Calcined Clay Geopolymer Concrete

XRD is a very popular technique used for the characterization of Portland cement systems that are composed of crystalline and semi-crystalline phases. Likewise, XRD analysis is applicable to geopolymer binder system, which is composed of amorphous and semi-crystalline phases. Casarez, Soberón and Sánchez (2014) noted that XRD nevertheless is often used in the analysis of geopolymer systems to identify newly formed phases, define the degree to which starting materials have reacted, and assess the level of amorphicity of the reaction products. Wang, Li and Yan (2005) reported that besides the amorphous and semi-crystalline phases, metakaolin-based geopolymers contained adsorbed atmospheric water and small amounts of inert ingredients (quartz and mullite) which originated from the metakaolinite. The distinction of the liquid water in the sample was possible using FTIR analysis. Specifically, their findings

showed that the broad band in the XRD pattern of the metakaolinite (between 18° and 25°) is an indication of its mixed semi-crystalline and amorphous structure, while the reaction products between 18° and 25° (with relatively smaller intensities after the geopolymerisation) is an indication that the geopolymer material has an almost complete amorphous structure.

Moreover, for lateritic clay-based geopolymers, Davidovits and Davidovits (2020) argued that because of the inherent limitation of NMR spectroscopy in characterizing iron-rich compounds, XRD techniques and Mossbauer spectroscopy are presently the analytical techniques that can effectively characterize the structure of this kind of geopolymeric binder.

2.9 Functional Groups of Calcined Clay Geopolymer Concrete

In Portland cement-based materials, FTIR spectroscopy is used to estimate the relative quantities of different constituents in samples, as well as assess the molecule's vibrations – when combined with the calcium-silicate (C/S) values – to give facts on the CSH network (Lawan, Kaura and Bature, 2016). Accordingly, the technique has been used previously to determine the functional group of metakaolin based geopolymer systems. Wang, Li and Yan (2005) showed in Fig. 2.18, the IR spectra of the metakaolin and the corresponding geopolymer which is synthesized using blended sodium silicate solution (Molecular Ratio (MR)=3.2) and 8 mol/L NaOH solution.

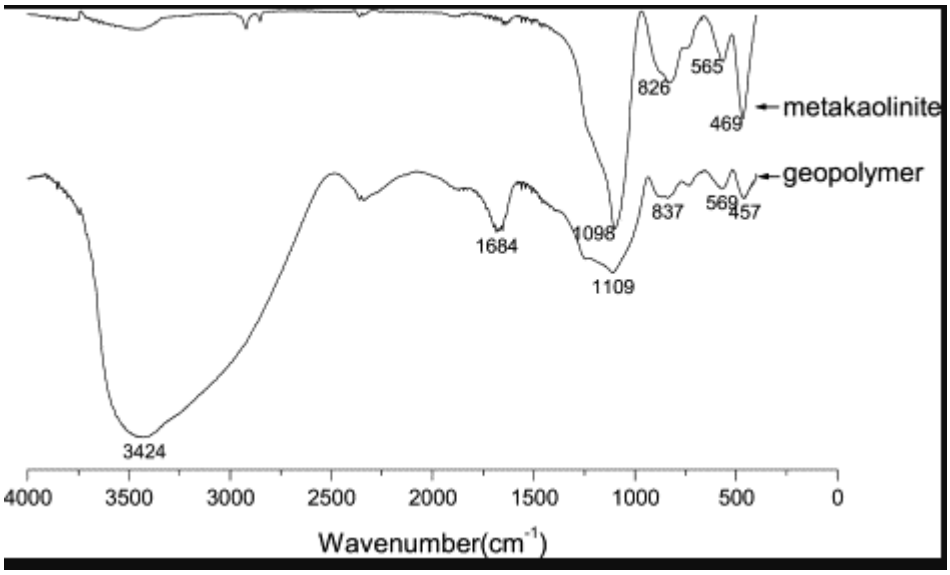

Fig. 2.18 FTIR spectra of raw metakaolin and corresponding geopolymer (Wang, Li and Yan, 2005)

From the Infrared (IR) spectrum of the geopolymer in Fig. 2.18, it can be seen that the broad band of around 3420 cm^{-1} together with that around 1680 cm^{-1} indicates adsorbed atmospheric

water, which exists in the moulded geopolymer sample. Meanwhile, the broad adsorption bands of the IR spectrum of the raw metakaolin around 1098, 826, and 469 cm^{-1} are assigned with Si-O stretching vibration, Si-O-Al vibration, and flexural vibration, respectively. Interestingly, Wang, Li and Yan (2005) concluded that since only a little difference exists between the IR patterns of the raw metakaolin and the corresponding geopolymer within 450–1200 cm^{-1}, it can be suggested that most vibrant forms of the molecular chains existing in the raw metakaolin are retained in the geopolymerization product.

2.10 Global Warming Potentials (GWP) of AAC

AAC is generally associated with low CO_2 emissions due to their synthesis, mostly, from waste and the low-embodied energy required for their production. According to Duxson *et al.* (2007), the Green House Gases (GHG) savings of AAC is about 80% relative to Portland cement concrete. However, (Habert, D'Espinose De Lacaillerie and Roussel, 2011) showed that GGBS, PFA and metakaolin geopolymer concrete have higher environmental impacts in all the categories considered in their LCA except Global Warming Potential (GWP) compared to PC concrete. The study further showed that the fresh water ecotoxicity impact of the geopolymer concretes is about 1000 times higher than that of PC concrete as shown in Fig. 2.19. Meanwhile, Davidovits (2015) challenged these values by showing that the data used in this LCA did not correspond to the irritant silicate used for geopolymer formulation.

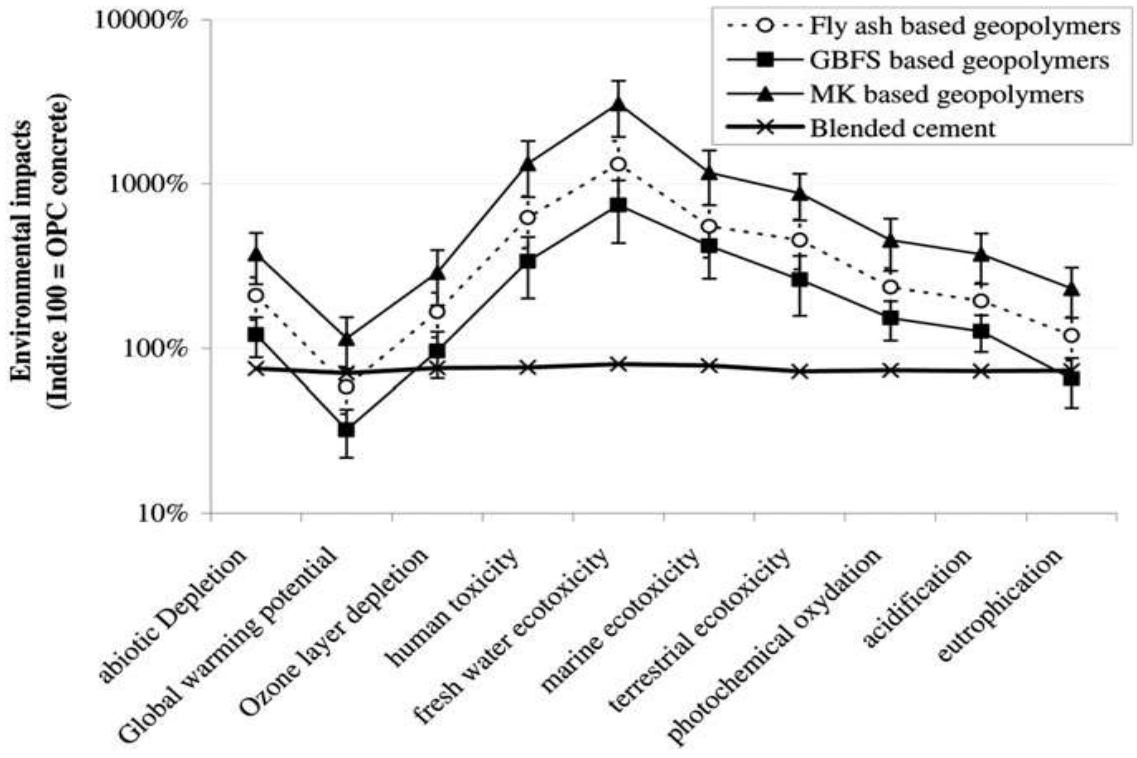

Fig. 2.19 Eco-profile of PFA, GGBS and Metakaolin geopolymer concretes (Habert, D'Espinose De Lacaillerie and Roussel, 2011). The blended cement composed of 70% CEM I and 30% mineral admixture which can be either GGBS, PFA or metakaolin

Thermal curing, production of water glass, and the caustic soda that are used for alkali activation are the major processes associated with the increased environmental impact of AAC (Passuello *et al.*, 2017). According to Andrew, Quillin and Kofi (2011), processing sodium silicate from calcination of sodium carbonate and hydrothermal process is the dominant cause of environmental impact of AAC, because of the energy intensiveness of the processes and the water usage involved.

On the other hand, the sodium silicate activators derived from wastes have the potential of significantly lowering the environmental impact of AAC. Passuello *et al.* (2017) studied geopolymer paste mixes based on sodium silicate derived from chemically modified rice husk ash (RHA) and reported lower impacts in LCA per unit of compressive strength in acidification, GWP, eutrophication, and photochemical oxidation potentials compared to the OPC paste. The study further reported up to 150% higher impact values in fresh water ecotoxicity, human toxicity, marine ecotoxicity and terrestrial ecotoxicity potential relative to OPC paste.

2.10.1 GWP of GGBS based AAC

Generally, GGBS-based AAM have the least GWP compared to other aluminosilicate sources because they require lower concentration of activator for their synthesis. This is in addition to the fact that, they are a by-product that do not require extraction and calcination process (Zografou, 2015). However, the granulation and grinding processes of refining GGBS have a noticeable contribution to the GWP of GGBS based AAC (Andrew, Quillin and Kofi, 2011). Furthermore, the use of GGBS as a precursor for AAC eliminates the necessity of thermal curing which is one of the major factor responsible for increasing the environmental impact of AAC (Davidovits, 2015).

2.10.2 GWP of Calcined Clay Geopolymer Concrete

According to Scrivener, John and Gartner (2018), Alkali-activated calcined clays are a scalable option that has the potential to reduce global CO_2 emissions. For instance, previous studies showed that the use of smectite- rich bentonite as a meta-clay source has the potential to reduce the GWP of AAC significantly. Also, Heath, Paine and McManus (2014) reported a 30% reduction in GWP of geopolymer binder when PC binder is replaced with bentonite-based

meta-clay. Similarly, (Maddalena, Roberts, and Hamilton 2018) reported that metakaolin based geopolymer binders for non-structural applications (mortars, rendering cement) have a carbon footprint of between 23 to 55% lower than Portland cement.

However, the main drawback of calcined clay based AAC is that it requires significant amounts of alkali metal silicate whose current production technology is both capital and energy intensive. As such, the lowering of the environmental impact of alkali-activated calcined clay depends on the development of low-CO_2 alkali silicate production methods.

2.10.3 Waste Derived Activators and GWP of Geopolymers

The growing interest in valorising various industrial wastes and by-products, as well as the need to reduce the production cost and improve the carbon footprint of geopolymer binders, has encouraged the development of alternative alkali-activators. Examples of industrial wastes are agricultural residues, cleaning solutions, *etc*. For instance, an alkaline aqueous solution is generated as a by-product of the aluminium foundry industry and is used to wash the extrusion sand moulds and other tools used in the moulding process. Another example is Bayer liquor residue that results from the well-known Bayer process of refining bauxite for the production of alumina. Fernández-Jiménez *et al.* (2017) reported good strength performance when a waste alkali solution was used as an activator for geopolymer.

Similarly, many authors have studied the combination of alkalis with waste derived amorphous silica sources such as RHA, waste glass cullets, *etc.*, and reported that they are effective activators for geopolymers (Passuello *et al.*, 2017). However, Vinai and Soutsos (2019) noted that the development of a waste-derived solid activator, which can be premixed with a precursor and thus obtain a one-part binder system is more desired by the construction industry. The one-part system require mixing with water only to produce geopolymer.

2.10.4 One-part Geopolymer and GWP

Luukkonen *et al.* (2018) reviewed published data on the environmental impact of PC, two-part (synthesized with liquid activator) and one-part (synthesized with solid activator) geopolymers. Their conclusion was that the environmental impact is 24% and 60% for one-part and two-part geopolymers respectively, relative to the environmental impact of PC. Thus, one-part geopolymers are more environmentally friendly than two-part geopolymers. However, Davidovits (2015) argued that although one-part geopolymers follow the routine practices of Portland cement materials traditionally used in the construction industry and have lower

embodied energy, their synthesis is based on dry NaOH/KOH which are corrosive in nature and therefore not user-friendly systems. After reviewing recently published patents on one-part geopolymers, Davidovits (2015) summarized two major drawbacks of their mass production considering their reliance on the use of KOH or NaOH and nano-silicafume. These drawbacks are:

I. A limited amount of silica fume is produced globally and therefore insufficient for mass production of one-part geopolymers.
II. The global supply of KOH and NaOH (which are generally manufactured by the electrolytic dissolution of NaCl or KCl) is threatened by the decreasing market of chlorine (due to its toxicity) and therefore may affect its economical availability for mass production for one-part geopolymers.

It may be interesting to note that Davidovits coined the term geopolymer in 1978 and founded the geopolymer institute, which continue to provide cutting-edge research in the field. He also presents the annual state-of-art research and development in the field of geopolymer, where he highlights the salient breakthroughs in the preceding year and draws attention on the gaps that needs to be researched in the field.

2.11 Controlled Low Strength Binder (Calcined Clays Semi-dry Paste)

According to Scrivener, John and Gartner (2018), one of the most effective strategies towards improving the sustainability of the construction industry is to discontinue the use of Portland cement for low strength applications and soil stabilization. This practice will significantly reduce the amount of clinker production and consumption, as well as encourage a massive utilization of various industrial wastes that have pozzolanic properties. ACI Committee (2013) defined controlled low-strength material (CLSM) as engineered material that has a compressive strength of less than 8.3 MPa, but slightly higher than that of well-compacted soil (1.2 MPa). The CLSM is a self-consolidating cementitious material used in applications that include backfill, structural fills, pavement bases, conduit bedding, erosion control, void fillings, *etc*.

Previous works on CLSM showed that industrial waste and recycled materials that are commonly agreed to be a promising application as cement substitutes are GGBS, cement kiln dust (CKD; Lachemi *et al.*, 2008, 2010; Le and Nguyen, 2016), PFA, RHA and quarry dust (QD; Nataraja and Nalanda, 2008). Also, Taha *et al*. (2007) evaluated the potential use of by-

pass dust (BPD), incinerator bottom ash (IBA) and copper slag as a CLSM. Their conclusion was that the waste materials should always be used in combination with Portland cement in order to activate their pozzolanicity.

However, collaborative research by Coventry University, Skanska and Lafarge Plasterboard under the Waste & Resources Action Programme (WRAP) developed a viable binder using recycled gypsum from waste plasterboard and other mineral wastes for construction of road foundations. The research optimized a mix (plasterboard-derived recycled gypsum (15%), BPD (5%) and BOS (80%)) which gave a compressive strength of 11 MPa at a water to binder ratio of 0.3 (Ganjian *et al.*, 2008). A site trial based on the optimized ternary blend was carried out in three applications: soil stabilization, semi-dry roller compacted paste, and roller compacted concrete. The semi-dry roller-compacted paste – using the ternary blend with 13% water – achieved the highest compressive strength of 31MPa at 28 days, and was therefore used for the base course in the road site trial shown in Figs. 2.20a and 2.20b.

Fig. 2.20a Placing the semi-dry paste

Fig. 2.20b Compacting the semi-dry paste

More recently, Bai Kamara, Ganjian and Khorami, (2019) optimized a semi-dry paste mixture based on nine industrial by-products for road base foundation. In their work, mixture design based on a statistical programme (Minitab 18) was used for the design of the experiment (DoE). They then used extreme vertices design (EVD) method to set the boundaries of the various components in the mixture designs. Their conclusion was that the ternary mixture with the proportions of 15% vitamin B5 gypsum, 37.5% reclaimed asphalt filler, and 47.5% GGBS with 15% water gave the highest compressive strength of about 30 MPa at 28 days.

Considering the fact that the supply sustainability of GGBS may be difficult to secure in the long term, coupled with the proven viability of Portland cement-free semi-dry paste for road base foundation, this work sought to determine the possibility of replacing GGBS in the already

reported optimized ternary mixes in the literature with the iron-rich flash calcined clay. The potency of the calcined clay was also compared with white metakaolin.

2.12 Summary

From the aforementioned reviewed literature, it has been established that geopolymers are one of the viable options being explored presently to improve the sustainability of the construction industry. The mass production of geopolymers can best be guaranteed by rock-based aluminosilicate sources; specifically, lateritic clay, which was considered as an unsuitable precursor until recently due to its large iron content. The reactivity of iron and the structural implication of its inclusion in the binding gel has not been understood in details. Two-part geopolymers – based on user-friendly activators – remain the best route for the wide commercialization of geopolymers due to its inherent superior performance. The impracticality of prescriptive recipe-based standard for geopolymers due to its ability to utilize an ever-growing range of materials makes it always necessary to characterize the mechanical, rheological and durability performance of every formulation. Also, the internal mechanisms of any formulated geopolymer system need to be examined, in addition to its carbon saving estimation.

Consequently, the viability of producing geopolymer based on flash calcined lateritic clay sourced from Northern Ireland as precursor was studied. The effect of mix design parameters such as type, proportion and dosage of activators, curing conditions etc were evaluated for this precursor. This is because broad range of optimized molar ratios have been prescribed in the literature for correct geopolymer formulation. But, even within the recommended range, diverse performance have been recorded which are largely determined by the precursor use in the system. This study also sets out to characterize the internal mechanisms of the calcined lateritic clay geopolymer to gain insight into the cause of the recorded mechanical or durability performance. The study further explored the potential of the calcined lateritic clay as a replacement for scarce GGBS for a ternary hydraulically road binder mixture.

CHAPTER 3 RESEARCH METHODOLOGY

3.1 Introduction

In the preceding literature review chapter, the current research trends in the field of geopolymer as an alternative binder for the construction industry had been highlighted. The prospects of exploring low purity, iron-rich kaolin clay as a precursor for geopolymer binder had been stressed and some research gaps identified. It can therefore be seen that for the study to achieve its outlined objectives - the investigations into the mechanical properties, durability performance and microstructural characterizations of the geopolymer binder system – broad range of experiments needs to be carried out. This chapter introduces the research design and methodology that was used for this work. Also, the research approach adopted in this study and the reasons for its adoption, the research strategies that were followed in this study coupled with the Justification for following them have been highlighted.

3.2 Research

Kothari (2004) noted that research is the search for fact through study, observation, comparison or experiment. Research is a systematic approach that comprises of defining the problem, formulating a hypothesis, data collection and analysis, and drawing conclusion as well as recommendation to solve the identified problem. According to Saunders et al (2016), research is a structure that justify the research strategy used in collecting and analyzing data for the purpose of answering the research question and satisfying the research aim and objectives. Based on the foregoing definitions, it can be seen that this study fulfils the features of a research.

3.2.1 Research Design

Research design is a strategy for selecting the research themes and the data collection methods that answers the selected research questions (Blessing et al. 2009). Richey and Klein (2014) noted that a research design is a framework that determines the information that needs to be collected, the sources of the information and how it should be collected. It also provides guidance on the data collection and the analysis phases of the research.

Claisse et al (2010) recommend that research on construction materials should be experiment based that involves broad range of testing including durability performance, as well as site trials where possible. The research design of this study enabled identification of the relevant

tests that provided the necessary insights into the performance of the calcined clay geopolymer binder.

3.2.2 Research Methodology

Research methodology is a systematic way of approaching, solving and presenting a problem (Saunders et al. 2009). In other words, it is a science of reviewing how a good research should be carried out (Flick 2015). The research methodology determines the type of problem to be investigated, testable hypothesis and appropriate method of data collection. Although there are different research methods, Saunders (2016) suggest that the preferred method should be one that align with the research aim and the relevant theories. The two common Research methods are: quantitative and qualitative research methods.

Quantitative research method is the method that uses numbers or any measurable item or object in a systematic way to enable investigation of a cause - effect relationships (Teo, 2013). This method usually answers questions that are within the measurable variables in order to clarify, predict and control a phenomenon (Leavy 2017). The four main types of quantitative research are: descriptive, correlational, causal-comparative and experimental.

From the foregoing definition and classification, and also based on the research questions of this study, it can be seen that the research method adopted is quantitative – experimental type.

3.3 The Research Process

The research process provides a platform for proper structuring of the research methodology. It is normally composed of research philosophy, research approaches, research strategies, time zone and data collection.

Research philosophy is defined by Saunders (2016) as a system of beliefs and assumptions with regards to the development of knowledge. These assumptions enable selection of both the research strategy and research approach. The research philosophy provides the patterns, different perspectives, and approaches that can be used for the acheivement of research aim, which have to be justified from the relevant literature. Some of the classses of reseach philosophy include: positivism, objectivsm, subjectivism, functionalism, realism, interpretivism and pragmatism etc.

The positivist phylosophy of research required that only factual data generated through logical observations and measurement can be used by the researcher rather than personal assumption or interest (Kothari, 2004).

Research approach provides a platform that enables selection of the most appropriate research design and strategies. It also describes method of data collection and analysis that concur with the research's aim and objectives (Collis and Hussey 2013). The two basic types of approach that can be adopted in a research are the deductive and Inductive research approaches. According to Collins (2010), deductive research approach is generally related with scientific systematic enquiries. It is an approach that explores existing theory and variables in order to test a hypothesis.

In this research, positivism philosophy and deductive approach were adopted. This is because the study applied experimental type of quantitative method that align with the research aim and objectives.

3.4 Research Strategy

Research strategy is an activity that needs to be undertaken to ensure availability of resources throughout the study and within the specified time frame. Ketchen and Bergh (2004) noted that, research strategy ensures the approach used to design the study is consistent with the aim and objectives of the study. Depending on the nature of the research, these strategies can be applied either independently or together. According to Saunders et al. (2016), the six common research strategies are: experiment, survey, case study, grounded theory, action research and time horizon.

Based on the research questions for this study, the research strategies adopted are experimental and cross-sectional time horizon strategies. The experimental research strategy was adopted in this study because of its suitability concerning the cause-and-effect relationships. Also, the cross-sectional time horizon was adopted because the study was carried out within the time bound deliverables specified by the PhD framework of Coventry University i.e. it has a defined start and completion date. According to Flick (2015), academic research prefers cross-sectional time horizon strategy because of their time bound nature.

3.5 Techniques and Procedures

The techniques and procedures used in collecting the data for this research are based on the specification of either BS EN or ASTM standard test method for the experiment that was carried out. The data generated from each experiment was considered as a primary data. Saunders et al. (2009) defined primary data as the original data collected by a researcher for the purpose of addressing the research question of a study. In other words, it involves original information that was not interpreted, summarized or analyzed from someone else work. However, the Life Cycle Inventories (LCI) data that was used in the Life Cycle Analysis (LCA) of this study was a secondary data compiled by Econvent.

3.6 Data Analysis

Because of the experimental nature of this research, the quantitative data obtained was presented descriptively in form of graphical charts. Also, images obtained from SEM were presented and analyzed descriptively.

3.7 Legal and Ethical Consideration

From the onset, the research passed through the Coventry University ethics approval process. Details of the experiments were provided, as well as the health and safety guidelines for the experimental works were outlined.

3.8 Chapter Summary

This chapter defined and highlighted the applications of the various research methods, designs and strategies, as well as data collection techniques. It also justified the adoption of the appropriate method that was suitable for this kind of research as inferred from the relevant literature. It can be seen in this chapter the argument that support adoption of experimental methodology – a type of quantitative method, due to the method's appropriateness to the research's objectives. A combination of primary and secondary data was used for the different component of the study. The primary data was obtained from the various experiments that were carried out, while the secondary data compiled by ecoInvent database was used for the LCI computation. It can also be seen that deductive research approach was followed, and positivist research philosophy was adopted in this study.

CHAPTER 4 EXPERIMENTAL PROCEDURES

4.0 Introduction

This chapter outlines the experimental procedures adopted for this research. The chapter provides detail characterization of the various materials used in the study. The focus material for this study is the flash calcined lateritic clay. It has been identified as the precursor that can potentially replace the scarce aluminosilicate materials currently used in the UK for the production of geopolymers. The chapter further provides the detail mix designs for the various mortars and concretes that were produced and characterized. Also, detail description of the samples' preparations have been given, as well as the standard tests that were carried out in the study.

4.1 Materials

The basic materials used for this study are:

I. High-strength Portland cement (CEM-I) for the controlled mortar and concrete mixes.
II. Aluminosilicate sources: Calcined clay and GGBS supplied by Banah UK and Hanson Cement UK, respectively (shown in Fig. 4.1).
III. Alkali metal sources: Reagent grades $Na_2SiO_3.5H_2O$ and NaOH purchased from Fisher Scientific UK, and` 54.5% and 37% Na_2SiO_3 solutions obtained from Inoxia UK, 45% K_2SiO_3 solution produced by Woellner GmbH.
IV. Fine and coarse aggregates supplied by local suppliers.
V. Tap water from the lab's main supply.
VI. High purity metakaolin calcined at 1000 and 1100 °C from Eastern Europe.

a.

Fig. 4.1a GGBS

b.

Fig. 4.1b calcined clay

4.1.1 Portland Cement

High strength EN 52.5 N Portland cement conforming to BS EN 197-1 was used for the control mortar and concrete mixes. The chemical composition of this CEM-I obtained from the XRF is given in Table 4.1. The mineralogical composition computed using Bogue's equation was 61.5 wt.% C3S, 13.8 wt.% C2S, 7.1 wt.% C3A and 8.2 wt.% C4AF.

4.1.2 Properties of the GGBS

The GGBS used for this study was supplied by Hanson Cement UK ltd. from their Teesside plant and is EN 15167-1 standard compliant with an amorphous content of more than 95%, volumetric mass density of the particles of 2.92 g/cm^{3,} and the d_{50} of 15 µm. The oxide compositions of the GGBS obtained from the XRF are presented in table 4.1.

Table 4 1: Major oxide compositions (wt. %) of the Portland cement, GGBS and Calcined clay

Oxide (% by weight)	SiO_2	Fe_2O_3	Al_2O_3	TiO_2	MgO	CaO	LOI
CEM I	21.0	2.7	4.4	-	1.6	64.7	3.2
GGBS	29.38	0.36	11.2	0.7	6.9	43.7	2.4
Calcined clay	35.18	25.4	29.6	2.9	1.3	0.9	< 2%

4.1.3 Properties of the Calcined Clay

The calcined clay used for this study was supplied by Banah UK ltd. The sourced clay was obtained from grinding the altered basalt (lithomarge) in Northern Ireland. It was processed from flash calcining the low purity kaolin clay (70.1% kaolin content) at 750 °C and residence time of less than 1s. The calcination results in the dehydroxylation and transformation of the goethite and magnetite phases of the precursor into hematite but maintained its layered structure (McIntosh *et al.*, 2015). The calcined clay (marketed as banahMETA) has a 31% reactive silica, specific surface (BET) of 75 m^{2}g, specific gravity of 2.89 and particle sizes which are 50% (d_{50}) and 90% (d_{90}) finer than 6 µm and 20 µm respectively. The oxide

composition of the calcined clay obtained from the XRF and the loss on ignition (LOI) are presented in table 4.1.

4.1.4 Alkali Metal Sources

Four forms of alkali metal sources were used in this research; namely: sodium hydroxide pellets, granular sodium metasilicate pentahydrate, high and low viscosity sodium silicate solutions, and a low viscosity potassium silicate solution, shown in Fig. 4.2. The sodium hydroxide (NaOH, SH) was a reagent grade in pearl form with 97% purity purchased from Fisher Scientific UK. Various concentrations between 4-12 molar (M) were prepared as a solution by dissolving the corresponding mass of pellets in a litre of water. For example, the 8M NaOH solution was prepared by dissolving 8 x 40 = 320 grams of NaOH solid in 1 litre of distilled water where 8 and 40 are the molar and molecular mass of NaOH respectively.

The sodium metasilicate pentahydrate ($Na_2SiO_3.5H_2O$, SSP) was a reagent grade in salt form purchased from Fisher Scientific UK which had a SiO_2 to Na_2O molar ratio (MR) of 1.0. The solution was prepared such that the quantity of Na_2SiO_3 in the solution was 44.1%. The two alkaline solutions were prepared 24 hrs prior to the mixing to ensure complete dissolution and cooled before used in the experimental works.

1. 

54.5% Na_2SiO_3 solution

2. 

NaOH flakes

3. 

$Na_2SiO_3.5H_2$

4. 

37% Na_2SiO_3 solution

5. 

45% K_2SiO_3 solution

Fig. 4.2 Activators used in the study

The third source of alkali metal used in this study were the commercially available sodium silicate solutions produced by Inoxia UK ltd. The high and low viscosity sodium silicate solutions have a 54.5% and 37% solid component, as well as an MR of 2.05 and 3, respectively. These alkali metal sources were produced hydrothermally in a pressure reactor vessel.

The fourth source of alkali metal used in this study was the potassium silicate solution produced by Woellner GmbH. This activator marketed as the Geosil had a 45% solid component and an MR of 1.7. It is also produced hydrothermally in a pressure reactor vessel.

4.1.5 Fine and Coarse Aggregate

The sharp sand that is finer than a 4.5 mm sieve size and larger than 75 µm was used as the fine aggregate component of the mortar and concrete mixes. An uncrushed aggregate with a maximum size of 10 mm was used for the concrete mixes. The coarse aggregate had a specific gravity of 2.65, crushing value of 23.5%, and water absorption of 0.6 respectively. The grading curve of the coarse aggregate is presented in Fig. 4.3. The aggregates were obtained from local suppliers in Coventry.

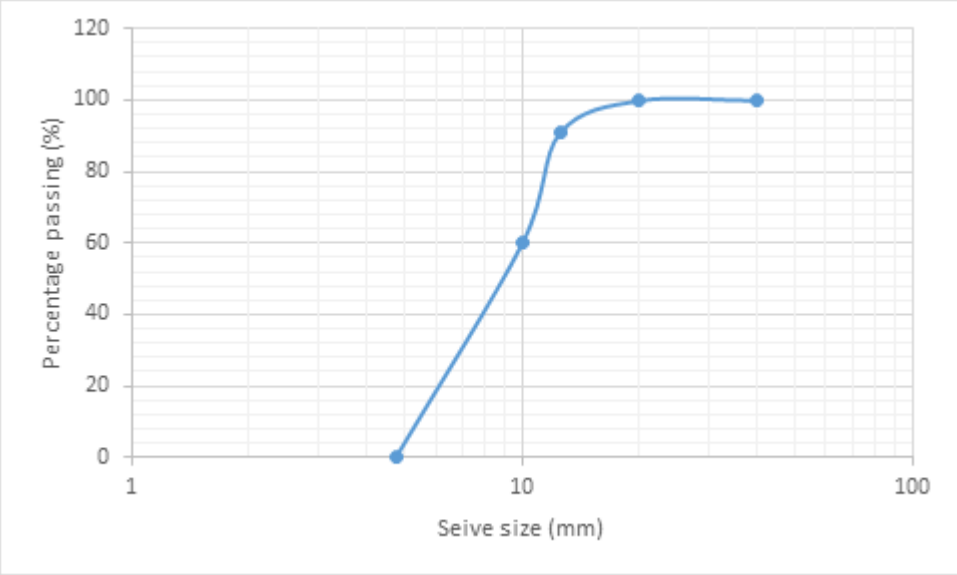

Fig. 4.3 Particle size distribution curve of the coarse aggregate

4.2 Mix Design

The control mortar was designed based on aggregate to binder ratio of 3. The GGBS alkali activator and some of the calcined clay geopolymer mortars were designed based on the water demand of the precursors. Other groups of calcined clay geopolymer mortars were designed based on the molar oxide compositional ratios prescribed in the scientific literature. Table 4.2 defined the codes used for the various mortar mixes.

Table 4 2: Definitions of mortar mixes codes

Code	Meaning
GGBS–32SH	32% sodium hydroxide solution activated GGBS mortar
GGBS– 44.1SSP	44.1% sodium metasilicate pentahydrate solution activated GGBS mortar
CC–32SH	32% sodium hydroxide solution activated CC mortar
CC–44.1SSP	44.1% sodium metasilicate pentahydrate solution activated CC mortar
SSP:CC =0.7	Mortar mix based on sodium metasilicate pentahydrate solution to CC ratio of 0.7
SS:CC = 0.7	Mortar mix based on sodium silicate solution to CC ration of 0.7

SH:CC = 0.7	mix based on sodium hydroxide solution to CC ratio of 0.7
CC-54.5SS	54.5% sodium silicate solution activated CC geopolymer mortar mixes
GGBS–SH (35%)	Mortar mixes based on 32% sodium hydroxide solution to GGBS ratio of 0.35
CC-37SS	37% sodium silicate solution blended with 32% sodium hydroxide solution activated CC geopolymer mortar mixes
CC-45KS	45% potassium silicate solution activated CC geopolymer mortar mixes

The control concrete mix was designed based on the Building Research Establishment (BRE) guidelines. One of the four geopolymer concrete mixes was designed based on Rangan guidelines, while the other three mixes were modified by increasing the binder content.

4.2.1 Control Mortar and Concrete Based on Portland Cement

The control reference mortar was designed based on an aggregate to binder ratio of 3, and water to cement ratio of 0.45. Accordingly, the control concrete mix was designed according to the BRE method for normal concrete mixes with a targeted mean compressive strength of 35 MPa at 28 days, slump of 80 mm, 10 mm maximum size for uncrushed coarse aggregate, and 35% passing sieve 600 µm fine aggregate. The control mixture composition is given in table 4.3.

Table 4 3 Control mortar and concrete mixes (kg/m^3)

Control mixes	52.5 CEM I (kg/m^3)	Sand (kg/m^3)	Coarse aggregate (kg/m^3)	Water (kg/m^3)
Mortar	455	1365	-	205
Concrete	404	921	725	221

4.2.2 Calcined Clay Geopolymer and GGBS Alkali Activated Mortars

Seven groups of mortar mixes were designed using different precursors, different alkali metal sources, variable alkali solution to precursor ratios, variable aggregate proportions, *etc.* in order to assess the strength performance of the developed mortars and determine the mix variables

that gave peak strength. The mass ratios of group 1, 2, 3 and 5 mixes were designed based on the water demand of the precursors. According to Messina *et al.* (2017), the solution of precursors (S/P) mass ratio of metakaolin based geopolymers is generally close to 1 due to its water demand. This formed the basis of using L:B ratios of between 0.7 and 1 in the group 2 mixes. Furthermore, group 4, 6 and 7 mixes were designed to satisfy the prescribed molar oxide ratios for geopolymers. The description of the details of the six groups of the mortar mixes is given in table 4.4, while their various mixture proportions are presented in table 4.5.

Table 4 4 Description of the seven groups of mortar mixes

Group	Sample Label	Activator	Mix variable	Sand: precursor
1	GGBS – 32SH	NaOH solution made up of 32% solid	Ratio of NaOH solution to GGBS varies from 0.3 to 0.5	Sand to GGBS ratio is 2
	GGBS – 44.1SSP	$Na_2SiO_3.5H_2O$ solution consisting of 44.1% solid	Ratio of 44.1% $Na_2SiO_3.5H_2O$ solution to GGBS varies from 0.3 to 0.5	Sand to GGBS ratio is 2
2	CC – 32SH	NaOH solution made up of 32% solid	NaOH solution proportion varies from 0.8 to 1.0	Sand to CC ratio is 1
	CC – 44.1SSP	$Na_2SiO_3.5H_2O$ solution consisting of 44.1% solid	44.1% $Na_2SiO_3.5H_2O$ varies between 0.8 and 1.0	Sand to CC ratio is 1
3	SSP:CC =0.7 (ratio of mass of $Na_2SiO_3.5H_2O$ solution to calcined clay)	$Na_2SiO_3.5H_2O$ solution consisting of 54.5% solid		
	SS:CC = 0.7 (ratio of mass of 54.5% Na_2SiO	Na_2SiO_3 solution consisting of 54.5% solid		Sand to calcined clay ratio is 1

	solution to calcined clay)		Chemical activator type and mixture ratio	
	SH:CC = 0.7 (mass ratio of NaOH solution to calcined clay)	NaOH solution made up of 32% solid blended with 54.5% Na_2SiO_3 solution in a ratio of 2.5		
4	CC - 54.5SS	Na_2SiO_3 solution consisting of 54.5% solid	Ratio of mass of calcined clay to Na_2SiO_3 solution varies from 0.5 to 1.5	Sand to calcined clay ratio is 3
5	GGBS – SH (35%)	NaOH solution	Varied molarities from 4 – 12 M	Sand to GGBS ratio is 2
6	CC-37SS	Na_2SiO_3 solution consisting of 37% solid	SS:SH = 2.5	Sand to calcined clay ratio is 3
7	CC-45KS	K_2SiO_3 solution consisting of 45% solid	KS:CC = 1.25	Sand to calcined clay ratio is 3

Table 4 5 Mortar mixes (kg/m^3)

Group 1	**Sand**	**GGBS – 32SH**			**GGBS – 44.1SSP**		
L:B		GGBS	32% NaOH	Free water	GGBS	44.1% $Na_2SiO_3.5H_2O$	Free water
0.3	1227	614	185	0	614	185	0
0.35	1209	604	212	0	604	212	0
0.4	1191	596	238	0	596	238	0
0.45	1174	587	264	0	587	264	0

0.5	1157	579	289	0	579	289	0

Group 2	**Sand**	**CC – 32SH**			**CC – 44.1SSP**		
L:B		CC	32% NaOH	Free water	CC	44.1% $Na_2SiO_3.5H_2O$	Free water
0.8	723	723	579	0	723	579	0
0.85	711	711	604	0	711	604	0
0.9	698	698	628	0	698	628	0
0.95	686	686	652	0	686	652	0
1	675	675	675	0	675	675	0

Group 3	**Sand**	**CC**	**32% NaOH**	**54.5% Na_2SiO_3**	**54.5% $Na_2SiO_3.5H_2O$**	**Free water**
SSP:CC =0.7	1482	484	0	0	344	64
SS:CC = 0.7	1482	484	0	344	0	64
SH:CC= 0.7	1482	484	246	98	0	64

Group 4	**Sand**	**Calcined clay**	**54.5% Na_2SiO_3**	**Free water**
0.5	1221	396	198	84
0.75	1221	339	255	84
1	1221	297	297	84
1.25	1221	264	330	84

1.5	1221	238	356	84
Group 5	**Sand**	**GGBS**	**NaOH (32%)**	**Free water**
4 M (SH 16%)	1209	604	212	0
6 M (SH 24%)	1209	604	212	0
8 M (SH 32%)	1209	604	212	0
10 M (SH 40%)	1209	604	212	0
12 M (SH 48%)	1209	604	212	0

Group 6	**Sand**	**CC**	**37% Na_2SiO_3**	**NaOH (32%)**	**Free water**
SS:SH = 2.5	1301	352	251	101	19

Group 7	**Sand**	**Calcined clay**	**45% K_2SiO_3**	**Free water**
KS:CC = 1.25	1308	310	388	19

4.2.3 Calcined Clay Geopolymer Concrete

Four distinct geopolymer concrete mixes were designed and tested using different types of activators. Mix 1 was labelled GC/Na-R and designed according to the guidelines specified by (Rangan, 2008). The Rangan guidelines focus on workability and compressive strength performance of the designed concrete based on water to geopolymer solid ratio, which had similar effect with water to cement ratio of Portland cement concrete. The Rangan guidelines also considered the influence of aggregates in the geopolymer concrete mixes to be similar to that of Portland concrete. This method specifies the mass of total aggregates to be between 75 and 80% of the mass of the concrete, and that the fine and coarse aggregate proportions should be determined from the grading curves used in the design of normal concrete mixes.

The other three concrete mixes were modifications of the first mix: by decreasing the proportion of the aggregates in the mixes to 70% while maintaining a constant water to solid

ratio of 0.48. The 70% aggregate content was used by Kwasny *et al.* (2016) in geopolymer concrete formulation as the optimized composition for rotary calcined lateritic clay. Moreover, all the mixes were designed to give a Si:Al, H_2O:Na_2O and Na:Al ratios that fall within the recommended compositional ranges (compiled in table 2.1) for geopolymer concrete, which were similar to the ones obtained for the peak-strength calcined clay geopolymer mortar mix. The details of the concrete mixes are given in table 4.6, while their computed molar oxide ratios are presented in table 4.7

Table 4 6 Concrete mixes (Kg/m^3)

Mixes	GC/Na-R	GC/Na-RM	GC/Na-M-RM	GC/K-RM
CC	276	315	315	311
54.5% Na_2SiO_3	276	315	-	-
37% Na_2SiO3	-	-	225	-
45% K_2SiO3	-	-	-	390
32% NaOH	-	-	90	-
FA	554	756	756	756
CA	1294	924	924	924
Free water	80	91	2	20

Code: GC = Geopolymer concrete; /Na= 54.5% sodium silicate solution; /Na-M = 37% sodium silicate solution blended with 32% sodium hydroxide solution; /K = 45% potassium silicate solution; -R = designed based on Rangan specification *i.e.* aggregate to binder ratio of 4.33; -RM = modified designed based on aggregate to binder ratio of 3.46.

Table 4 7 Molar oxide ratios of the concrete

Mix	Na_2O/Al_2O_3	SiO_2/Al_2O_3	Na_2O/SiO_2	H_2O/Na_2O
GC / Na - R	1	4.11	0.24	14.2
GC / Na - RM	1	4.11	0.24	14.2
GC/Na-M-RM	0.9	3.2	0.28	14.6
Mix	**$(Na_2O + K_2O)/Al_2O_3$**	**SiO_2/Al_2O_3**	**$(Na_2O + K_2O)/SiO_2$**	**$H_2O/(Na_2O + K_2O)$**
GC / K - RM	0.8	4.1	0.2	18.6

The details of the designed GC/Na–R based on Rangan guidelines is as follows:

Density of the concrete = 2400 kg/m^3 (4.1)

Combined mass of aggregates = 77% of the concrete mass = 0.77 × 2400 = 1848 kg/m^3 (4.2)

Proportion of fine aggregate = 30% of the combined mass of aggregate (4.3)

Fine Aggregate content = 0.3 × 1848 = 554.4 kg/m^3 (4.4)

Coarse Aggregate content = 1848 – 554.4 = 1293.6 kg/m^3 (4.5)

Mass of calcined clay and alkaline solution = Density of concrete – combined mass of aggregate = 2400 – 1848 = 552 kg/m^3 (4.6)

Mass ratio of Na_2SiO_3 solution: $Calcined\ Clay$ = 1 (mortar mix optimization) (4.7)

From steps (4.6) and (4.7):

Mass of Calcined clay = Mass of Na_2SiO_3 solution = 0.5 × 552 = 276 kg/m$^{3.}$ (4.8)

Free water was incorporated into the mix in order to achieve the desired H_2O:Na_2O ratio while maintaining a water to solid ratio of 0.48 that was the value obtained for the peak strength mortar. In comparison, Rangan (2008) used a lower water to solid ratio because of the low surface area of their precursor – PFA, which required less water to wet its surface relative to the calcined clay. The resulting designed mixing quantities for the GC/Na-R mix are presented in table 4.8.

Table 4 8 Calcined clay geopolymer concrete mix based on Rangan method (GC/Na–R)

Quantities (kg)	Calcined clay	Na_2SiO_3 solution	Fine Agg.	Coarse Agg.	Free water
1 m^3	276	276	554	1294	80

The details for the molar oxide ratios computed for the GC-Na/R mix are as follows:

The Na_2SiO_3 solution is made up of 54.5% solid and 45.5% water.

Mass of Na_2SiO_3 solid = 0.545 × 276 = 150.42 kg/m^3;

Mass of Na_2SiO_3 water = 0.455 × 276 = 125.6 kg/m^3

Water: Geopolymer solid ratio = (125.6 +80) / (276 + 150.42) = 0.48

To determine the molar oxide ratios of this GC/Na–R mix based on stoichiometry, the oxide composition of the sodium silicate solution and calcined clay presented in tables 4.9 and 4.10 respectively were used.

Table 4 9 Oxide composition of the Na_2SiO_3 solution

Na_2SiO_3 solution (kg)	SiO_2 (%)	Na_2O (%)	H_2O (%)
276	36.63	17.87	45.5

Table 4 10 Oxide composition of the calcined clay

Calcined clay (kg/m^3)	SiO_2 (%)	Na_2O (%)	Al_2O_3 (%)	Fe_2O_3 (%)	Others
276	35.18	0.13	29.6	25.4	9.69

Also, the molecular mass of the various oxides obtained from the periodic table presented in table 4.11 were used for the computation of the respective molar oxide ratios of the mix.

Table 4 11 Oxides molecular mass

Oxide	SiO_2	Na_2O	Al_2O_3	Fe_2O_3	H_2O
Mass (g/mol)	60.07	61.97	101.93	159.66	18.01

The total molar oxides for this GC/Na–R mix computed based on stoichiometry are presented in table 4.12, while their ratios are presented in table 4.13.

Table 4 12 Total molar oxides for the GC/Na–R mix (mol/m3)

Oxide	Calcined clay	Na_2SiO_3 solution	Free water	**Total**
SiO_2	161.6	168.3	0	329.9
Na_2O	0.58	79.6	0	80.2
Al_2O_3	80.2	0	0	80.2
Fe_2O_3	43.9	0	0	43.9
H_2O	0	697.3	444.2	1141.5

Table 4 13 Calculated molar oxide ratios for the GC/Na–R mix

SiO_2:Al_2O_3	Na_2O:Al_2O_3	Na_2O:SiO_2	H_2O:Na_2O	Fe_2O_3:Al_2O_3
4.11	1	0.24	14.2	0.55

4.2.4 Semi-Dry Mixes for the Calcined Clay Pastes

(Karami, 2008; Mahieux, Aubert and Escadeillas, 2009; Bai Kamara, Ganjian and Khorami, 2019) have optimized semi-dry mixtures that can be used as a Hydraulic Road Binder (HRB) based on ternary mixture composition of GGBS, basic oxide slag (BOS), by-pass dust (BPD), run-off-station ash (ROSA), plasterboard gypsum (PG), *etc.*

In this work, the iron-rich flash-calcined clay and high-purity white metakaolin clays (flash calcined at 1000℃ (MK1000) and 1100℃ (MK1100) respectively) from Eastern Europe were studied for controlled low strength applications. The oxide compositions of the BOS, BPD, MK1000 and MK1100 obtained from the XRF are presented in table 4.14.

Table 4 14 Oxides composition of the pozzolans used for the semi-dry mixtures

Oxide (% by weight)	SiO_2	Fe_2O_3	Al_2O_3	TiO_2	MgO	CaO	SO_3	K_2O
BOS	11.43	28.24	1.6	0.39	8.27	41.29	0.44	0.02
BPD	12.79	1.88	3.47	0.19	0.82	44.03	12.22	10.06
WMK	47.19	0.77	35.06	1.29	0.06	0.2	0.19	0.12

The conversion of pig-iron to raw steel in a basic oxygen furnace produced basic oxygen slag (BOS). For every one ton of crude steel produced about 100-150 kg of slag was generated as a waste material (Reddy, Pradhan and Chandra, 2006). The BOS used in this research was obtained from Corus at Scunthorpe works and was ground before being used in the mixtures. The grinding of the BOS was done using a laboratory ball mill and sieved through a 600 µm sieve.

The BPD was generated as a solid waste during the production of the cement clinker using the dry process. This resulted from the precipitation of some volatile constituents in the kiln feed that were not recycled back. The BPD was generated from the kiln when the temperature was about 1000℃. The BPD used in this research was obtained from Castle Cement, Clitheroe, Lancashire.

The WMK was made up of over 90% pure kaolinite obtained from Eastern Europe, with the remainder being quartz and a trace of anatase (TiO_2). The WMK was flash calcined at 1000 °C and 1100 °C respectively in a gas suspension calciner for a residence time of less than 1s. The fineness is a sieve residue of around 25% on 45µm, achieved during pre-processing in a pilot-scale drier crusher.

The mixture composition for the controlled low-strength application of the calcined clay was carried-out based on the optimized ternary mixes undertaken by other researchers reported in the scientific literature (Karami, 2008; Bai Kamara, Ganjian and Khorami, 2019). These previous works produced an HRB10 (a standardized mortar that has compressive strength more than 10 MPa) after 28 days. Mahieux, Aubert and Escadeillas (2009) optimized that the ternary binder was made up of GGBS (52.5%), BOS (42.5%), and a catalyst (5%). Karami (2008) optimized ternary binder composition (ROSA (45%), BOS (50%) and BPD (5%)) had a compressive strength of 11.1 MPa at 28 days. Bai Kamara, Ganjian and Khorami (2019) reported an optimum ternary mix (GGBS (80%), BPD (10%) and PG (10%)) that had a compressive strength of 22 MPa at 28 days. These optimized ternary mixes were based on a water to binder ratio of 0.15.

In this work, a constant water to binder ratio and BOS and BPD proportions were used for the ternary mixes. The main pozzolan was varied in the mixes, but the proportion was constant. The semi-dry ternary mixtures are presented in table 4.15.

Table 4 15 Semi-dry ternary mixtures

SYSTEMS	Main Pozzolan	BOS	BPD	Water
GGBS/BOS/BPD	40%	50%	10%	15%
CC/BOS/BPD	40%	50%	10%	15%
MK1100/BOS/BPD	40%	50%	10%	15%
MK1000/BOS/BPD	40%	50%	10%	15%

4.3 Sample Preparations

The various pastes, mortars, and concrete samples were produced based on designed quantities, according to the mixing sequence discussed in the next section.

4.3.1 Portland Cement Control Mortar and Concrete Mixing, Moulding, and Curing

The mixing of the control mortar mix was carried out using a five-litre Hobart mixer based on the procedure specified by British Standards Institution. (2005). The fresh control mortar was

poured into the 50 x 50 mm plastic moulds in two layers and compacted using a vibrating table. The surface of the cube was flattened and then allowed to harden at room temperature for 24 hrs. The cubes were then demoulded and placed in a curing tank at 20 ±1°C until the testing age of 7 and 28 days.

The control concrete was mixed in a horizontal concrete mixer. The aggregates and Portland cement were first mixed for a few minutes, then water was added and mixed for a further few minutes until homogeneity was achieved. Upon completion of the slump and rheology tests, the fresh concrete was poured into the 100 x 100 mm plastic moulds in 3 layers and compacted using the vibrating table. The surfaces of the cubes were flattened and allowed to harden at room temperature for 24 hrs. The cubes were then demoulded and placed in the curing tank until the testing age of 7 and 28 days.

4.3.2 Calcined Clay Geopolymer Mortar and Concrete Mixing, Moulding and Curing

The preparation of the various calcined clay geopolymer mortar mixes was carried out using a five-litre Hobart mixer. The binder was prepared and shear mixed for about five minutes to ensure that the solution had penetrated all the layered sheets of the calcined clay for an effective reaction. The quartz sand was then added until a homogenous mix was achieved. The mixes were then placed in the 50 mm x 50 mm plastic cubes moulds and compacted uniformly using the vibrating table. The samples were then demoulded after 24 hrs and cured in the air or sealed conditions as required for the various mixes. The sealed cured specimens were wrapped in cling film and stored in an air-tight plastic box with some water at the bottom in the conditioning room until testing. The temperature and relative humidity were maintained at 20 °C and >95% respectively. Two of these mixes are shown in Fig. 4.4. The sealed curing prevented the samples from atmospheric carbonation, as well as avoided lost or gain of moisture.

Fig. 4.4 (a) CC-SSP90 mortar mix

Fig. 4.4 (b) CC-SH90 mortar mix

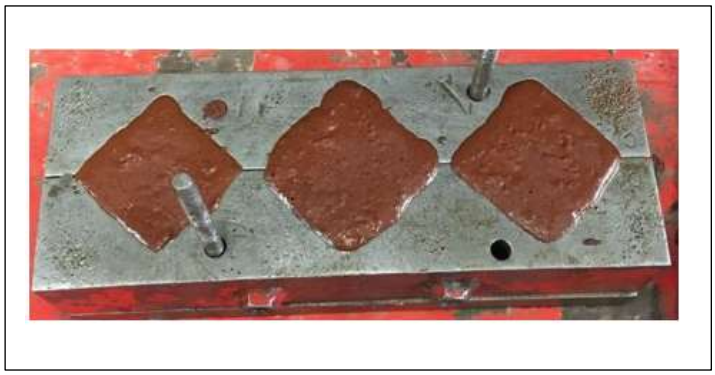

Figure 4.4 (C) CC – 54.5SS mortar cubes

The geopolymer concrete samples were prepared by mixing the calcined clay, extra water and the silicate solution in a horizontal concrete mixer until a homogenous mix was achieved. The fine aggregate was then added into the mix. The uncrushed aggregate was subsequently added into the mix until it was fully coated by the mortar as shown in Fig. 4.5. This mixing sequence had proven to limit the occurrence of atmospheric carbonation on the hardened samples significantly by visual appearance (free from white crystals that are formed by the reaction of sodium oxide in the system and carbon dioxide in the atmosphere). The resultant concrete was then poured into moulds and compacted on a vibrating table. The moulds were then covered with plastic sheets under laboratory conditions for 24 hours. Subsequently, the samples were demoulded and then sealed-cured until the testing age of 7 and 28 days. The sealed curing was done by wrapping the samples with cling film and placed in an air-tight plastic box in the conditioning room with a controlled temperature of 20 ± 1 ^{o}C and relative humidity of 85%.

Fig. 4.5a GC/Na- R mix

Fig. 4.5b GC/Na- R cubes

4.3.3 Semi-Dry Pastes Mixing, moulding and curing

The mixing procedure for the semi-dry pastes mixes was as follows:

1- Dry mixing of the materials for 1 minute at level 1 speed.
2- Addition of half of the mixing water during the first 30 seconds of mixing at level 1 speed.
3- Continuation of mixing for 30s with level 2 speed.
4- Scraping off the pastes at the sides of the mixing bowl and blades.

5- Addition of the remaining water and continuation of mixing for two minutes at level 3 speed.

The resulting pastes were placed in the 50 mm cube moulds in three layers. Each layer was compacted by 25 blows using the square tamping rod (25 mm x 25 mm x 300 mm). The samples were further compacted using the JJ100 hydraulic press. The hydraulic pressure was set at 90 KN for a gang of three sets of 50 mm cube moulds. The 90 KN pressure was used to reflect field applications, whereby a vibrating or pneumatic-tyre roller with an axle load of no less than 30 KN followed by at least eight passes was used for compacting hydraulically bound mixtures. The specimens were air-cured at room temperature for 12 hours and sealed-cured afterwards. Fig. 4.6 shows the compaction and sealed curing of the semi-dried samples.

Fig. 4.6 Compaction and sealed curing of semi-dried samples

4.4 Tests

4.4.1 X-ray Fluorescence Test

The XRF analysis was conducted to determine the chemical composition of the calcined clay, WMK, BPD, BOS and 52.5 CEM 1 samples. A wavelength dispersive X-ray fluorescence spectrometer (Bruker AXS S4 explorer) was used for the oxide composition test. It measures elements within the range of ^{11}Na to ^{92}U in the atomic number order. The spectrometer operates based on the principle that, when high energy X-rays are emitted against an atom, they become

unstable thereby ejecting an electron from its inner orbit. The electrons that lie in the outer orbits and possess a higher energy fall into the inner orbit and fill the space created by the removed electron. Energy is released as a secondary X-ray due to the migration of the electron between the two orbits. The energy is quantitatively equivalent to the energy difference of the two involved orbits, while the secondary X-ray is characteristic of the element. XRF analyser is capable of doing both the qualitative and quantitative composition analysis by recording the characteristic wavelengths and intensities of secondary X-ray radiations from a sample.

4.4.2 Strength Activity Index Test

The pozzolanic activity of the calcined clay, WMK, and GGBS were determined using the strength activity index test (SAI). This test compared the compressive strength of the pozzolans replaced Portland cement mortar mixes relative to the control mortar. Details of these mixes are presented in table 4.16. All the samples were cured in a water bath and tested under surface saturated dry conditions for 7, 28, and 56 days. The SAI result is reported as:

$$SAI = A/B * 100$$

Where: A = unconfined compressive strength of the pozzolans replaced mortar specimen (MPa) at 7, 28, and 56 days
B = unconfined compressive strength of the control mortar (MPa) at the corresponding age.

Table 4 16 Details of Strength Activity Index (SAI) test for the mortar mixes

Mortar mixes	Fine aggregate: binder	Water: binder[1]	OPC	Pozzolan	sand as cement replacement
Control	3	0.6	100%	0%	0%
CC	3	0.6	80%	20%	0%
GGBS	3	0.6	80%	20%	0%
MK1000	3	0.6	80%	20%	0%
Mk1100	3	0.6	80%	20%	0%

Filler	3	0.6	80%	0%	20%

[1]Binder (consists of Portland cement and pozzolan)

4.4.3 Slump Test

The slump tests for the four geopolymer and control concrete mixes were carried out in accordance with British Standards Institution (2000) specifications for determining the consistency of the fresh concrete mixes. Fig. 4.7 shows the slump measurements for the calcined clay fresh geopolymer concrete. Also, a slump test was undertaken for the peak strength geopolymer mortar using a mould of 90 mm in height, 66 mm internal diameter of the bottom end and 38 mm internal diameter of the top end. The mould was then placed in the centre of the flow table and filled with the mortar in three layers. Each layer was compacted with 10 strokes and the surface was flattened. The mould was then removed and the drop in vertical height was measured.

Fig. 4.7 Slump measurement for the geopolymer concrete mixes

4.4.4 Stress Growth Test

This test was carried out to determine the peak torque and static yield stress of fresh concrete using an ICAR rate controlled concrete rheometer based on the specifications of the manufacturer. The peak torque indicates the energy required to shear mix and pump fresh concrete, while the static yield stress is the stress required to initiate the flow of the concrete. Large values of these parameters indicate a stiff concrete, while low values indicate a self-compacting concrete. For the SGT, 0.024 m^3 of fresh control and the four geopolymer concrete mixes were placed in the ICAR concrete rheometer to determine the static yield stress. The rotational speed of the vane was set at 0.025 rp/s and was applied to the concrete materials for

at least 40 seconds. The peak torque and static yield stress of the geopolymer concrete were computed using equation 4.9.

$$\tau_o = \frac{2T}{\pi D^3 (\frac{H}{D}+\frac{1}{3})} \quad (4.9)$$

Where: τ_o = yield stress
T = maximum torque
H and D = height and diameter of the vane

4.4.5 Flow Curve Test

This test was carried out to determine the relationship between the shear stress and shear rate using the ICAR rate controlled concrete rheometer based on the manufacturer's specifications by obtaining the dynamic yield stress and plastic viscosity of the fresh control and four geopolymer concrete mixes. The test commenced from a pre-shear period followed by a set of flow curve points to reduce the effect of thixotropy and provide a consistent shear history. During the pre-shear period, the vane maintained a constant high speed equal to the maximum test speed without recording any measurement. The flow curve then followed the pre-shear period with the speed of the vane in descending order by following the number of points. The test was calibrated such that the breakdown time was 20 seconds, with an initial speed of 0.5 rp/s, a final rotational speed of 0.05 rp/s, and the numbers of points set as 7 points. The speed points were divided between the initial and final speed points. The value of dynamic yield stress and plastic viscosity for the fresh concrete that is considered to be within the annulus flow was then computed using the Bingham equation expressed in equation 4.10 and Reiner-Riwlin equation expressed in equation 4.11.

$$T = \tau_o + \mu N \quad (4.10)$$

Where: τ = shear stress
τ_o = yield stress
μ = plastic viscosity
N = shear rate

$$\Omega = \frac{T}{4\pi h\mu}\left(\frac{1}{R_1^2} - \frac{1}{R_2^2}\right) - \frac{\tau_o}{\mu}\ln\left(\frac{R_2}{R_1}\right) \quad (4.11)$$

Where: Ω = rotation speed (rad/s)
T = torque (Nm)
h = vane height (m)
R_1 = vane radius
R_2 = outer container radius

Fig. 4.8 presents the rheology test set-up using the ICAR rheometer.

Fig. 4.8 Rheology test for the calcined clay geopolymer concrete

4.4.6 Viscometer Test

The workability of geopolymers is best characterized by determining their rheological parameters against the predominantly used single-point tests (Laskar and Bhattacharjee, 2011). Consequently, the rheological properties (shear stress and plastic viscosity) of the geopolymer grout that has similar molar oxide ratios with that of the peak strength mortar were measured using the Rheology International Series 2 Viscometer Model RI:2:M. These parameters define the character of flow of the grouts such that high values indicate its resistance to flow, which may results in weak adhesion forces when used as a binder in a mortar or concrete matrix The rheometer was operated by rotating its spindle in the fresh grout, which measured the torque that overcame the viscous resistance of the movement as shown in Fig. 4.9. The four-bladed vane spindle had four rectangular blades of radius Rv = 9.5 mm, and height h = 38 mm and was placed in a container of radius 27.5 mm mounted in the middle of the lower plate. The shear stress, Ƭ, was computed from the measured torque based on equation 4.12 specified by Banfill and Kitching (1990).

$$\tau = 3T/(2\mu\ (Rv3+3\ Rv3h)) \qquad (4.12)$$

Where: T = torque

Fig. 4.9 Rheology test for the geopolymer grout

4.4.7 Setting Time Test

The initial and final setting times of the geopolymer pastes for different water to solid ratio were determined based on the procedure specified by ASTM International (2019). The set up for this experiment is presented in Fig. 4.10. At regular time intervals, the penetration of the standard 1 mm needle on the sample was measured, until a penetration of 25 mm was achieved. The elapsed time between the initial mixing of the paste and the penetration of 25 mm was computed as the initial setting time of the mix. The pastes's final setting time was calculated as the elapsed time between the initial mixing of the paste and the first measured penetration that did not mark the specimen surface with the needle's circular impression.

Fig. 4.10 Setting time test for the calcined clay geopolymer grout

4.4.8 Density Test

The density of three replicate geopolymer mortar and concrete cubes were determined at 7 and 28 days for the investigated mixes using a specific gravity balance based on Archimedes' principle. For each mix and testing age, the mean density was computed and reported. The set up for the density experiment is shown in Fig. 4.11.

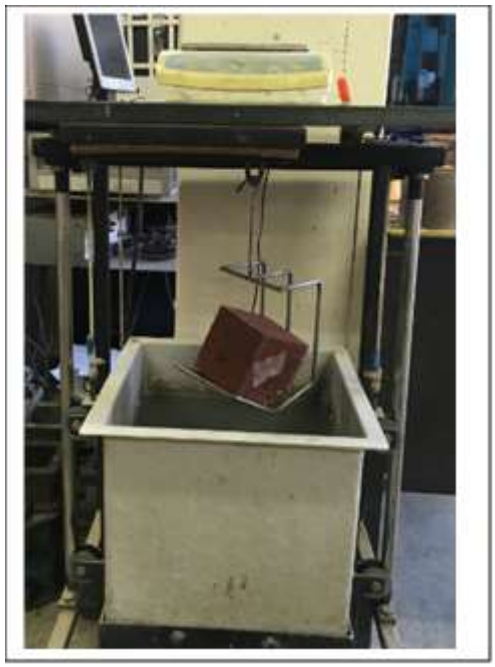

Fig. 4.11 Density test for GPC/Na-R concrete sample

4.4.9 Ultrasonic Pulse Velocity Test

At 7 and 28 days, a UPV test was carried out on the mortar cubes which provided an insight into the dense structure of the various mortar and concrete samples. A large UPV value indicates a dense sample with few pores, while a low value indicates otherwise. The UPV test was carried out by measuring the time required for a pulse to pass through parallel sides of the mortar (approximately 50 mm) and concrete cube (100 mm) samples using the UPV measurement device by Control. and the two ultrasonic transducers set to a frequency of 1 kHz as shown in Fig. 4.12. The velocity is then computed using equation 4.13.

$$Velocity\ (km/s) = Distance\ travelled\ by\ the\ pulse\ time \quad (4.13)$$

Fig. 4.12 UPV test for GPC/Na-R concrete

4.4.10 Compressive Strength Test

The compressive strength for the three replicates surface-saturated 50 mm x 50 mm GGBS alkali-activated mortar cubes samples, for each of the GGBS and calcined clay based mixes, was determined at 7 and 28 days according to the procedure specified by British standard institution (2019). A JJ Lloyd testing machine, with a loading rate set at 1KN/s to accommodate the low strength of many of the samples, was used as shown in Fig. 4.13a.

On the other hand, the compressive strength test for the saturated dry surface 100 x 100 mm control and the four calcined clay geopolymer concrete samples was carried out in accordance with British standard institution (2019) using Avery Denison 2000 compressive strength testing machine and the loading rate set at 0.6 MPa/s as shown in Fig. 4.13b.

(a) 

(b) 

Figs. 4.13 (a) compression test using JJ Lloyd LS100 & (b) Compression test using Avery 2000

4.4.11 Split tensile test

A split tensile strength test for the four geopolymer concrete mixes was performed as specified by the ASTM C496 (ASTM International, 2004). The sealed cured cylindrical samples were loaded at a rate of 0.6 MPa in a surface saturated dry condition. The set-up for the experiment is presented Fig. 4.14a, while the split concrete sample is shown in Fig. 4.14b.

(a) 

(b) 

Figs. 4.14 (a) Split tensile set-up (b) Split GC/Na-R cylindrical concrete

As can be seen, the load was applied normal to the length rather than to the cross-section as is done for the unconfined compressive strength. The tensile strength was then obtained using equation 4.14.

$$T = \frac{2P}{\pi LD} \tag{4.14}$$

where T is the tensile strength; P is the applied load at failure; D and L are the concrete cylinder diameter and length respectively.

4.4.12 Freeze-thaw Resistance Test

The freeze-thaw resistance test for the geopolymer and control concrete mixes was performed by measuring the mass and strength loss of the 56 days cured concrete cube sample. The program was run up to 300 cycles using the environmental chamber shown in Fig. 4.15.

Fig. 4.15 Environmental chamber for freeze-thaw resistance test

Each cycle took about 5 hours (285 minutes). The concrete samples were subjected to 300 cycles of freezing (at –17.8 ^{o}C) and thawing (at 4.4 ^{o}C). Fig. 4.16 shows the temperature changing during freeze-thaw cycles.

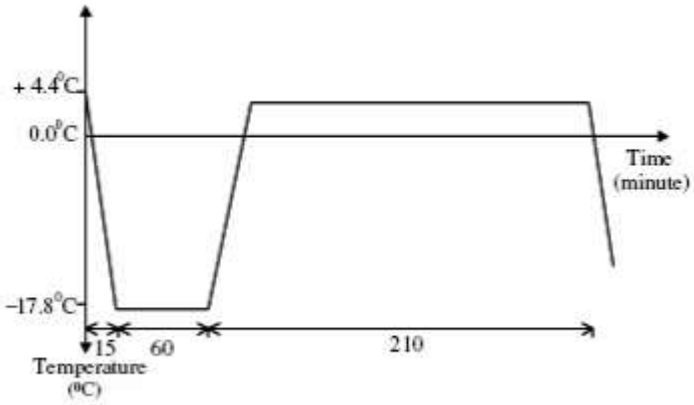

Fig. 4.16 Temperature variation in freeze-thaw cycle

4.4.13 Chloride Permeability Test

A rapid chloride permeability test (RCPT), in accordance with ASTM International (2018), was used to determine the electrical conductance of the concrete mixes to provide a rapid indication of their resistance to the penetration of chloride ions. The total charge passed, in coulombs, has been found to be related to the resistance of the specimen to chloride ion penetration.

The RCPT test method involved measuring the amount of electrical current that passed through 50 mm thick slices of 100 mm diameter cores for a period of 6 hrs. Two specimens, one of which was immersed in a sodium chloride solution and the other in a sodium hydroxide solution, were used. A potential difference of 60 V direct current was maintained across the ends of the specimen. The experiment set-up is shown in Fig. 4.17.

Fig. 4.17 RCPT test for the GC/Na-R concrete

4.4.14 Scan Electron Microscopy Test

The microstructures of the various control, GGBS, and calcined clay mortar samples were probed using the SEM technique. Also, the microstructures of the control and four geopolymer concrete samples were examined. In all cases, the fragments from the compressive tests of the 28 days cured samples were vacuum dried, and the fractured surfaces were examined by SEM using the Jeol SEM instrument (JSM-6060LV model) shown in Fig. 4.18. Different micrographs that revealed the morphology of the reaction products were obtained and reported.

Fig. 4.18 SEM test set-up using the Jeol instrument

4.4.15 X-Ray Diffraction Test

The XRD enabled the geopolymer concrete characterization through a mineralogical phase identification (Davidovits, 2020). It is an analytical method suitable for determining the structure of the geopolymeric binder produced from iron-rich kaolinitic clay. In this study, powders obtained from the crushed mortar and concrete samples were evaluated using the Panalytical XRD equipment, in order to identify the various phases present in the samples. This Panalytical Empyrean system, with a Co (1.7903Å) Kα X-ray source shown in Fig. 4.19, has a longer wavelength than the more common Cu Kα tubes (~ 1.54 Å), avoided the fluorescence that can occur from Fe in the sample. The testing was conducted by varying the diffraction angles (2-theta) from 5^{o} to 90^{o}. The intensity of the diffracted X-rays was observed as the detector and sample continued to rotate for 2 hrs via their corresponding angles. The data obtained was analysed to determine the different phases using the expert database in the system.

Fig. 4.19 XRD set-up for the various mortar and concrete samples

4.4.16 Fourier Transform Infrared Spectroscopy Test

An FTIR spectroscopy technique was used in this study to investigate the functional groups of the various calcined clay geopolymer mortar and concrete samples. This was used because, compared to XRD, an IR spectrum provided more detailed information on the amorphous phases of the samples through identification and confirmation of its compound. A molecule is known to absorb radiation only at certain frequencies that match the frequencies at which the molecule itself vibrates. This implies that a molecule has its own characteristic wavelengths in infrared absorption spectroscopy. This enabled the quantitative analysis of an unknown substance by understanding its IR spectrum. The FTIR spectroscopy was performed on the crushed fragments of the mortar and concrete samples using a Nicolet iS5 FT-IR machine shown in Fig. 4.20. Background data was first obtained using the OMNIC software before testing the dried samples. Afterwards, the data for all the samples analysed were obtained for a range of 600-4000 cm^{-1} wavelength. The data acquired for each sample was presented as the wavelength in cm^{-1} against transmittance in percentage.

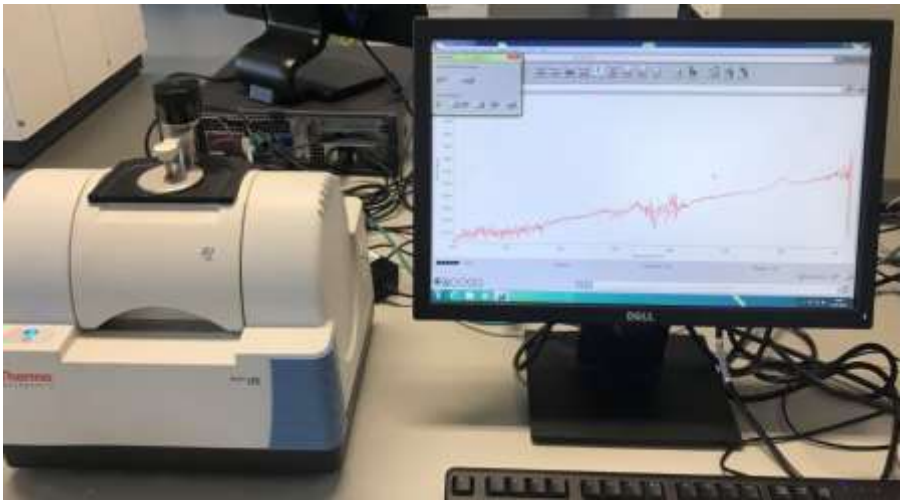

Fig. 4.20 FTIR experiment using Nicolet iS5 FT-IR machine

CHAPTER 5 RESULTS AND DISCUSSION

5.0 Introduction

In this chapter the results obtained from the various experiments are presented and discussed in eight sub-sections; as summarized in Fig. 5.0.

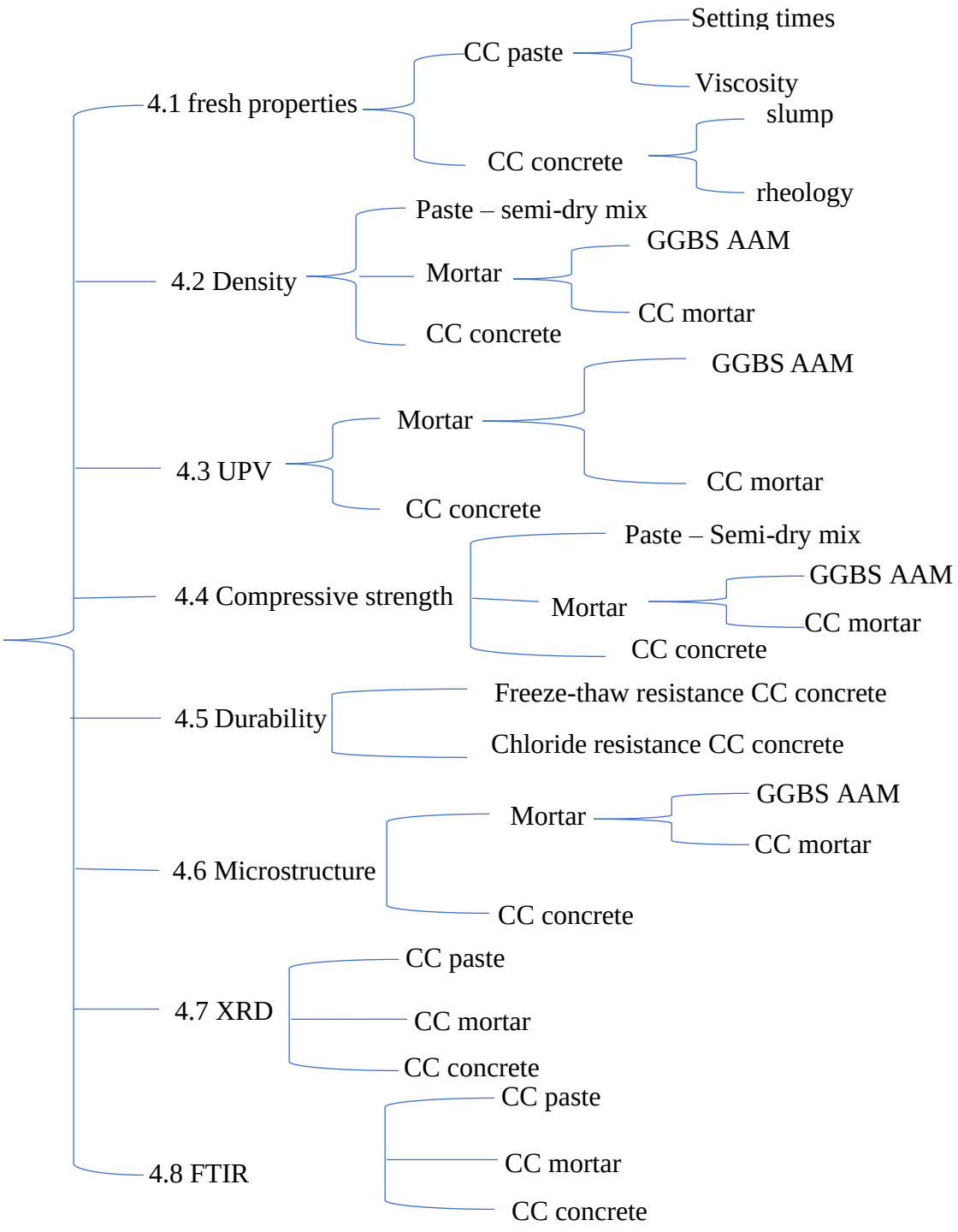

Fig 5.0 Schematic of the result and discussion section

5.1 Fresh properties

The results reported in this sub-section on the fresh properties of calcined clay geopolymers are:

- The setting times and rheological performance of the calcined clay geopolymer paste based on variable liquid to binder ratios (sum of alkali solution and free water divide by the precursor). The pastes Liquid to Binder ratio (L:B) of 1.3 and 1 correspond to that of the peak strength mortar with and without added water respectively in the mix (see Group 4 of table 4.5).
- The measured slumps and rheological properties of the geopolymer concrete mixes.

5.1.1 Effect of liquid to binder ratio on setting times and viscosity of the calcined clay geopolymer grout

The setting time indicated the setting development of the geopolymer paste of the two mixes that had a calcined clay to sodium silicate solution mass ratio of 1, but L:B of 1 and 1.3 respectively. The paste based on L:B of 1 have lower initial and final setting times of 7.5 and 8.25 hrs respectively as shown in Fig 5.1. Nevertheless, these values are higher than what is obtainable from for a CEM I paste based on W:C of 0.5 which can have a maximum final setting time of 4 hrs.

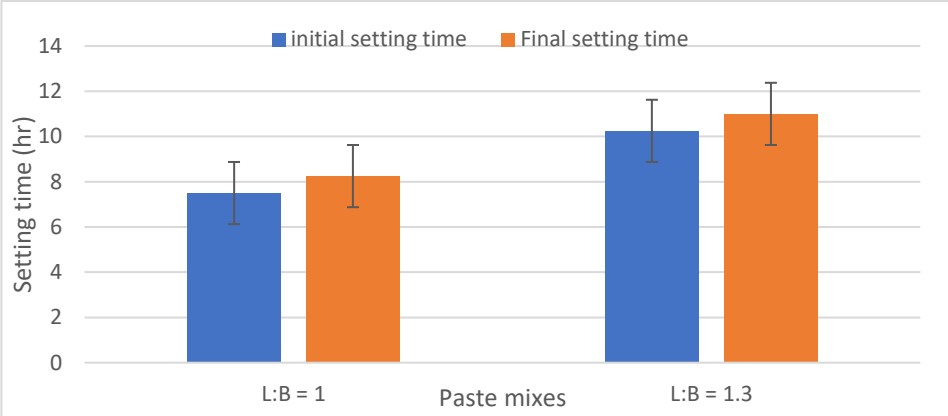

Fig 5.1 Setting times of the calcined clay geopolymer grout

It can be seen in Fig 5.1 that increasing the L:B of the geopolymer pastes from 1 to 1.3 resulted in extending the setting times of the grout. This result concurs with Blackstock, Neill, and McIntosh (2017) who reported that the setting process of geopolymers derived from calcined lithomarge takes several hours. However, a relatively short setting time was achieved by Kwasny *et al.* (2018) by blending calcined clay with GGBS that supplied calcium into the

system and thereby lowered the setting times through quick precipitation of C(N)-A-S-H gel. In other words, the calcium supplied by the GGBS coupled with its angular shape, speed up the reaction that lowered the setting times of the GGBS blended calcined clay geopolymers. Meanwhile, it can be seen that the two geopolymer pastes produced, hardened and gained sufficient strength such that they could be demoulded within 20 hours when cured at room temperature. This hardening behaviour is desired for the daily turnaround of moulds, especially in precast industries. Also, the delayed setting times may be useful in the transportation and handling of the calcined clay based geopolymer concrete, especially in applications where extended workability is required.

A consistent and controlled rheology, which can be described with the Herschel-Bulkley (power-law) model, was achieved by the calcined clay geopolymer grout that had a L:B of 1.3. The shear stress (Ƭ), was computed from the measured torque shown in equation 5.1 specified by Banfill and Kitching (1990).

$$\tau = 3T/(2\mu\,(Rv3+3\,Rv3h)) \qquad (5.1)$$

Where: T = torque

At a shear rate of 40 Pas^{-1}, the grout shear stress measured at 42 Pa and the viscosity at 241 Pas. At the shear rate of 20 Pas^{-1}, the grout shear stress was 24 Pa and the viscosity was 133.4 Pas. The measured shear stress of the grout was influenced by both the high H_2O/Na_2O ratio of 14:1 and L:B of 1.3. Fig 5.2 shows the flow curves of the two geopolymer grouts that attained an $r^2 \geq 0.98$ for their line fits. Geddes, *et al.* (2018) applied power law model and obtained similar flow curve for a flash calcined clay activated by potassium silicate solution. The high plastic viscosity measured was due to the viscous nature of the sodium silicate solution that was used as the alkali metal source of the grouts.

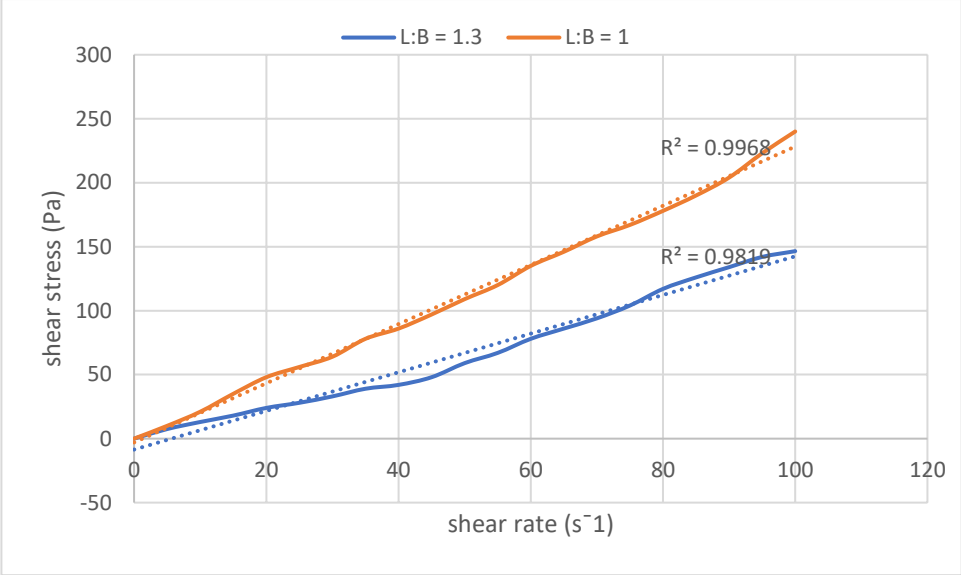

Fig 5.2: Comparing the flow curves of the calcined clay geopolymer grouts

5.1.2 Effect of activator type on the consistency of calcined clay geopolymer concrete

The measured slump values for the PC control and four geopolymer concrete mixes (see table 4.3 and 4.6 for the mix designs) are presented in Fig 5.3. The values obtained can be described as a collapsed slump based on a BS EN 12350-2 classification. The control mix had lower slump value of 160 mm (despite it having a high water to cement ratio of 0.5) compared to the other geopolymer concrete mixes; except for the blended mix. This demonstrates the flowable character of the calcined clay geopolymer concrete irrespective of the type of activator used in the formulation.

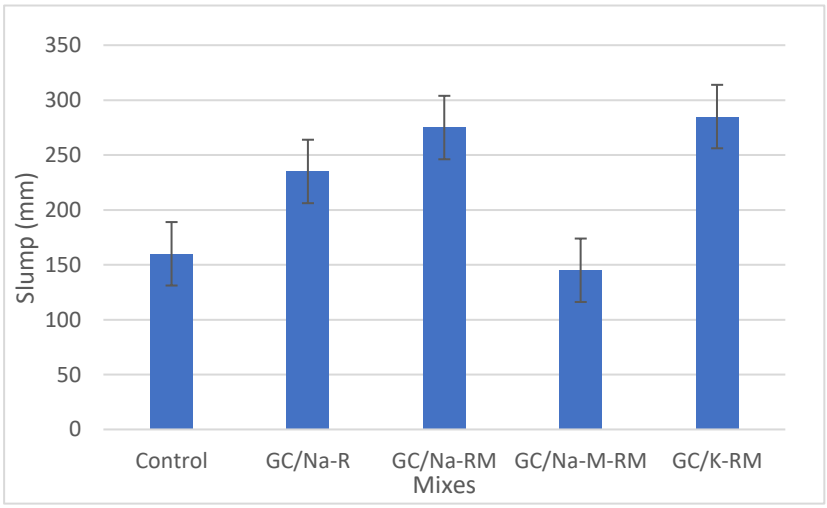

Fig 5.3 Slump for the control and geopolymer concrete mixes

From Fig 5.3, it can be seen that the mix formulated by blending the sodium-based silicate and hydroxide solutions produced the lowest slump of 145 mm among the geopolymer concrete

mixes. This was because the mix had the lowest free water content, coupled with the rapid reaction of the 8 M concentrated hydroxide solution. Another reason for the relative low slump value for the blended activator mix is the part replacement of the silicate solution activator which enhance concrete flow with hydroxide solution. The results also show that decreasing the aggregate content of the mix increased the flowability of the concrete. However, the overall workability of the four geopolymer concrete mixes was significantly affected by the viscous nature of the activators used as illustrated by the rheological properties result.

5.1.3 Effect of activator type on rheological properties of calcined clay geopolymer concrete

The dynamic yield stress measured for each concrete mix was the minimum stress required to maintain the flow of the concrete, while the static yield stress was the stress required to initiate the flow of the concrete, which is often associated with a higher value. This is in agreement with the result of this study as presented in table 5.1 that show a higher static yield stress compared to the dynamic yield stress of the control and geopolymer concrete mixes. The measured peak torque and Bingham parameters are also presented in table 5.1, while the relationship between the torque and speed is presented in Fig 5.4. The result showed a positive linear relationship between the yield stress and plastic viscosity for the control, GC/Na-RM, and GC/K-RM concrete.

Table 5 1 Rheological parameters of the geopolymer concrete mixes (see table 4.6 for mix design)

	Stress measurement		Relative parameters		Bingham parameters	
Mix GC/	Peak torque (Nm)	Static yield stress (Pa)	Yield Value (Nm)	Viscosity value (Nm. s)	Dynamic yield stress (Pa)	Plastic viscosity (Pas)
Control	9.58	2232.1	5.76	1.14	1655.7	4.5
Na-R	27.06	3308.2	15.19	39.54	-	-
Na-RM	1.5	348.5	0.52	8.2	81.7	161.9
Na-M-RM	12.69	2958.2	20.39	45.12	-	-
K-RM	0.63	146.4	0.04	3.40	5.3	68.0

From the results, the static and dynamic yield stresses of the GC/Na -RM is relatively low compared to the GC/Na-R mix which was activated with the same alkali solution but a varied

aggregate content. This suggested that increasing the paste volume of geopolymer concrete improved its workability. It can also be seen that the plastic viscosity of the geopolymer concrete mixes was significantly more than what was obtained for the Portland cement-based control concrete. This increased viscosity was caused by the Na_2SiO_3 solution (a viscous liquid) used as the alkali metal source (activator) for the geopolymer concretes. The result also showed that the parameters obtained by applying the Bingham model indicated that the PC control, GC//Na-RM and GC/K-RM mixes exhibited a Bingham fluid character. Additionally, the rheological values obtained for the PC control concrete was within the range for conventional concrete as reported by Khayat *et al.* (2019).

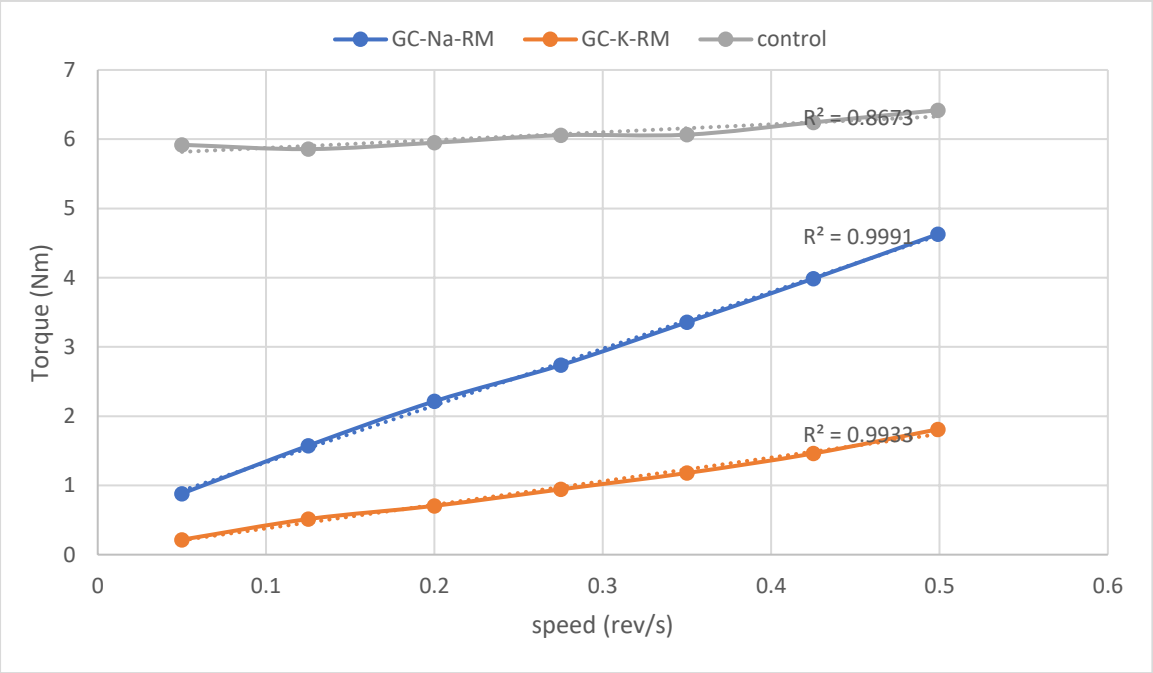

Fig 5.4 Flow curve for the PC control, GC/Na-RM and GC/K-RM concrete

The torque-velocity curve (Fig 5.4) also showed a decreased rotational velocity from the pre-shearing applied at the highest shear rate. This ensured a full breakdown of the samples and controlled the effect of thixotropy (a structural build-up that occurred in the sample after mixing) during the rheology measurement.

Furthermore, it can be seen from the results presented in table 5.1 that the mix with the higher aggregate content (GC/Na-R) have the highest peak torque of 27.1 Nm. The increased torque for the mix with higher volume fraction of aggregates is caused by reduced spacing between aggregates in the mix, which induced greater resistance to flow of the concrete. Meanwhile, the potassium silicate activated mix had the lowest peak torque of 0.63 Nm. This indicates that

increased binder content is associated with the low energy required to shear (mix) and pump geopolymer concrete. Also, the blended activator had a significantly higher peak torque of 12.69 Nm as compared to other geopolymer concrete mixes with similar aggregate contents. This indicates that it requires more energy for shearing and pumping compared to a lone silicate activated mixes.

5.2 Density

The mean densities for the seven groups of mortar and the four concrete mixes were measured at various ages (the values are reported in this sub-section). Comparing the densities of a given group of mixes can be used to indicate the advancement of hydration/geopolymerisation reaction in the system.

5.2.1 Influence of type and dosage of activator on the density of GGBS AAM

Fig 5.5 shows the density of the GGBS mortar mixes. These decreased due to the increase in proportion the of NaOH solution in the mix. Also as expected, the density increase was observed across all the mixes as the mortar samples hardened from 7 to 28 days. Even at 28 days, the density of the mortar samples was around 60% that of the PC control mortar due to the weak binding gel caused by the limited silicate in the system. This low density mortar can be associated with the weak strength of the resulting binder (C-N-A-S-H gel) due to the partial hydration reaction in the system which was caused by the high Na:Si ratio.

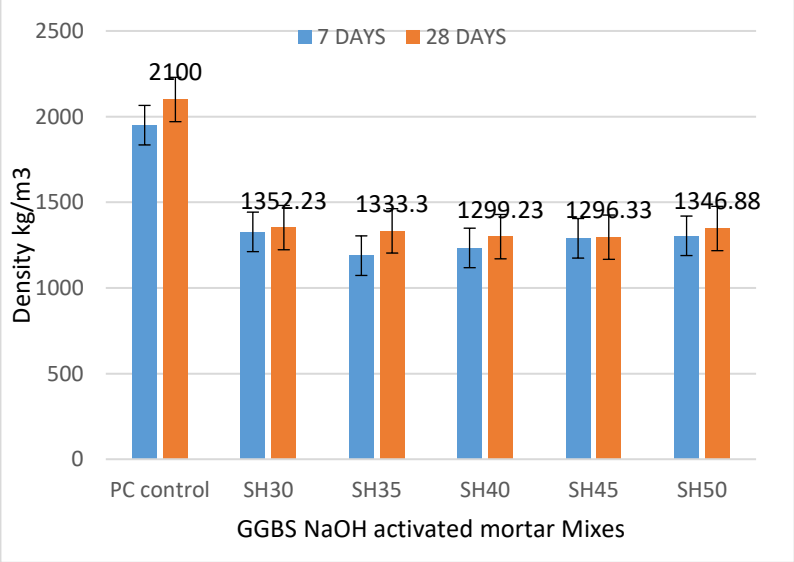

Fig 5.5: Density of GGBS mortar mixes activated by variable proportion of NaOH solution

5.2.2 Effect of type and dosage of activator on the density of calcined clay geopolymer mortar

In Fig 5.6, the effect of 54.5% sodium silicate solution to precursor ratio ranged from 0.5 to 1.5 on the density of CC geopolymer mortar (see group 4 in table 4.5) with constant free water and aggregate content is presented. It can be seen that the density measured of the calcined clay geopolymer mortar samples are more than that of the PC mortar, which also increased slightly with an extended curing age. The increase in density with age was caused by the hardening and drying of the samples characterised by the loss of moisture and the accompanied reduction of voids over time. The results shown in Fig 5.6 indicate that the hydrous sodium silicate activated calcined clay geopolymer mortar samples are within the range of a normal weight PC mortar. Meanwhile, the low density measured for the PC control mortar in comparison to the CC geopolymer mortars is due to the high W:C of 0.5 of the control mortar.

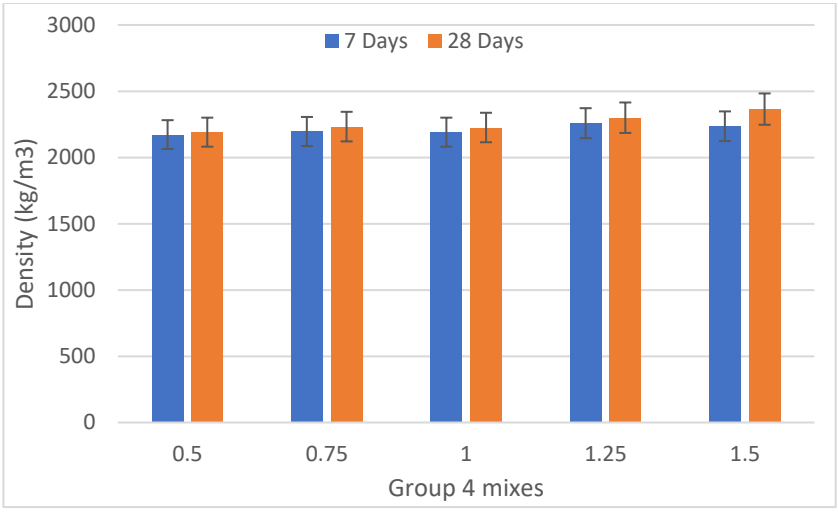

Fig 5.6 Density of calcined clay geopolymer mortar mixes

It can also be seen in Fig 5.6 that the density of the geopolymer mortar did not significantly increase with age. This indicates that the hardening and geopolymerisation processes had almost been completed at seven days.

5.2.3 Effect of activator type on the density of calcined clay geopolymer concrete

The density measurements of the PC control and geopolymer concrete mixes after 28 days fall within the range of normal weight concrete (defined by Neville 2011 to be between 2240 – 2400 kg/m^3) as shown in Fig 5.7. This is because a normal weight aggregate was used for all the mixes. The result also showed that the values obtained for the GC/Na-R and GC/Na -RM after 28 days of sealed curing showed a decrease in density of the concrete samples, which was caused by a decrease in the aggregate proportion.

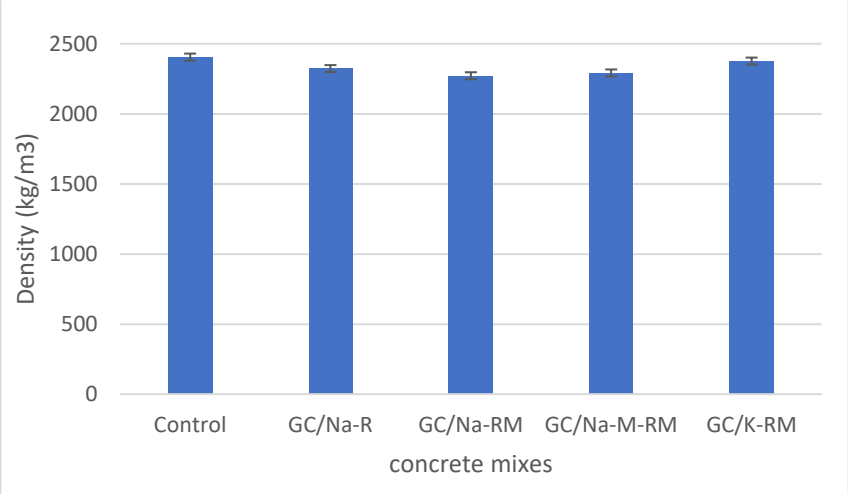

Fig 5.7 Density of the PC control and calcined clay geopolymer concrete mixes

Fig 5.7 also shows that the blended activator mix (GC/Na-M-RM) produced a relatively denser concrete compared to the sodium silicate activated geopolymer concrete (GC/Na-RM) with equal aggregate content (see table 4.6). This was thought to be caused by the mix having the lowest free water content, thus resulting in fewer voids. Furthermore, the potassium silicate activated concrete showed a slightly higher density compared to the other geopolymer concrete mixes. This was probably due to the presence of K^+ in the gelation product, as well as its enhanced coagulation characteristic compared to the Na^+ in the geopolymerisation reaction.

5.2.4 Effect of the main pozzolan on the density of semi-dry ternary paste

The ternary mix that had calcined lateritic clay as its main pozzolan was the densest semi-dry paste (Fig 5.8). Moreover, all the samples could be described as normal-weight pastes and this can be associated with the samples' adequate compaction that resulted in fewer voids.

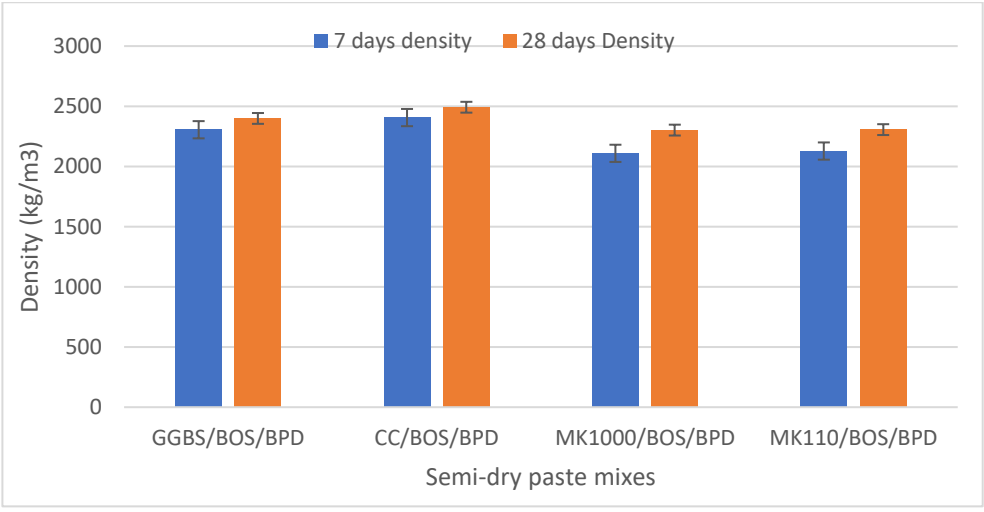

Fig 5.8 Density of the ternary mixes semi-dry pastes

Fig 5.8 also shows that the density of each semi-dry paste increased slightly with age under sealed curing conditions.

5.3 Ultrasonic pulse velocity (UPV)

Measured UPV values indicate the quality of the internal structure of mortar and concrete samples (Khatib, 2008). The results obtained from the UPV tests for the various mortar and concrete samples are presented under this sub-section.

5.3.1 Influence of type and dosage of activator on UPV of GGBS AAM and calcined clay geopolymer mortar

The results obtained from the UPV test presented in Fig 5.9 showed a decrease in the computed pulse velocities that were caused by an increased dosage of NaOH solution in the mortar mixes. This indicated that increasing the alkali solution proportion in the mix beyond the optimum dosage resulted in the presence of more pores in the sample. These trends are as expected with any mix having increased water content form the activator dosage. The UPV results also showed all the mixes fall within the UPV range of 2.5 to 4.5 km/s. This can be classified as good mortar (Şimşek *et al.* 2019).

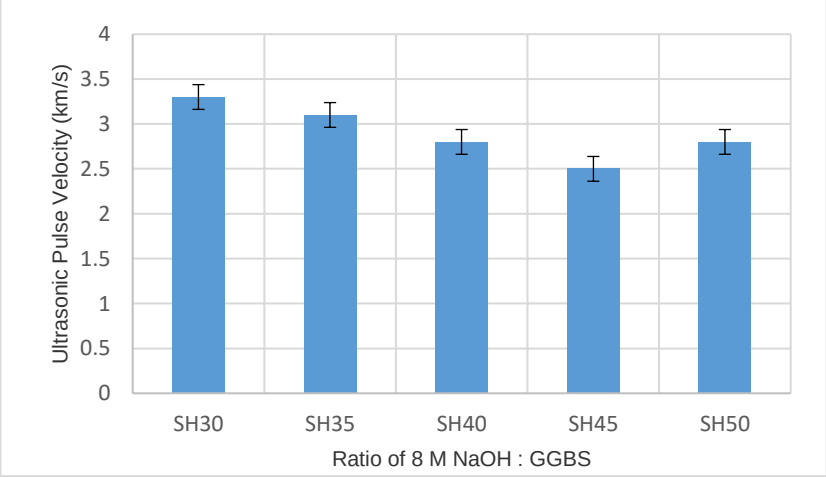

Fig 5.9 Ultrasonic Pulse Velocity of sodium hydroxide activated GGBS mortar

The UPV result in Fig 5.9 also shows that the SH30 GGBS AAM sample - which is the 8 M sodium hdyroxide activated mix with L:B of 0.3, that have the highest UPV value had a better packed internal structure with fewer pores. The improved density of this internal structure is an indication that the workable mix had an appropriate alkali solution dosage. However, the SH50 mix which is supposed to have longer signal travel time due to increased pores resulting from increase activator dosage indicate otherwise. This is an outlier which may be caused by

the SH50 samples having better compaction or more homogenous shear mixing and can be counted as an experimental error. Nevertheless, the UPV results indicate that the internal structure of the mortars across the solution to precursor ratios range of 0.3 – 0.5 are homogenous and compact that are of good quality.

Furthermore, the computed UPV for the peak strength calcined clay geopolymer mortar at 7 and 28 days were 2.3 km/s and 2.4 km/s, respectively. This increase in the measured pulse velocities (i.e a shorter signal travel time through the sample) with an increase in curing age of the peak strength mortar is an indication of a decrease in the number of pores present in the sample due to advancement of the geopolymerization reaction. The UPV results also showed that at both 7 and 28 days, the values obtained fall within the UPV range of 2 to 4.5 km/s that is classified as good mortar (Şimşek *et al.* 2019).

5.3.2 Effect of activator type on UPV of calcined clay geopolymer concrete

The UPV computed for the two geopolymer concrete mixes activated with 54.5% sodium silicate solution that have equal water to solid ratios of 0.48 and H_2O:Na_2O ratios of 14.2 (see table 4.7) but varied aggregate proportion (see table 4.6) was found to be within the same UPV range for concrete classification. On the one hand, the computed UPV value of 3.3 km/s at both 7 and 28 days for the GC/Na - RM geopolymer concrete was the same. On the other hand, the GC/Na-R mix that had a higher aggregate content had UPV values of 3.1 and 3.2 km/s at 7 and 28 days, respectively. These values obtained from the UPV experiment fall within the range classified by the UPV test standard of good concrete (Khatib 2008).

5.4 Compressive strength development

Compressive strength development is a property that is known to have a good correlation with other mechanical properties and durability of concrete. The results obtained from the compressive strength test of the various mortar and concrete mixes at different ages is presented in this sub-section.

5.4.1 Effect of type, concentration, and dosage of alkali solution on compressive strength of GGBS AAM

NaOH concentration is associated with the dissolution and release of the silicate and aluminate ions from the precursor. From the results presented in Fig 5.10, it can be seen that increasing the concentration of the NaOH solution above 8 M slightly decreased the 28 days compressive strength of the NaOH-activated GGBS mortar. This reflected the high viscosity of the alkaline

solution (above 8 M) that restricted ion mobility, thus affecting the reaction. Increased molarity is also associated with premature precipitation of the C-(N)-A-S-H gel and raising the Na:Si in the system. In other words, increasing the molarity of the NaOH solution above 8 M, resulted in a system with low amount of silicate in the binding gel, which produced a reduced strength mortar.

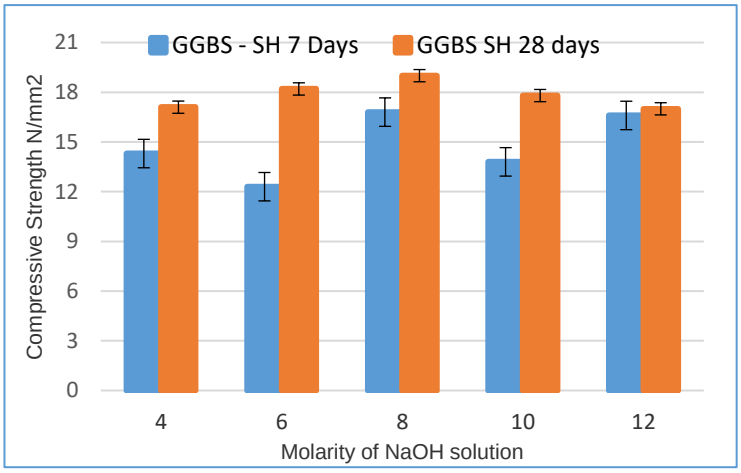

Fig 5.10: Compressive strength of GGBS mortar activated with variable molarity of NaOH solution

Fig 5.11 showed that the GGBS mortar samples activated with $Na_2SiO_3.5H_2O$ solution achieved significantly higher compressive strength compared to the mixes activated with 8 M NaOH solution. This strength improvement was largely due to the higher silicate content of the C-(N)-A-S-H gel precipitated by the $Na_2SiO_3.5H_2O$ solution, which enhanced the strength of the binding phase of the GGBS mortar. This is an agreement with the findings of Bernal et. al. (2014) that high strength binder system is produced by the alkalination of GGBS with silicate-based activator. Likewise, the remarkable strength produced by the hydrous metasilicate solution may also be associated with the latent hydraulic property of the GGBS, which may not be possible with low Ca precursor.

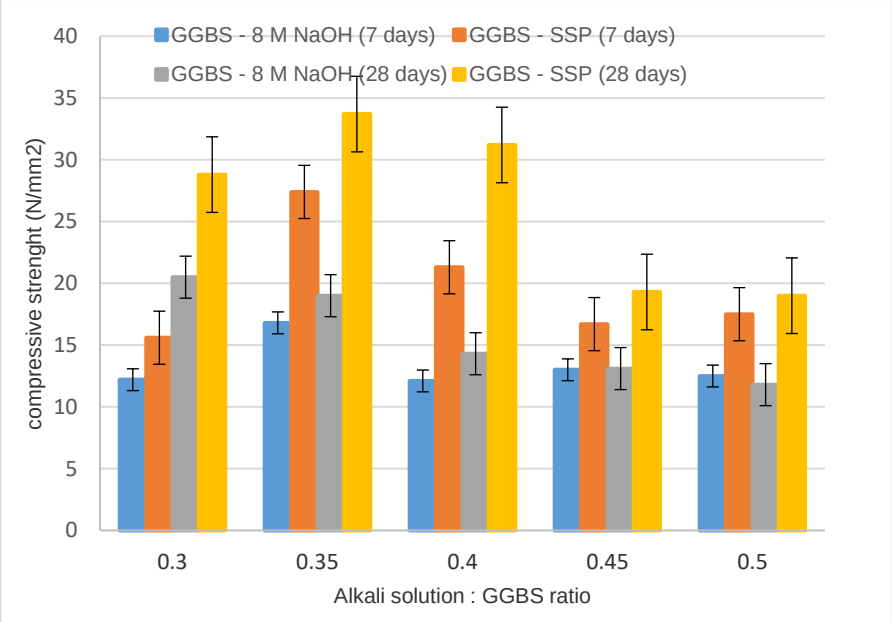

Fig 5.11 Compressive strength development of GGBS mortar activated with a different alkali solution to binder ratio

The results presented in Fig 5.11 also show that a ratio of alkali solution to GGBS of 0.35 produces a peak compressive strength of 34 MPa and 19 MPa at 7 days (for the $Na_2SiO_3.5H_2O$ and NaOH solutions activated mixes, respectively). Beyond the 35% alkali solution dosage, the liquid content in the GGBS mix can be described as high, such that not all the alkali solution was consumed in the reaction. This excess alkali solution produced more pores as the mortar hardened, thereby causing decreased strength of the mortar. However, at lower liquid content of below 35% a decrease in strength was observed. This may be associated with the increased energy required to provide full compaction to the mix. In addition to the semi-dry nature of the mix, it can also be argued that the alkali solution was inadequate to ensure the complete hydration.

Comparing the results of Fig 5.10 and 5.11, it can be argued that because of the high pozzolanic activity of the GGBS, its activation does not require significant Na_2O dosage that was provided by the NaOH solution. Rather, even a slight increase in SiO_2 in the reaction by the hydrous sodium silicate solution resulted in improve strength performance.

5.4.2 Effect of type and dosage of alkali solution on compressive strength of calcined clay geopolymer mortar

The compressive strength of the tested calcined clay mortars that were activated with an 8 M NaOH solution and a 44.1% $Na_2SiO_3.5H_2O$ solution with varied L:B (Liquid refer to the alkali solution and free water, while binder refer to the precursor) is presented in Fig 5.12. As noted

in sub-section 4.2.2, Menissa et. al. (2017) suggested that appropriate solution to precursor ratio of metakaolin geopolymers is generally around 1, because of its high water demand (about double the appropriate W:C of PC mortar). Also, some trial mixes were made with L:B of less than 0.8 but produced a stiff mortar. Consequently, due to the platy shape and layered structure of the calcined clay, a L:B of between 0.8 and 1 was used in order to produce a homogenous workable mortar for this group of mixes (group 2 of table 4.4). The result shows a strength development in the mortar for all the mixes with increasing age. This is an indication of the continuity of the reaction (dissolution of residual raw materials and gel formation) in the air-cured samples. The strength peaked at an L:B of 0.80 and dropped significantly as the ratio was increased to 1. The L:B ratio of 0.80 was thought to have a sufficient activator content to enable the dissolution of the aluminate and silicate from the precursor, while not hindering the coagulation and polycondensation rate during the gel synthesis. Furthermore, increasing the L:B resulted in a decrease in the strength of the mortar due to the presence of excess activator which may not all have been consumed in the reaction. This caused voids in the microstructure revealed by the SEM images (Figs 5.24 and 5.25) as the samples solidified in the air. Also, the high Na_2O content in the system – resulting from increasing the activating solution proportion – caused the excess Na^+ to react with the CO_2 through atmospheric carbonation. Thus, the geopolymerization process was disrupted and may have led to a reduction in strength. Although increasing the amount of alkali solution ensured a higher dissolution rate of the residual raw materials, it hindered the polycondensation rate by making the diffusion of dissolved species difficult (Liew et. al. 2012).

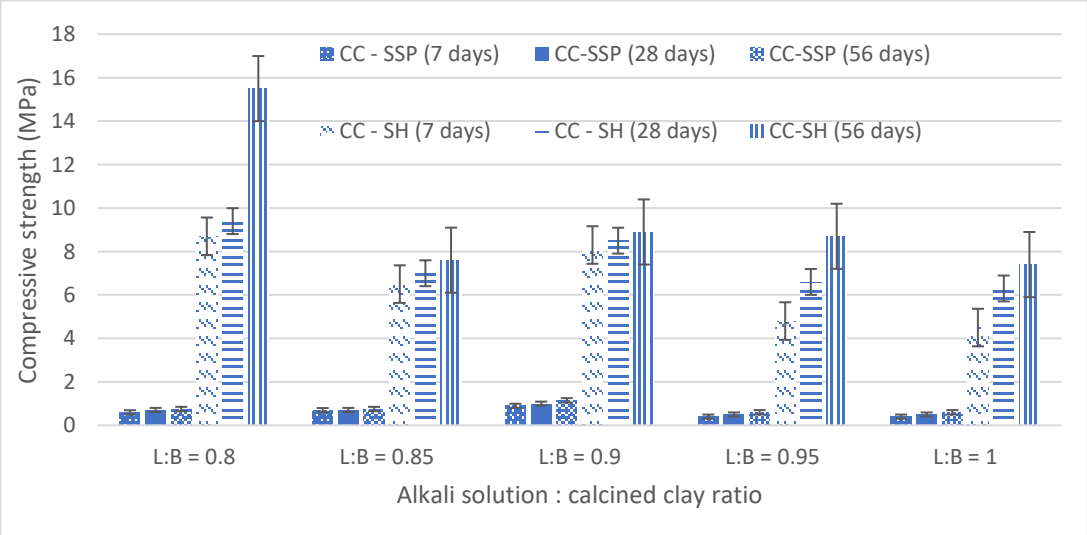

Fig 5.12 Compressive strength development of calcined clay geopolymer mortars activated by a variable proportion of two types of chemical activators

The results presented in Fig 5.12 further showed that up to 2000 % higher strength mortar was achieved by the alkalination of the calcined clay with the 8M NaOH solution, as compared to the hydrous sodium silicate solution (SSP). This observation is regardless of the age and proportion of the solution used in the mixes. The 32% NaOH solution had an enhanced leaching ability that dissolved the silicate and aluminate in the calcined clay, which enriched the binding phase (Bature, *et al.* 2018). Conversely, the 44.1% $Na_2SiO_3.5H_2O$ solution had reduced binding ability due to the dilution caused by the chemically bound water. Additionally, the dissolution of solid $Na_2SiO_3.5H_2O$ under normal atmospheric pressure conditions is shown to be not very effective (solubility value of 420 g/L at 20 ˚C compared to sodium hydroxide that has solubility value of 1000 g/L at the same temperature), thereby limiting the availability of the free silicate in the system that is required for the geopolymerization process.

Fig 5.13 presents the results of the compressive strength for the group 3 mixes designed with an equal alkali solution to a calcined clay mass ratio of 0.7. The variable for the mixes is the activator used: 8M NaOH solution, commercially available, high viscosity water glass and sodium metasilicate pentahydrate dissolved solution. The results show that the compressive strength of the mortar activated by the high viscosity sodium silicate solution at both 7 and 28 days was more than double that of the 54.5% $Na_2SiO_3.5H_2O$ dissolved solution. The significant strength difference was caused by a variation in the amount of Na_2SiO_3 solid in the two chemical activators. This variation resulted in varying the *alkali modulus* (ratio of $\%SiO_2$ to Na_2O), alkali dosage (ratio of $\%Na_2O$ to calcined clay), *etc* considerably in the system, despite the two mixes having the same activator solution to calcined clay mass ratio. Also, the chemically bound water in the SSP activator contributed to the dilution of the solution, thereby decreasing its binding effect. This is in agreement with the findings of Bernal *et al.* (2014) who reported that a low strength binder could be achieved by activating precursors with hydrated chemical activator. Moreover, the blended sodium hydroxide activated mortar achieved the highest strength for the group 3 mixes that have equal mass ratio of 0.7 due to the molar oxide composition ratios ($Na_2O:Al_2O_3$ of 1.1, $SiO_2:Al_2O_3$ of 2.4 and $H_2O:Na_2O$ of 9.8) of the mix. The detail molar oxide composition calculation is shown in appendix 1. However, for this group of mixes, which were cured in sealed conditions, the strength achieved was low and was caused by the insufficient amount of chemical activator in the mix that supposed to provide the required alkali dosage and modulus.

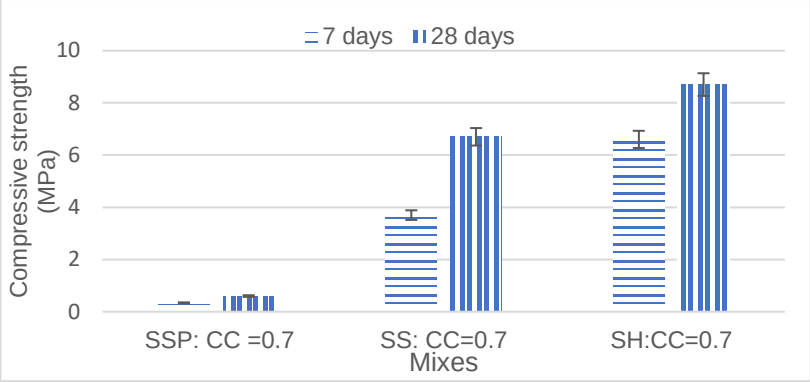

Fig 5.13 Compressive strength development of calcined clay geopolymer mortars activated by the three types of activators

The results in Fig 5.12 and 5.13 stress that geopolymer synthesis of calcined clay is very sensitive to molar oxide composition ratios. Thus, these mixes that were designed based on water demand of the precursor produced an alkali activated mortars. It is therefore necessary that the liquid to binder ratio, be formulated to satisfy the prescribed molar oxide ratios for geopolymer mortar to be achieved.

5.4.3 Effect of sodium silicate solution to calcined clay mass ratio on the compressive strength

Due to the relatively low strength achieved by group 2 and 3 mixes that were formulated based on activating solution demand, the effect of the variable proportion of silicate solution (group 4 in table 4.5) that had Si:Al and H_2O:Na_2O ratios within the prescribed optimised range were studied to determine which mass ratio (mix) would yield peak strength. The tested samples, which were seal-cured, showed an increase in strength with age for all mass ratios; with a rapid strength increase between 2 and 7 days as shown in Fig 5.14.

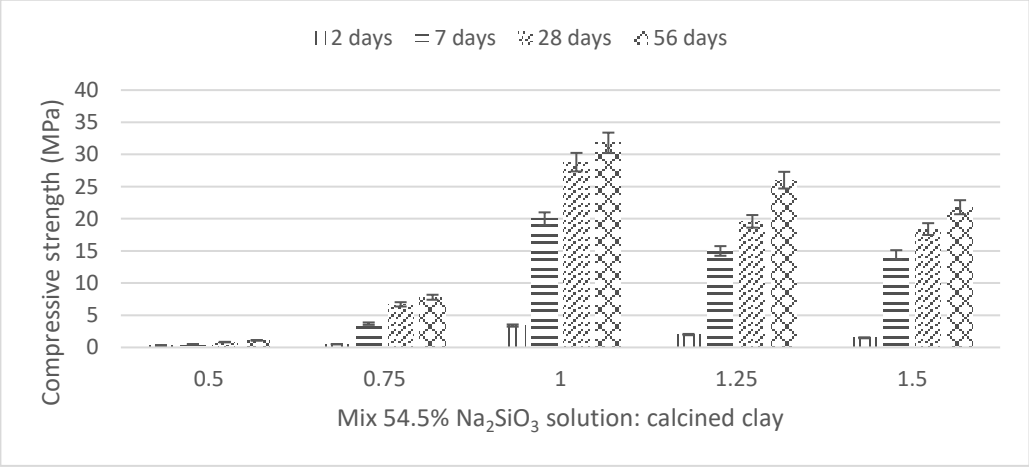

Fig 5.14: Compressive strength development of calcined clay geopolymer mortar activated by a varied proportion of 54.5% sodium silicate solution

From Fig 5.14, it can be seen that at 7 days, the geopolymer mortars had already achieved most of their strength due to the advancement of the geopolymerization reaction in the system. Also, peak strength at all ages was achieved with a mass ratio of 1. This suggest that the mortar mix formulated with a 54.5% sodium silicate solution to CC mass ratio of 1 have sufficient alkali modulus and dosage that were required for the reaction. Increasing the mass ratio above 1 may have precipitated more than the required free silicate. This disrupted the reaction and resulted in a decreased strength. This finding concurs with Liew, *et al.* (2012) and Bature, *et al.* (2019) who concluded that a deterioration in strength is expected when increasing the Na_2SiO_3 solution beyond the optimum dosage. This was due to the hindering of the geopolymerization reaction through the Al–Si phase precipitation that prevented contact between the reacting materials and the activating solution. Furthermore, the low mass ratio (below) 1 may have yielded insufficient free Si that was required to complete the geopolymerization. This resulted in a low strength mortar.

Moreover, it can be seen from table 5.2 that the mix that achieved the peak strength have SiO_2/Al_2O_3 and Na_2O/Al_2O_3 molar ratios of 4.12 and 1.0 respectively. These ratios corresponds to the ideal ratios prescribed by (Davidovits, 2015). Also, the Na_2O/SiO_2 of 0.24 and H_2O/Na_2O of 14.10 for the peak strength mix was similar to the optimum strength composition values reported by Singh *et al.* (2015). In summary, the mixes presented in Fig 5.14 reached a maximum strength and then decreased gradually due to the sensitivity of the geopolymer synthesis to variations in the molar oxide composition. Consequently, even though the molar oxide ratios of all the mixes fall within the range specified by Singh *et al.* (2015), a significant difference in strength was observed. This stresses the need for mix optimization in geopolymers.

Table 5 2 Molar oxide ratios for the group 3 mixes

Group 3 Mixes (CC:SS)	Na_2O/Al_2O_3	SiO_2/Al_2O_3	Na_2O/SiO_2	H_2O/Na_2O
0.5	0.5	3.07	0.16	16.69
0.75	0.7	3.51	0.2	12.22
1	1	4.12	0.24	14.10

1.25	1.25	4.64	0.27	13.58
1.5	1.49	5.16	0.29	13.24

Comparing the results presented in Fig 5.12 and 5.14, a significant difference in strength (up to 430% at 56 days for the mixes based on L:B of 1) can be clearly seen between the 54.5% Na_2SiO_3 solution and the hydrous $Na_2SiO_3.5H_2O$ solution activated calcined clay mortars. In fact, no meaningful strength was achieved by activating the calcined clay with both 44.1% and 54.5% $Na_2SiO_3.5H_2O$ solutions. Also, with a further comparison of the results presented in Fig 5.12 and 5.14, it can be observed that seal-curing enhanced the strength of geopolymer mortar compared to air-curing by limiting the carbonation that causes the decline in strength. It also prevented crack propagation and pore development associated with the rapid loss of moisture in the samples (Kumar, Saxena and Singh 2019).

5.4.4 Effect of activator type on compressive strength of calcined clay geopolymer concrete

At both 7 and 28 days, the GC/Na–R mix achieved a lower strength compared to the PC control and other geopolymer mixes (see Fig 5.15). This is mainly due to the lower binder content in the mix that had an aggregate to binder ratio (A:B) of 4.33 against 3.46 used for the formulation of the other three Rangan modified mixes. The potassium silicate activated mix achieved peak strength due to the enhanced alkalination capability of the potassium-based alkali metal source. This has been reported by other authors (Davidovits, 2015; Provis, 2018). Similarly, the potassium silicate activated mix showed less sensitivity to molar oxide variation; considering that it achieved peak strength with a (K+Na):Al of 0.8, which is slightly lower than the ideal ratio of 1 reported in the literature (Duxson et. al, 2007).

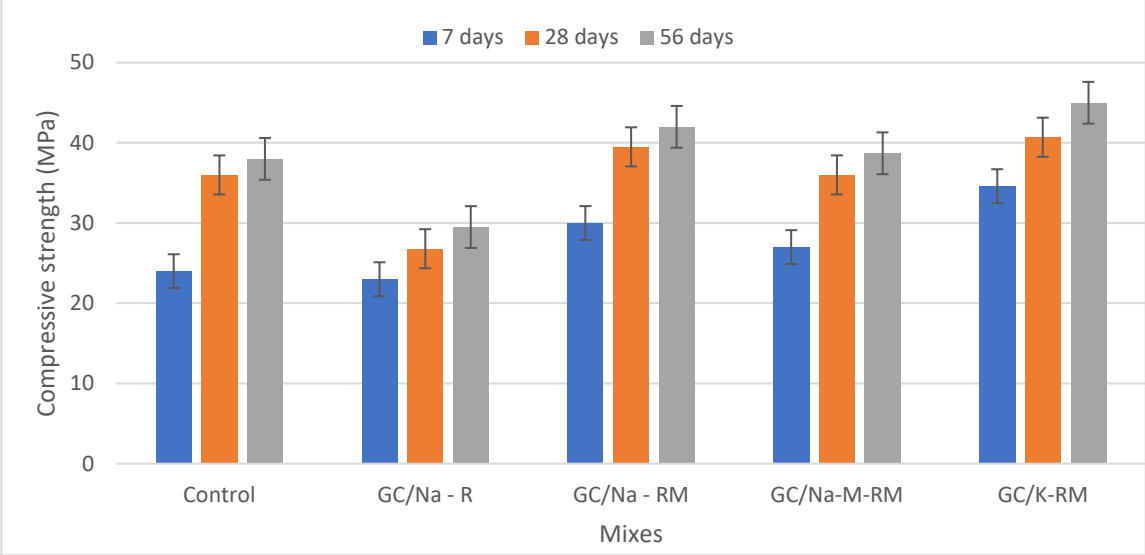

Fig 5.15: Compressive strength development of the control and calcined clay geopolymer concretes

In Fig 5.15, it can also be seen that the blending of the sodium silicate with the sodium hydroxide solution (GC/Na-M-RM) resulted in a lower compressive strength compared to the other two mixes (i.e GC/Na-RM and GC/K-RM) that have similar A:B ratio. This is despite the three mixes having similar molar oxide composition ratios that are prescribed for geopolymers. This decrease in strength can be associated with a high Molar Ratio (MR) of the silicate solution used as the activator. According to Davidovits (2015), increasing the MR of the silicate solution above 2.5 can be limiting and degrading to its alkalination potential in geopolymers.

5.4.5 Effect of activator type on tensile strength of the calcined clay geopolymer concrete

The split tensile test result obtained on the control and the four-geopolymer concrete samples at 28 days is presented in Fig 5.16. The principal characteristic tensile strength for each of the samples was computed using equation 5.1 (recommended by Neville (2011)) and these findings are shown in Fig 5.16. It can be seen that the split tensile strength for each sample is a fraction of its compressive strength at 56 days.

$$f_{ct} = 0.3(f_{cm})^{\frac{2}{3}} \qquad (5.1)$$

Where: f_{ct} = tensile strength

f_{cm} = compressive strength.

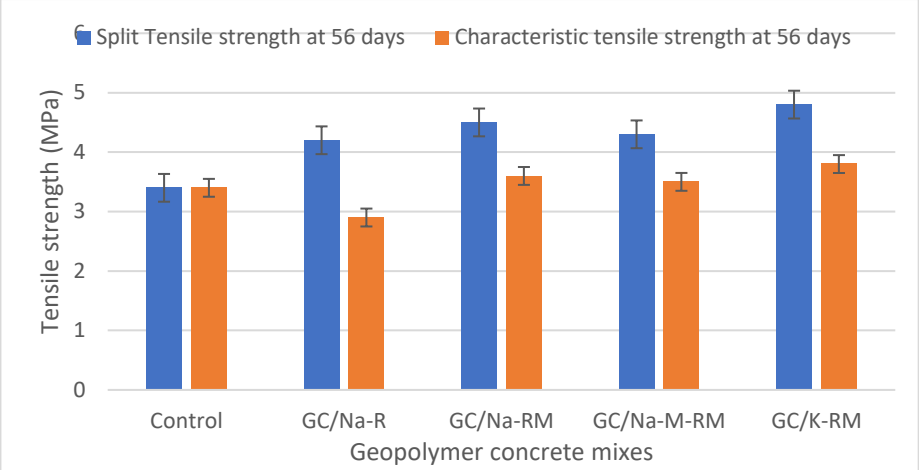

Fig 5.16: Tensile strength of the control and calcined clay geopolymer concretes

Fig 5.16 also shows that the principal tensile strength of the concrete samples had a lower value compared to the measured split tensile strength of the geopolymer concrete samples. This indicates that the geopolymer matrix had slightly enhanced tensile strength compared to traditional Portland concrete. It can also be argued that equation 5.1 provides a conservative value when applied to geopolymer concrete as it was designed primarily for Portland cement concrete.

5.4.6 Strength activity index of the semi-dry mix pozzolans

Fig 5.17 shows the compressive strength gain as age increases for the control mortar, as well as the various pozzolans used for the semi-dry mixes. In the control mortar, the strength gain indicated the continuity of the hydration reaction of the Portland cement in the mortar cured in water, which precipitated the C-S-H gel and $Ca(OH)_2$. For the binary mix mortars, the strength gain indicated a pozzolanic reaction between the portlandite and the respective pozzolans that precipitated additional C-S-H gel in the system, but with a lower calcium to silicate (C:S) ratio. The low strength of the control mortar compared to the binary mixes is caused by the high water-cement ratio of 0.6. This was used in the mix to accommodate the water demand of the pozzolans in the binary mixes. The MK1000 replaced mix achieved the highest compressive strength at 28 days.

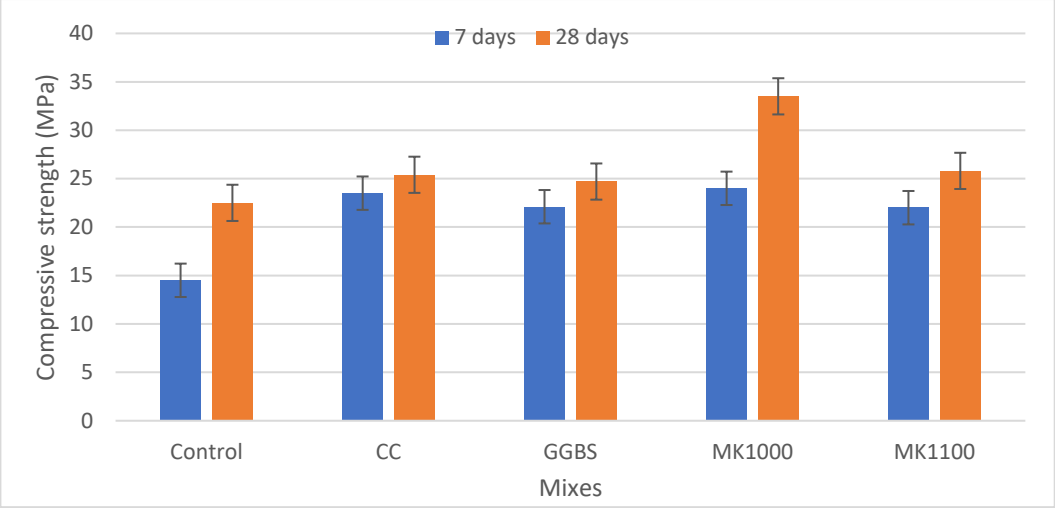

Fig 5.17: Compressive strength development of the pozzolans used for the semi-dry mix

The Strength Activity Index (SAI) of the calcined clay shown in Fig 5.18 for all the pozzolans was more than 0.75. This was an indication of considerable pozzolanic activity, as specified by the ASTM International (2019) standard that recommends mortars having a 20% pozzolan must achieve a strength more than 75% of the control mortar at both 7 and 28 days. According to Donatello, Tyrer, and Cheeseman (2010), if the pozzolans were merely fillers in the mixes and inert, there would be a decrease in the compressive strength of the binary mixes that would correspond to the replacement level of Portland cement in the mixes due to the dilution effect.

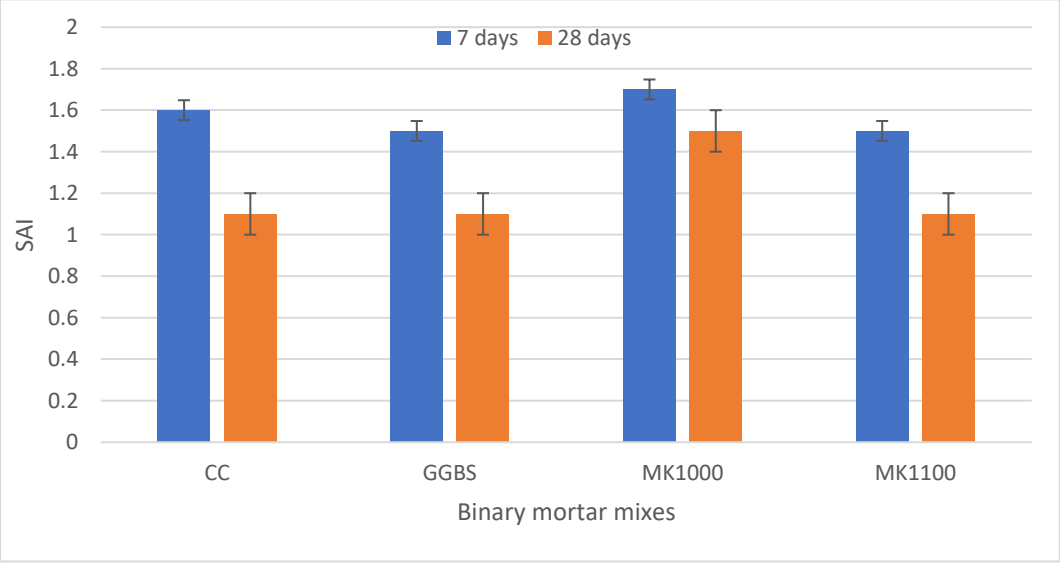

Fig 5.18: SAI of the pozzolans used for the semi-dry mix

5.4.7 Comparison of the compressive strength for variable types of calcined clays proportions of semi-dry pastes

The results of the compressive strength for the various ternary semi-dry pastes mixtures are shown in Fig 5.19. These mixes (see table 4.15) were designed to determine the potential of complete replacement of GGBS with the calcined clay, in a previously optimized ternary blend for a Hydraulically Road Binder (mix design details provided in sub-section 4.2.4). The strength development of the paste mixes that have the same proportion of BPD, BOS and water showed that the mix containing GGBS as the main pozzolan achieved the highest strength at 7 and 28 days. This increased strength could be due to the enhanced latent hydraulic binding property of the GGBS. The results achieved by the four mixes are higher than the optimized mixture of the 52.5%GGBS–42.5%BOS–5% catalyst reported by Mahieux *et. al.* (2007), which had a strength of 11 MPa at 28 days. However, the improvement in the compressive strength of the mixes can be associated with a reduction in the water content, which is known to result in fewer pores and improved paste pore structure. In contrast, Ganjian *et. al.* (2008) reported a higher strength of 30.55 MPa at 28 days for their semi-dry paste mixture 15%PG-5%BPD-80%BOS and water to binder ratio of 0.15. This improved strength produced in the previous study indicated that the BOS has better hydraulic activity compared to the main pozzolans used in this study.

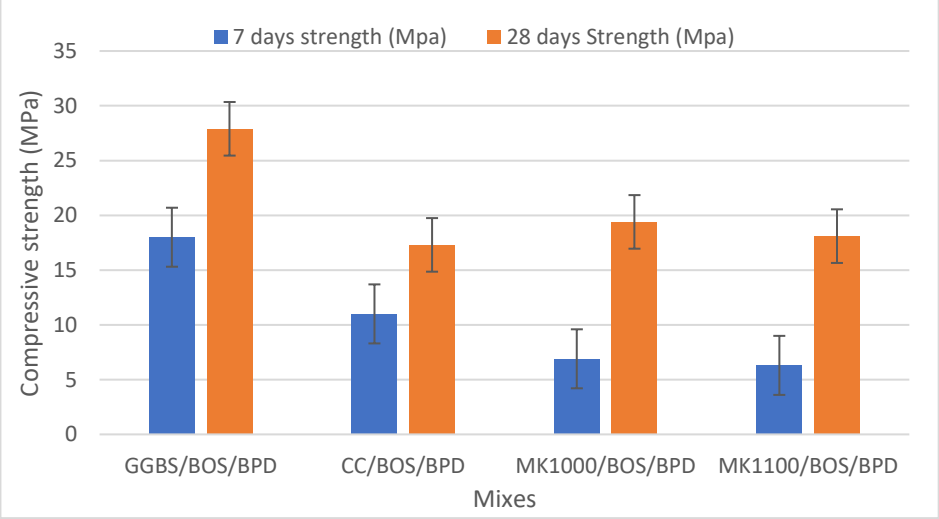

Fig 5.19: Compressive strength development of the ternary semi-dry mixes

From the results presented in Fig 5.19, it can also be noted that BOS has been used to activate the iron-rich calcined clay and produced a hydraulic road binder. In other words, the ternary binder composition showed that it was possible to replace the scarce GGBS with calcined clay

and produce an HRB10 (the 28 days compressive strength of standardized mortars higher than 10 MPa).

5.5 Durability

The four calcined clay geopolymer concretes mixes that were designed based on the molar oxide ratios obtained for the peak strength mortars were tested for durability. The results of the durability performance (chloride ion penetration and freeze-thaw resistances) of the four-geopolymer and PC control concrete mixes are presented in this sub-section.

5.5.1 Chloride permeability of calcined clay geopolymer concrete

ASTM C 1202 classifies chloride permeability as high when the charge passed in a concrete sample is above 4000 C, between 2000 – 4000 C as moderate, and between 1000 – 2000 C as low. (Chi 2016) reported that geopolymer concrete have a moderate to high ion chloride penetrability based on rapid chloride penetration test (RCPT) method. The chloride ion penetration of the control specimen (the Portland cement concrete) was low with the total charge of 1200 C passing through the sample. For the geopolymer concrete samples, the connecting cables generated enormous heat a few minutes after the commencement of the test. An enormous heat was also generated when replacing with connector cables of higher resistance (500 ohms). For safety reasons, the test had to be terminated. It can, therefore, be argued that RCPT is inadequate and unsuitable for geopolymer systems due to the presence of a high alkali concentration in the concrete. Claise (2016) concluded that RCPT tends to measure the current passed and not the actual permeability of the concrete when used for an alkali-activated system. This could be the reason for mixed chloride ion permeability results for geopolymer concrete reported in the scientific literature (Chi, 2016; Bernal *et. al.*, 2011; Al-Otaibi, 2008).

5.5.2 Freeze-thaw resistance of calcined clay geopolymer concrete

The mass loss and residual strength of the various concretes mixes that were subjected to 300 freeze – thaw cycles specified by ASTM C666 were obtained. The mass loss of the PC control and four geopolymer concrete specimens after the 125 and 300 freeze-thaw cycles is shown in Fig 5.20. A mass loss of 2.6% for the blended GC/Na-M-RM was more advanced and exhibited more surface deformation after 125 freeze-thaw cycles as compared to the other geopolymer concrete mixes. For the GC/K-RM, a mass loss of 2.3% was the lowest observed of the geopolymer concrete mixes after 125 freeze-thaw cycles. This improved performance may be

due to the better polycondensation of the potassium silicate activated geopolymer concrete that resulted in the samples having the lowest pore pressure induced by the frost cycles (Davidovits 2015). Moreover, the Portland cement control concrete samples had an accelerated mass loss and severe surface scaling beyond the 125 freeze-thaw cycles. The mass loss of the control concrete increased steadily with the number of freeze-thaw cycles and this is as a result of the internal cracking caused by its hydration product (Divanedari and Eskandarri-Naddaf 2020). Overall, the mass loss percentages of the geopolymer concrete samples were lower than the critical value of 5% after 300 freeze-thaw cycles and suffered slight scaling on the surface irrespective of the activator used.

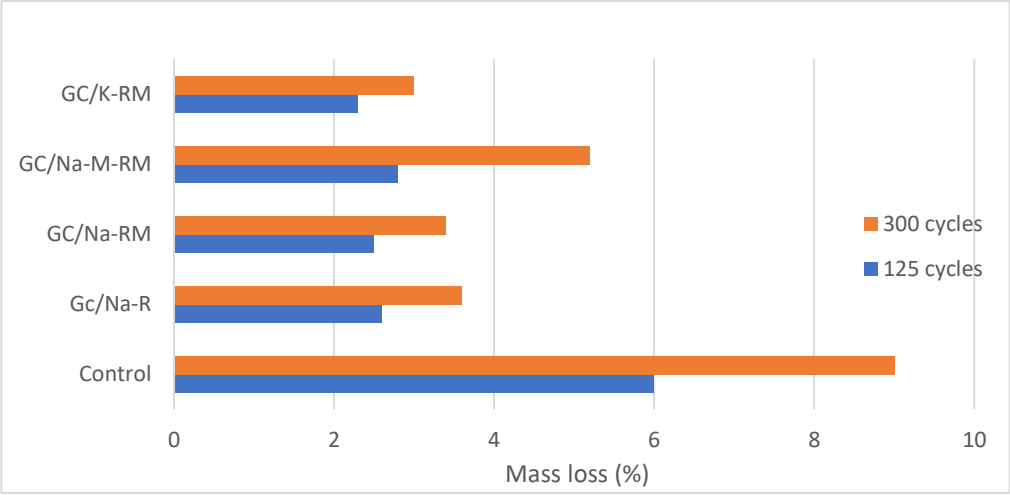

Fig 5.20: Mass loss rate of the concrete specimens

The residual compressive strength of the concrete specimens after 125 and 300 freeze-thaw cycles is shown in Fig 5.21. A decreasing trend in compressive strength of the concretes was observed between 150 and 300 freeze-thaw cycles. After 125 freeze-thaw cycles, the loss of compressive strength reached 25%, and the Portland cement control specimen could then be considered to have been damaged. The frost failure of the control concrete can be associated with the high water to cement ratio of 0.5 that may have induced significant pore pressure. This resulted in the internal cracking of the sample. Previous works had established that addition of 5% air entrainment agent is required for a frost-resistant PC concrete (Claisse, 2016). In this study, an air entrainment agent was not added to the PC control concrete in order to ensure a like to like comparison with the geopolymer concrete mixes.

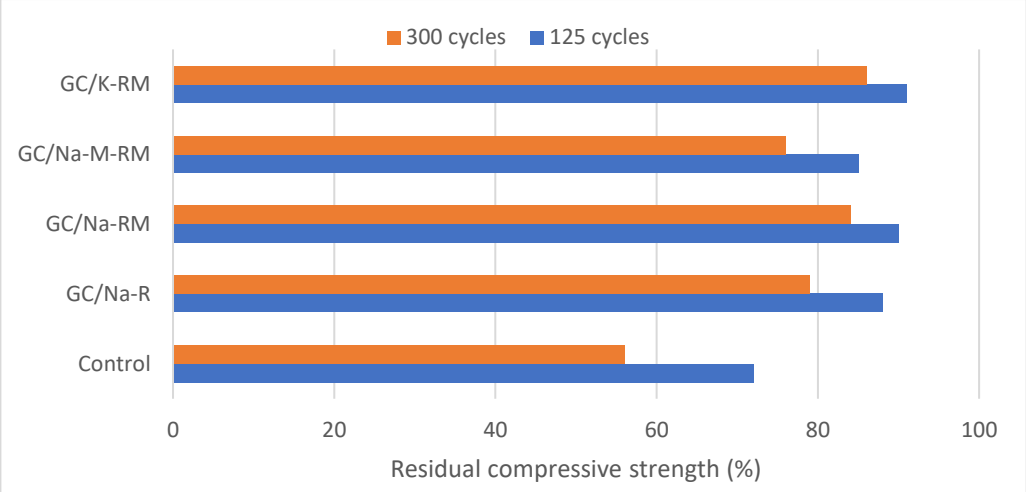

Fig 5.21: Residual compressive strength of the concrete specimens after freeze-thaw cycles

Moreover, Fig 5.21 shows a similar trend with the mass loss for the geopolymer concrete. Overall, the superior frost resistance of the geopolymer concretes compared to the PC concrete can be attributed to the reaction product (Zhao et al 2019). On one hand, the main reaction product of the PC concrete is a hydrated calcium silicate gel that suffers expansion and contraction as a result of freezing and thawing, that is accompanied by increase pore pressure in the sample. The increase pore pressure disturbs the internal structure of the concrete that then caused significant loss of mass and strength. On the other hand, the main reaction product of the geopolymer concretes is an aluminosilicate gel produced by polycondensation and polymerization reaction. Water is therefore released during the synthesis and not incorporated in the binding phase. This minimize the pore pressure that can be induced in the geopolymer concrete due to freezing and thawing. Thus, better frost resistance was observed.

Furthermore, it can also be seen from Fig 5.21 that the GC/K-RM suffered the least compressive strength loss of 14% after the 300 freeze-thaw cycles. Also, the blended mix had the least residual compressive strength of 76% after 300 freeze-thaw cycle for the geopolymer concrete mixes. This demonstrates relative weak performance of the blended activator for calcined lateritic clay, despite having similar molar oxides composition with the other geopolymer mixes. This is unlike PFA based geopolymers that achieve superior performance when activated using blended activator. This result suggest that a relatively less stable polymeric network structure is produced by the blended activator, which has enhanced potential to cause the cleavage of the calcined clay due to its sodium hydroxide component (Liew et al 2016). However, because of the reduced silicate component of the blended

activator, fewer silicate molecules are involved in the formation of the poly(sialate) as computed in table 4.7.

5.6 Microstructure of mortar and concrete

The micrographs obtained for the various mortar and concrete mixes are presented in this sub-section. The SEM images provide insight into the density, homogeneity and shape of the internal structure which is in part determined by the reaction.

5.6.1 SEM analysis of the GGBS AAM and calcined clay geopolymer mortar

The microstructure for the 8 M sodium hydroxide solution activated slag (GGBS –32SH) mortar cured under ambient conditions for 28 days (presented in Fig 5.22) revealed an undensified and loosely packed structure. The result further shows the precipitation of a sponge-like matrix globular unit on the surface with a propagated continuous crack depicted by the arrow (**a**). The uncompacted and dispersed structure of the sample can be associated with its fair strength performance (19 MPa at 28 days) and low density measured for this mix.

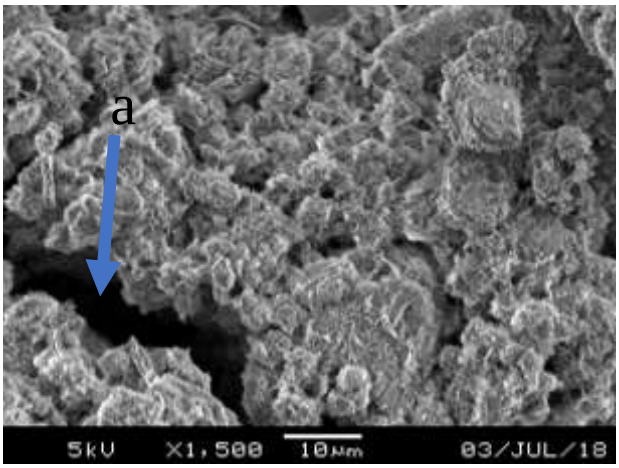

Fig 5.22 SEM micrograph of 8 M NaOH activated GGBS mortar

The microstructure of the 44.1% $Na_2SiO_3.5H_2O$ solution (GGBS – 44.1SSP) mortar cured for 28 days under ambient condition (shown in Fig 5.23) reveal a compact matrix that precipitated a hexagonal shape $Ca(OH)_2$ (**a**) and a dis-ordered tobermorite-like hydrated calcium alumionsilicatesilicate (C-A-S-H) gel (**b**), resulting in the high strength mortar (34 MPa at 28 days).

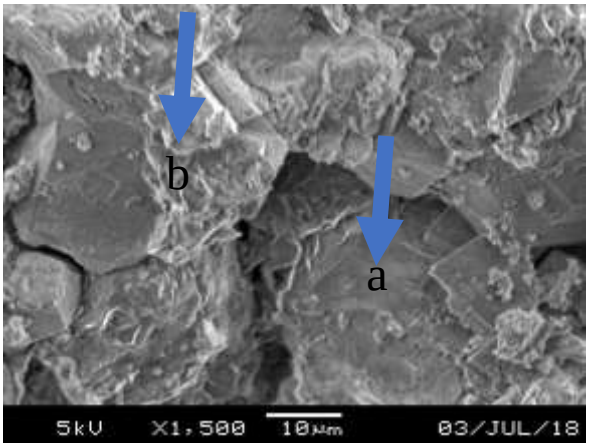

Fig 5.23 SEM micrograph of $Na_2SiO_3.5H_2O$ activated GGBS mortar

The SEM image for the CC–32SH mortar that was activated with an 8 M NaOH solution to calcined clay mass ratio of 1:1 and cured under sealed conditions for 28 days is presented as Fig 5.24. The micrograph revealed a densified and packed structure (**a**), as well as pores (**c**), which may be associated with the low strength achieved by the mix. The result further showed precipitation of a sponge-like, globular morphology on the surface resulting from the alkali activation. Also, Fig 5.24 revealed a propagated crack (b) on the surface of the sample. This crack may not necessarily be caused by drying shrinkage, but, by the loading applied on the sample during the compression test.

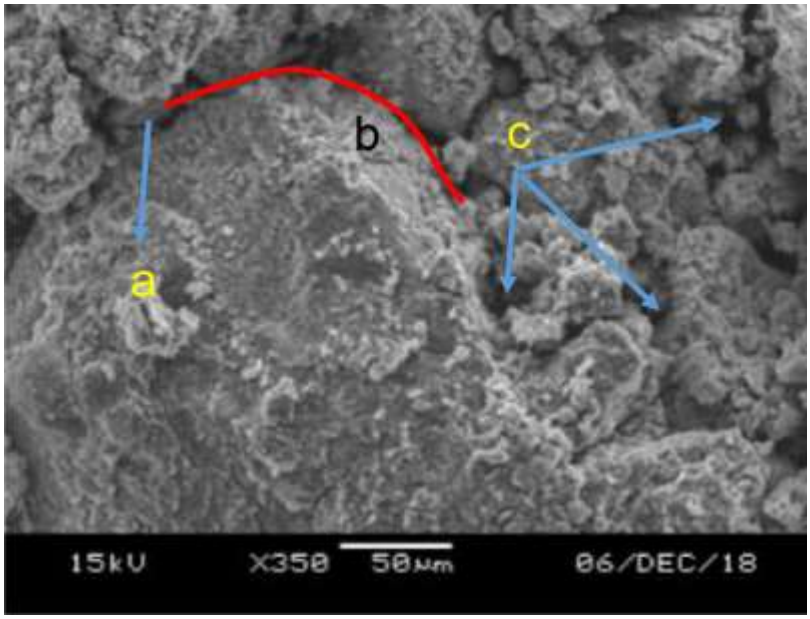

Fig 5.24 SEM micrograph for CC – 32SH mortar

Fig 5.25 presents the SEM image of the CC–44.1SSP mortar. The mortar was produced by activating the calcined clay with the 44.1% $Na_2SiO_3.5H_2O$ solution and cured for 28 days under sealed conditions. The micrograph showed a bulk, undensified and uncompacted, discrete structure (a). This may be the cause of the poor strength performance by this mix. The heavy

presence of the loose particles might have prevented the development of a uniform geopolymer network throughout the sample. The loose and dispersed structure was probably caused by the partial dissolution of the granular sodium silicate pentahydrate which was dissolved under normal atmospheric conditions. This is in addition to the dilution effect of the chemically bound water in the activator that may have hindered the dissolution of the residual raw materials and the precipitation of free silicate that will form the Si-O-Al polymeric network.

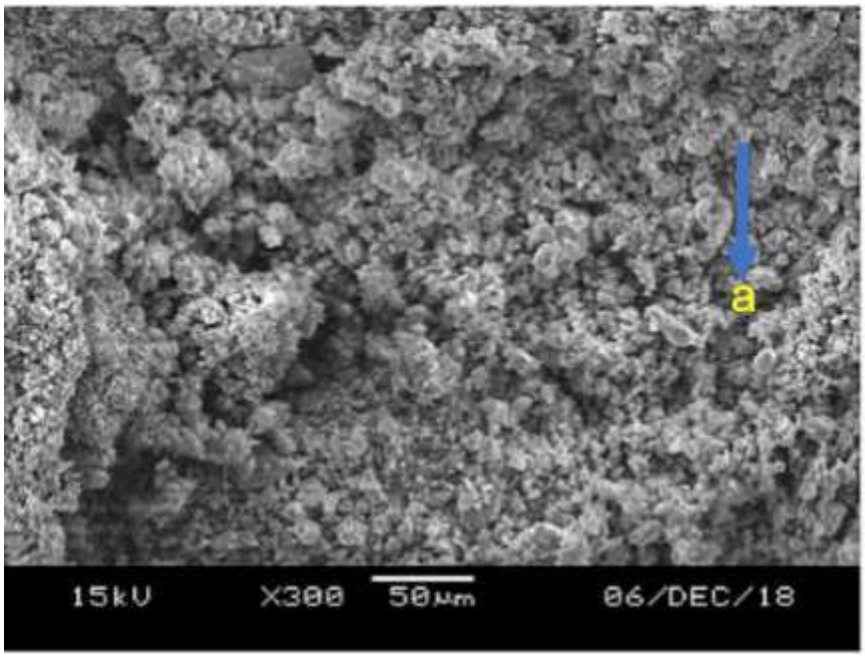

Fig 5.25: SEM micrograph for CC – 44.1SSP mortar

The micrograph of the CC-54.5SS mortar produced with a 54.5% Na_2SiO_3 solution to calcined clay mass ratio of 1:1 and cured for 28 days under sealed conditions is shown in Fig 5.26. The SEM image shows a glassy-like appearance typical of a geopolymer surface. The dense and compact structure has some sharp edges with the arrow (a) pointing to a saddle of sponge-like morphology precipitated on the surface matrix.

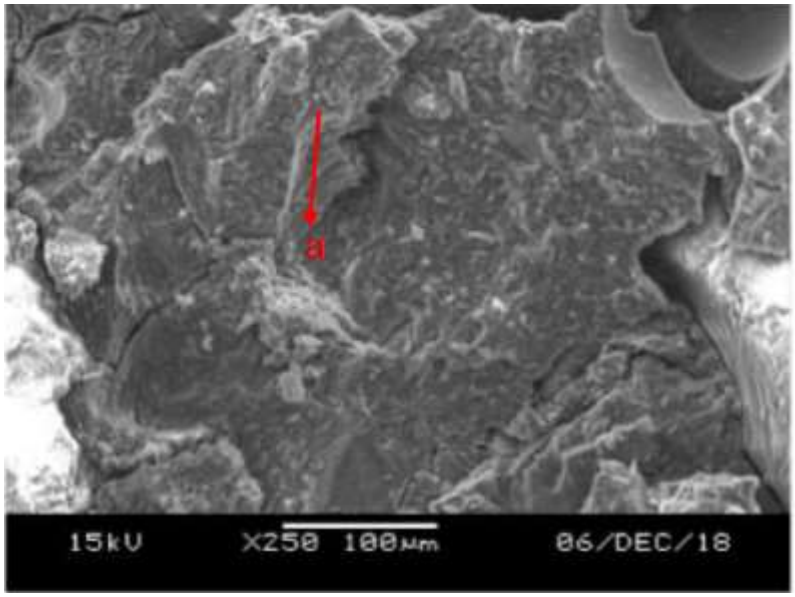

Fig 5.26: SEM image for CC - 54.5SS mortar

When comparing the SEM micrographs presented in Fig 5.24 to Fig 5.26, it is evident that the resulting mortar of Mix CC–44.1SSP consisted of more unreacted calcined clay and voids than Mix CC-54.5SS. It is also clear that the use of a 54.5% sodium silicate solution can be attributed to the increase in soluble silicate in the geopolymer system. This caused the development of a compact and dense structure due to the soluble silicate that enhanced the depolymerisation of the aluminosilicate and subsequent precipitations of more geopolymer gels.

5.6.2 SEM analysis of the calcined clay geopolymer concretes

Fig 5.27 – 5.30 present the SEM images of the four geopolymer concrete samples produced in this study. The SEM image of GC/Na-R samples shown in Fig 5.27 revealed a dense and homogenous morphology, with sponge-like globular unit geopolymeric gels on the surface. Similar but more dense morphology is revealed by Fig 5.28 for the GC-/Na-RM sample which had increased binder content in the system. The micrograph for the GC/Na-M-RM shown in Fig 5.29 reveals a densified and packed structure (**a**), as well as loose and discrete geopolymer matrix (**b**) that may be the cause of the reduced strength performance of the mix. In other words, the morphology shows precipitation of a sponge-like matrix indicated by globular units on the surface resulting from the geopolymerization.

A glassy morphology with fine grained matrix at the surface is revealed by the GC/K- RM mix (Fig 5.30) which is caused by the Si-O-Al polymeric network of the sample. A similar gel-type formation which is distinct from crystalline growths associated with C-S-H type cement was obtained by McIntosh and Soustous (2014) for a potassium silicate activated calcined

lithomarge geopolymer paste. An EDX analysis of the paste showed an elemental composition by weight (%) of: O K (19.94%), Al K (12.65%), Si K (27.17%), K K (22.17%), Fe K (9.29%) and Ca K (8.78%).

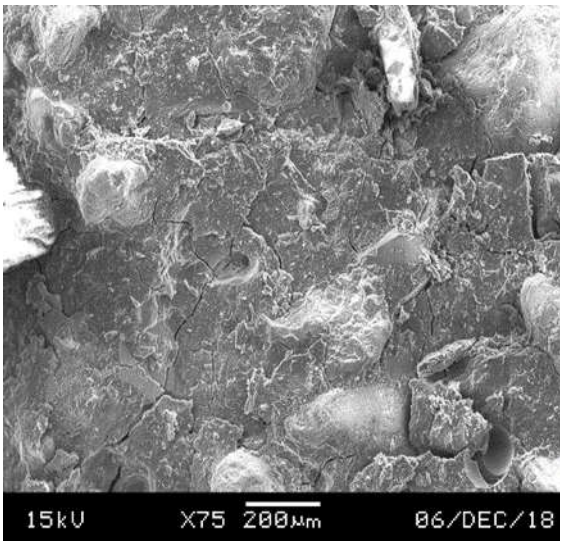

Fig 5.27 SEM images of the GC/Na –R

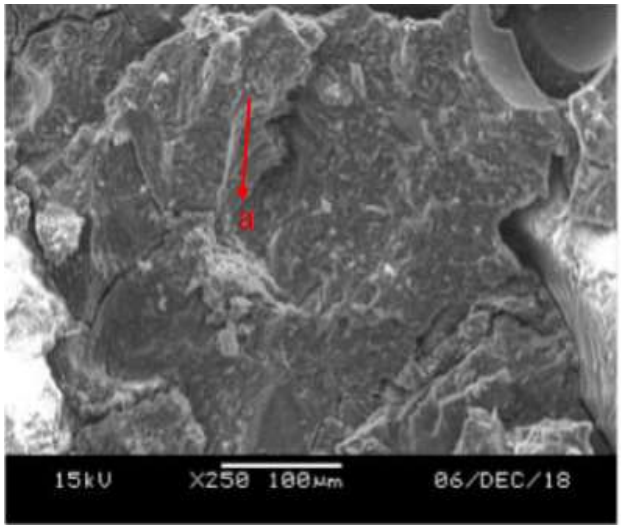

Fig 5.28 SEM images of the GC-Na/RM

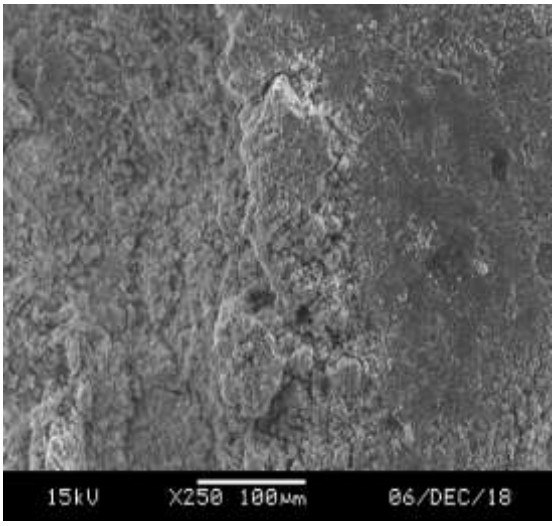

Fig 5.29 SEM images of the GC/Na-M-RM

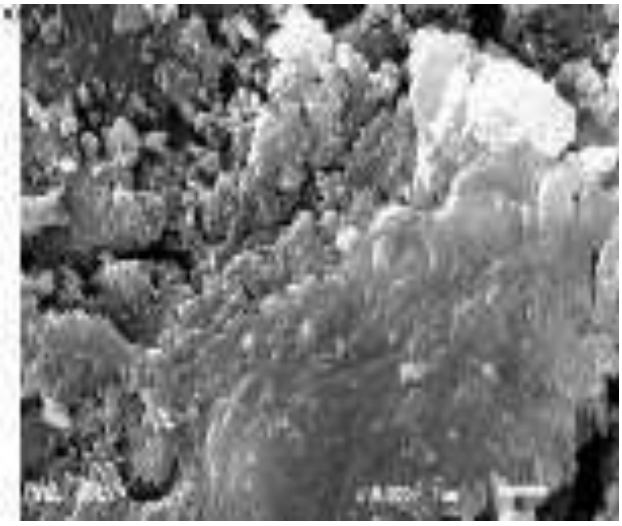

Fig 5.30 SEM images of the GC/K-RM

5.7 XRD analysis of the calcined clay geopolymer paste, mortar, and concrete

The XRD spectra and semi-quantitative analysis for the calcined clay and its resultant geopolymer paste, mortar and concrete are presented in this sub-section.

5.7.1 Mineralogical characterization of the calcined clay geopolymer paste

Fig 5.31 shows that the calcined clay powder and its sodium silicate activated geopolymer paste exhibited similar peaks and amorphous humps at the various 2θ positions. However, at all the 2θ angles, the paste had a lower intensity compared to the raw calcined clay: except at

the location 32–36° 2θ for the Co(Kα). The amorphous halo at this location in the paste can be assigned to the geopolymer matrix. This phase is similar and conforms to the geopolymer matrix at the location 27 - 29° 2θ for Cu (Kα) that was defined by Davidovits and Davidovits (2020). The slight shift to the right of the location was caused by the Co (1.7903Å) Kα x-ray source used in this study as they had a longer wavelength than the Cu Kα tubes (~ 1.54 Å) used by the referenced authors. The effect of this change of wavelength is, by Bragg's law, to shift the peaks to higher angles and can be seen in this context. Furthermore, the similarity of the XRD spectra in Fig 5.31 is an indication that the various crystalline materials in the calcined clay did not seem to have fully reacted in the geopolymerisation. This is in agreement with previous study (Lawther *et al.* 2016).

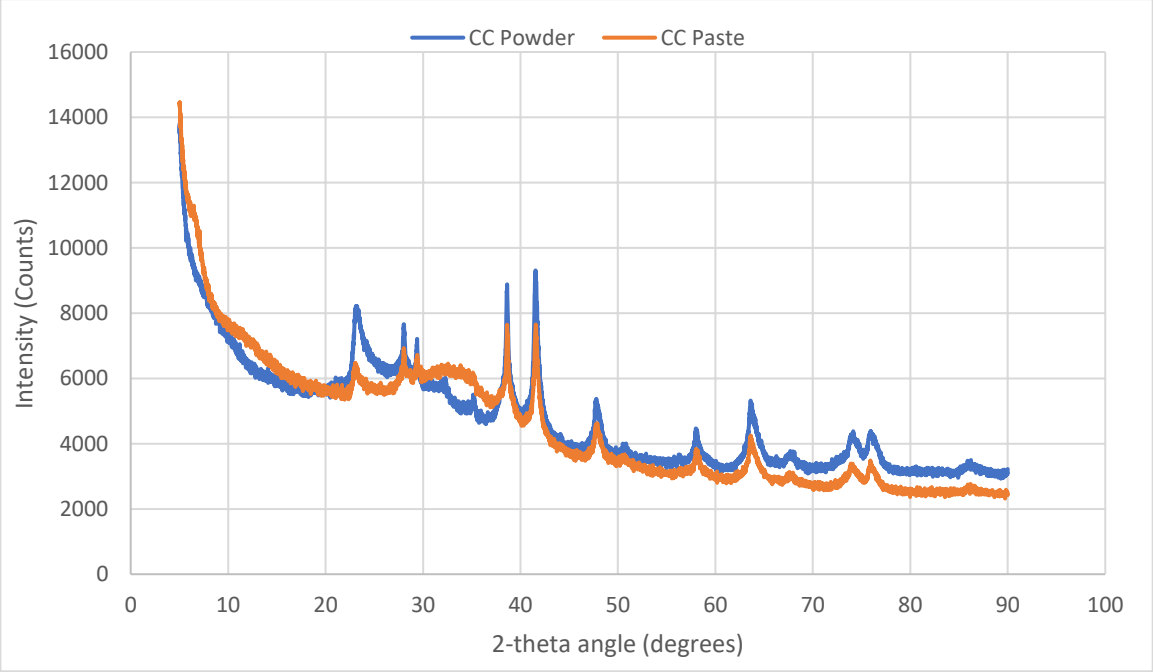

Fig 5.31 Comparing the XRD spectra of raw calcined clay and it's geopolymeric paste

Fig 5.32 presents the various minerals obtained by analysing the XRD spectra of the calcined clay geopolymer paste using the PANalytical X'pert high score software which has a database for semi-quantitative minerals identification. The sanidine mineral identified in Fig 5.32 has been shown in a structural molecular model for Ca based geopolymer matrix by Davidovits (2015) to be the analogue of the geopolymeric framework of K-Poly(sialate-disiloxo) corresponding to Si:Al of 3.

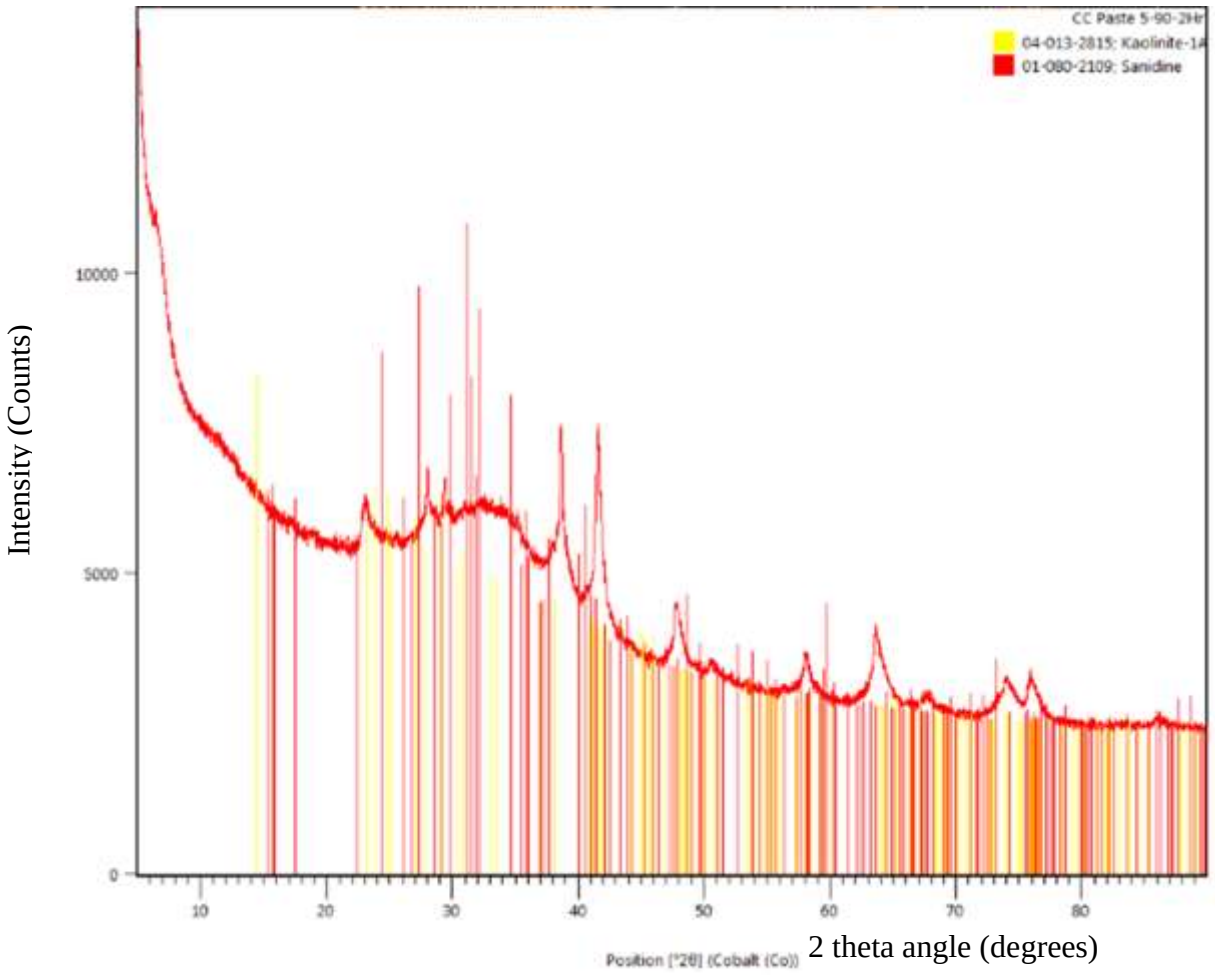

Fig 5.32 XRD analysis of calcined clay geopolymer paste

The semi-quantitative analysis of the various mineral phases shown in Fig 5.32 is presented in table 5.3. It can be seen that no trace of the dubious goethite and magnetite minerals was found in the XRD spectra of the calcined clay. This confirmed that they had been transformed into hematite during the calcination. This is in agreement with the findings of (McI*ntosh et al.*, 2015).

Table 5. 3 semi-quantitative analysis of the XRD spectra of calcined clay geopolymer paste

Compound name	Chemical formula	Crystal system	Semi Quant.(wt%)
Sodium Iron Phosphate	Na Fe P O_4	Orthorthombic	6
Iron Oxide	Fe_2O_3	Rhombohedral	7
Calcium Sodium Aluminium Silicate Hydroxide Phosphate Carbonate	Ca6.235 Na1. 594 (Al4 Si6 023) (OH)1.528 (PO4)0.5 (CO3)0.5	Tetragonal	17
Sodium Calcium Aluminium Silicate	(Ca, Na)(Si, Al)4 O8	Anorthic	10

Potassium Aluminium Silicate Hydroxide	K. Al3 Si3 O10 (O H)2	Monoclinic	12`
Potassium Magnesium Aluminium Iron Silicate Hydroxide	K.Mg0.18 Fe0.16 Al2.35 Si3.3 O10 (O H)2	Hexagonal	9
Aluminium Silicate Hydroxide	Al2 Si2 O5 (O H)4	Anorthic	2
Potassium Aluminium Silicate	K (Al Si3 O8)	Monoclinic	10
Potassium Aluminium Hydrogen Phosphate	K Al (H P O4)2	Anorthoc	15
Magnesium Silicon Oxide	Mg Si O3	Orthorhombic	12

5.7.2 Phase characterization of the calcined clay geopolymer mortars

The XRD spectra of the samples - SSP 0.7, SH 0.7 and SS 1.0 and 1.5 are presented in Fig 5.33 – 5.35 respectively. The geopolymeric activity of the samples were evaluated based on the peak intensity of some of the phases in the samples. It can be observed from Fig 5.33 that, the Quartz peaks of the sample at 2-theta angle of 24.2^{o} and 31^{o} is highest in the SSP 0.7 mix probably due to the partial reaction of the SSP which enriched the system with silicate. Analysis of the sodium hydroxide activated calcined clay mortar showed the zeolites peaks at 2-theta angle of 8.3, 27.9 and 35.9°, as well as muscovites (from the unreacted precursor) intensity peaks at 2-theta angle of 31 and 36°. These minerals phases are a result of the effective dissolution of the precursor by the 32% NaOH solution, which produced the less stable N-A-S-H in the system.

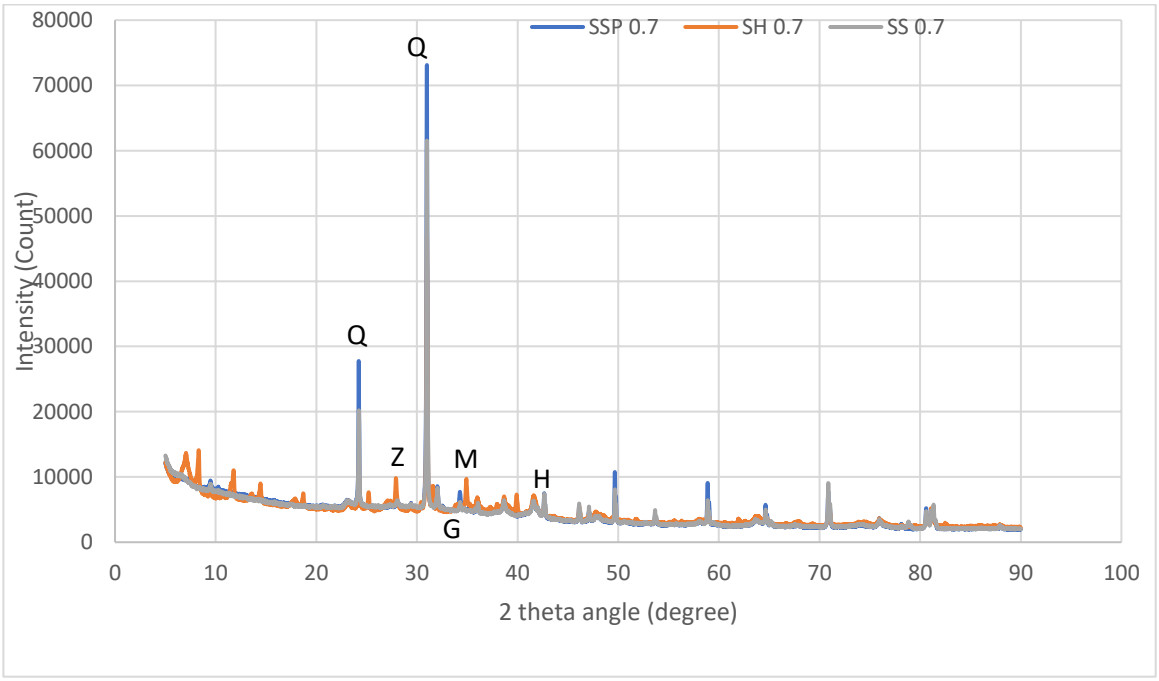

Fig 5.33 XRD spectra of group three mortar mixes at 28 days

(Z is zeolite, M is muscovite, G is Geopolymer matrix, Q is Quartz, H is hematite)

The XRD spectra presented in Fig 4.33 also shows the geopolymer matrix (Na/K–Al–Si–O) intensity amorphous halo at 32.5-36º, as well as hematite's peaks at 2-theta angle of 42.7 and 72°. A more details analysis of the XRD spectra of the group three mixes are presented in appendix 2. Moreover, the summary of the phases found in the group three mixes is presented in table 5.4.

Table 5 4 Summary of the mineralogical phases of group three mixes

Mineral	Chemical formula	SSP 0.7	SH 0.7	SS 0.7
Hematite	Fe_2O_3	X	x	X
Quartz	SiO_2	X	x	X
Muscovite	$K_{0.92}Na_{0.08}Al_{1.88}Fe_{0.12}Mg_{0.04}(Al_{1.08}Si_{2.92}O_{10})(OH)_{1.89}F_{0.11}$	X	x	X
Zeolite	$Na_{24}Al_{24}Si_{24}O_{96}(H_2O)_{64.8}$		x	
Na/K-Si-O-Al-O	Na/K ($AlSi_3O_8$)			X
Calcite	$CaCO_3$			X
Blodite	$Na_2Mg4(SO_4)4(H_2O)$		x	
Kaolinite	$Al_2Si_2O_5$4(OH)	X		

The XRD spectra in Fig 5.34 and 5.35 show similar mineralogical phases, but of varied intensities.

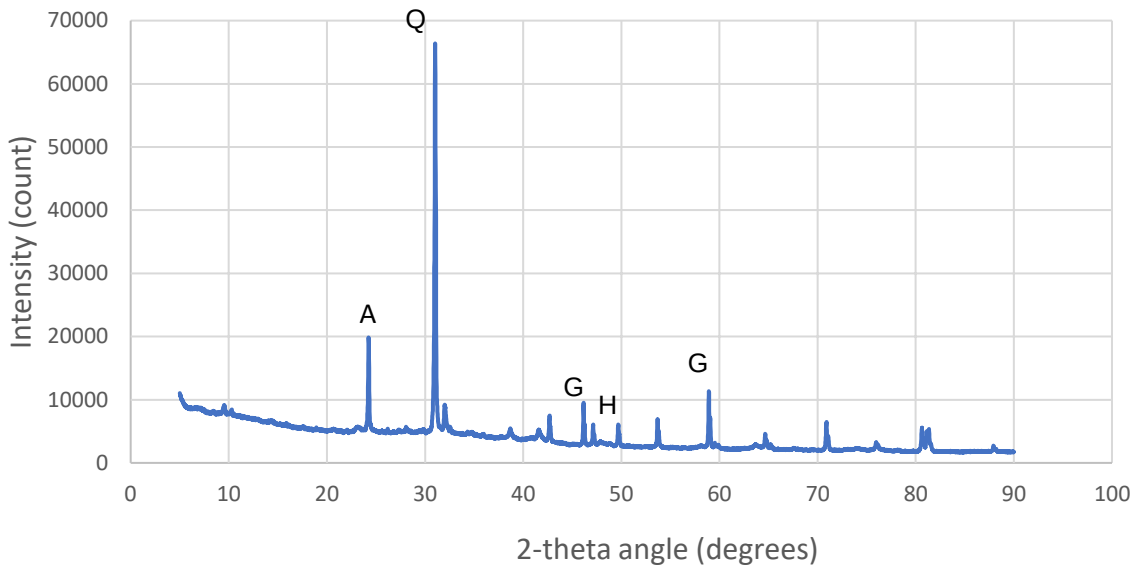

Fig 5.34 XRD for the CC SS 1 mortar at 28 days

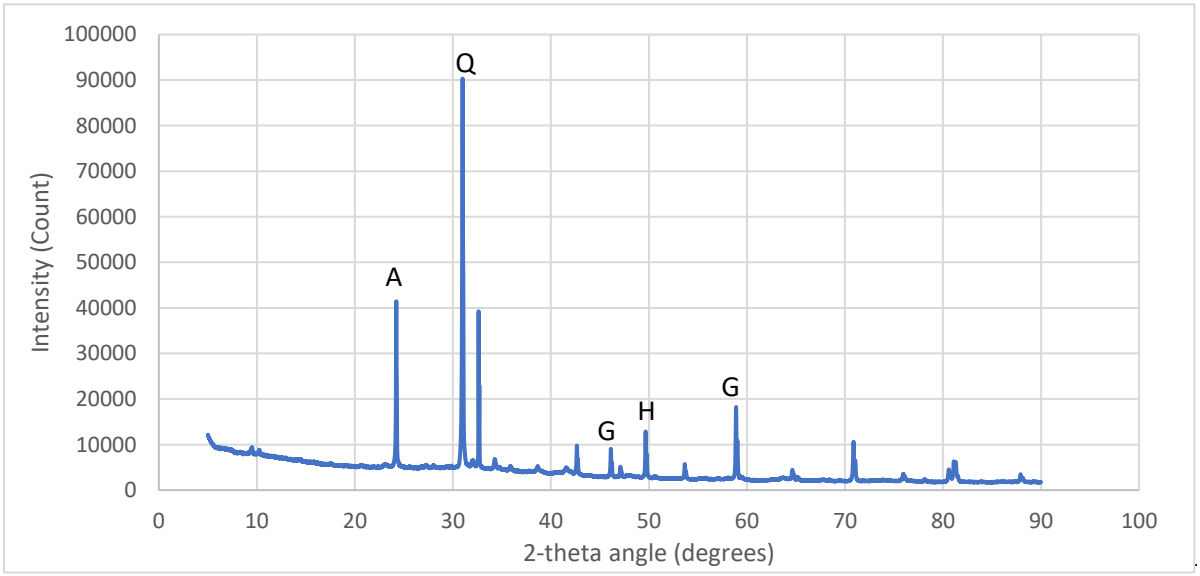

Fig 5.35: XRD for the CC SS 1.5 mortar at 28 days

(A is anatase; G is Geopolymer matrix;; Q is Quartz; H is hematite)

The XRD analysis of the SS1.5 mortar showing the geopolymer matrix and muscovite phases with the other mineral layers presented in Fig 5.36 hidden.

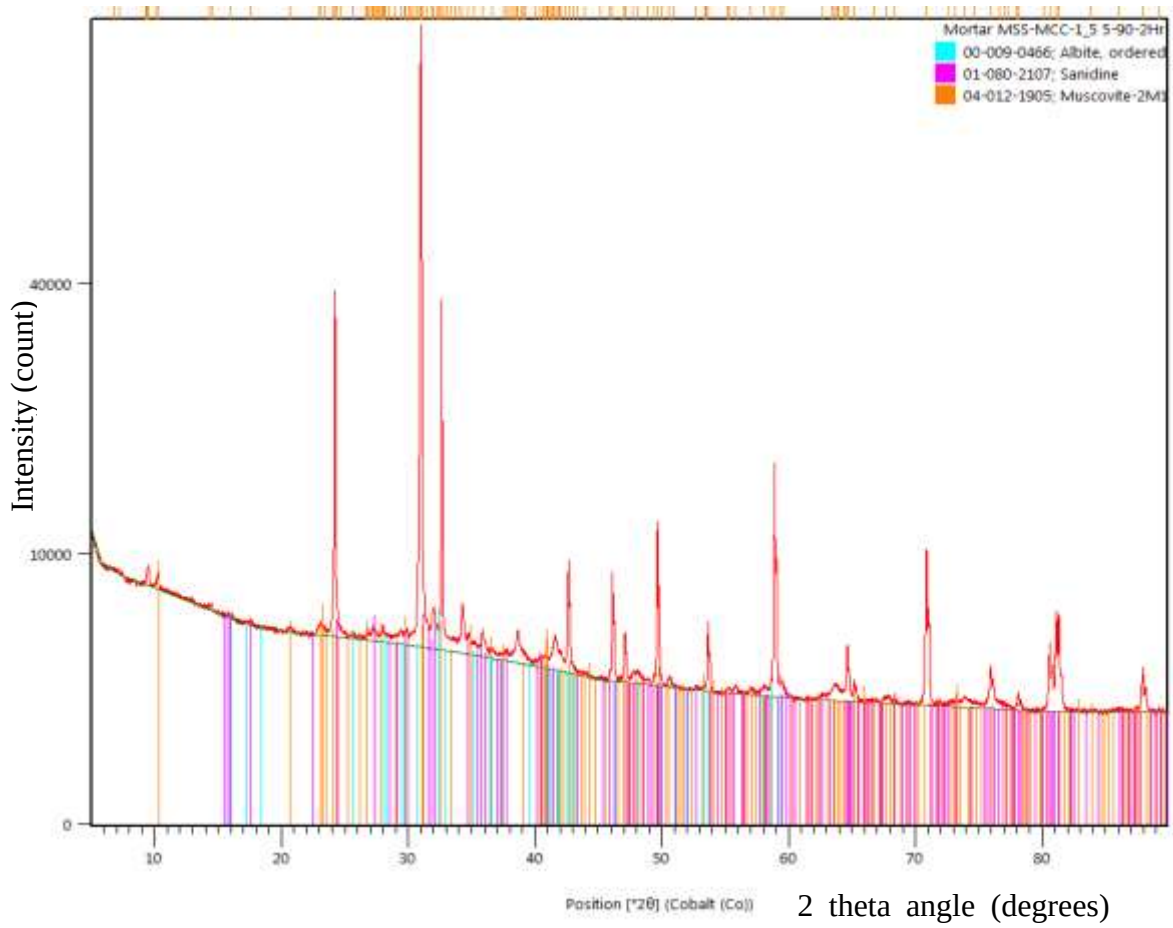

Fig 5.36: XRD analysis of the SS1.5 calcined clay geopolymer mortar

The albite and sanidine mineral frameworks identified in Fig 5.36 are geopolymeric frameworks that are similar to the Na-Poly(sialate-disiloxo) and K-Poly(sialate-disiloxo), as reported in Davidovits (2015). These geopolymeric frameworks have a Si:Al of 3. Thus, Fig 5.36 confirms that the calcined lateritic clay geopolymer is only partially crystalline, containing ordered domains with structures similar to the Na-feldspar, albite and the K-feldspar, sanidine.

5.7.3 Phase characterization of the calcined clay geopolymer concrete

Fig 5.37 and 5.38 show the XRD spectra for the calcined clay geopolymer concrete activated with the high viscosity sodium silicate solution, but varied binder content. The mix with the higher binder content (GC/Na-RM) exhibited more semi-crystalline mineral phases and broader amorphous humps. This feature is an indication of its advance geopolymeric activity. Furthermore, the XRD spectra for the geopolymer concrete showed traces of a synthetic goethite that was not found in the analysed paste, mortar, or raw calcined clay (see appendix 2 for more analysed spectra). The semi-quantitative analysis for the GC/Na-RM geopolymer concrete is presented in table 5.5.

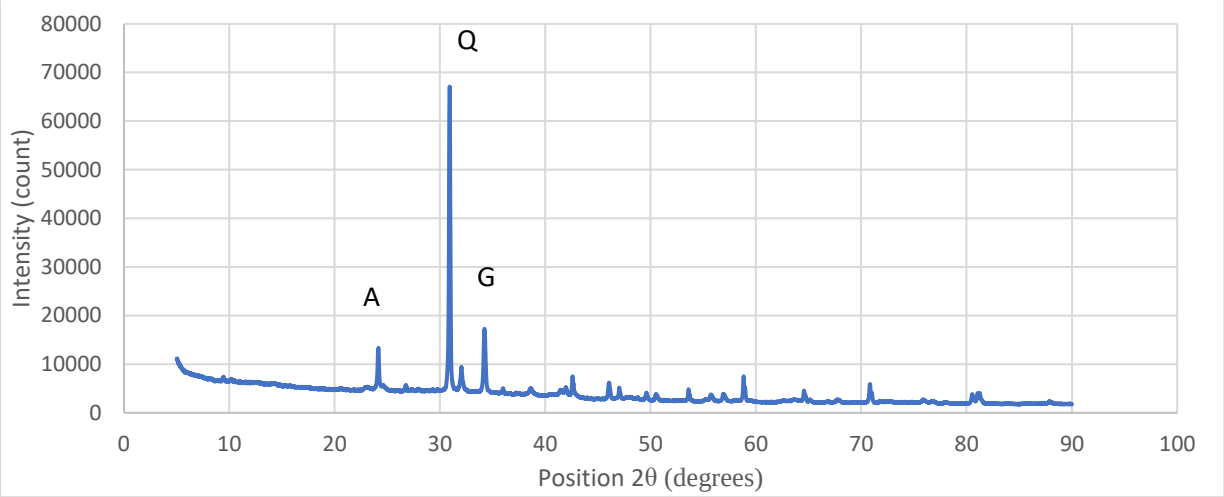

Fig 5.37: XRD results of GC/Na-RM concrete

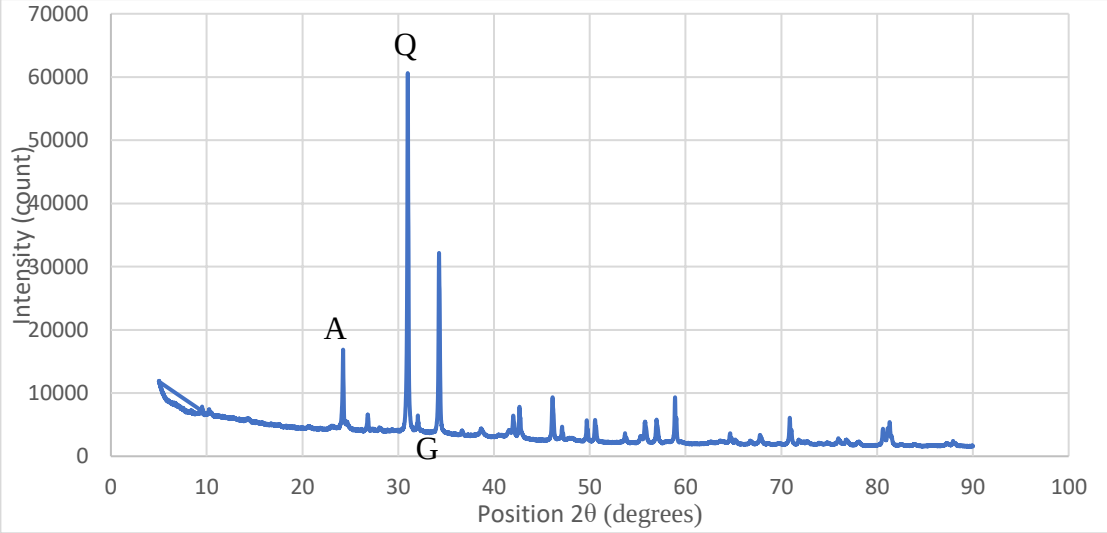

Fig 5.38: XRD results of GC/Na-R concrete

Table 5 5 Semi-quantitative analysis of the XRD spectra of GC/Na-RM concrete

Compound name	Chemical formula	Crystal system	Semi Quant.
Calcium Carbonate	Ca(CO3)	Rhombohedral	17
Iron Oxide	Fe_2O_3	Rhombohedral	2
Iron Oxide Hydroxide	Fe O (O H)	Orthomthombic	3
Titanium Oxide	Ti O2	Tetragonal	4
Potassium Sodium Aluminum Silicate	K.0.88 Na0.12 Al Si3 O8	Anorthic	18
Potassium Sodium Magnesium Aluminum Iron Titanium Silicate Hydroxide	(K0.99 Na0.05) (Al1.51 Mg0.32 Fe0.18 Ti0.03) (Si3.4 Al0.6 O10) (O H)2	Hexagonal	17
Potassium Aluminum Silicate Hydroxide	K (Al2.9 Si3.1 O10) (O H)2	Anorthic	20
Silicon Oxide	Si O2	Tetragonal	-
Potassium Sodium Aluminum Silicate	K0.5 Na0.5 Al Si3 O8	Anorthic	18

5.8 Functional groups identification by infra-red spectroscopy

The FTIR is a type of infra-red spectroscopy that works by measuring the amount of light absorbed by the bonds of vibrating molecules to provide a molecular fingerprint. In other words, the test is used to estimate the relative quantities of different constituents in samples, as well as assess the molecule's vibrations to give facts on the geopolymeric network. The FTIR spectroscopy was performed on the crushed dried fragments of the mortar and concrete samples using a Nicolet iS5 FT-IR machine in transmittance mode (interval of wave number ranging was 4000 – 600 cm^{-1}). The molecular vibration of the various calcined clay mortar and concrete that enabled the characterization of their functional groups are presented in this sub-section. The bands produced by the samples were compared with reference database which enabled correct assignment of functional groups. Non relevant functional groups were not considered. For instance, the functional group (C-O stretch) at ƛ= 1000 cm-1 was not analyzed because the band is not associated with geopolymers, as revealed by the various reference database

5.8.1 Functional groups identification for the calcined clay geopolymer paste and mortars

The infrared (IR) curve for the calcined clay geopolymer paste is presented in Fig 5.39. Four distinct broad peaks can be seen in the region of 950 cm^{-1}, 1350 cm^{-1}, 1650 cm^{-1} and 3350 cm^{-}

[1] which correspond to the Si-O, Al–O, H-O–H and O–H respectively. According to Elimbi, Tchakoute, and Njopwouo (2011), the bands at 3450 – 3480 cm^{-1} and 1650 cm^{-1} indicates adsorbed atmospheric water, that are notably present in metakaolin-based geopolymers. The non-smooth IR curve was due to the presence of iron in the calcined clay that caused the noise in the dried sample.

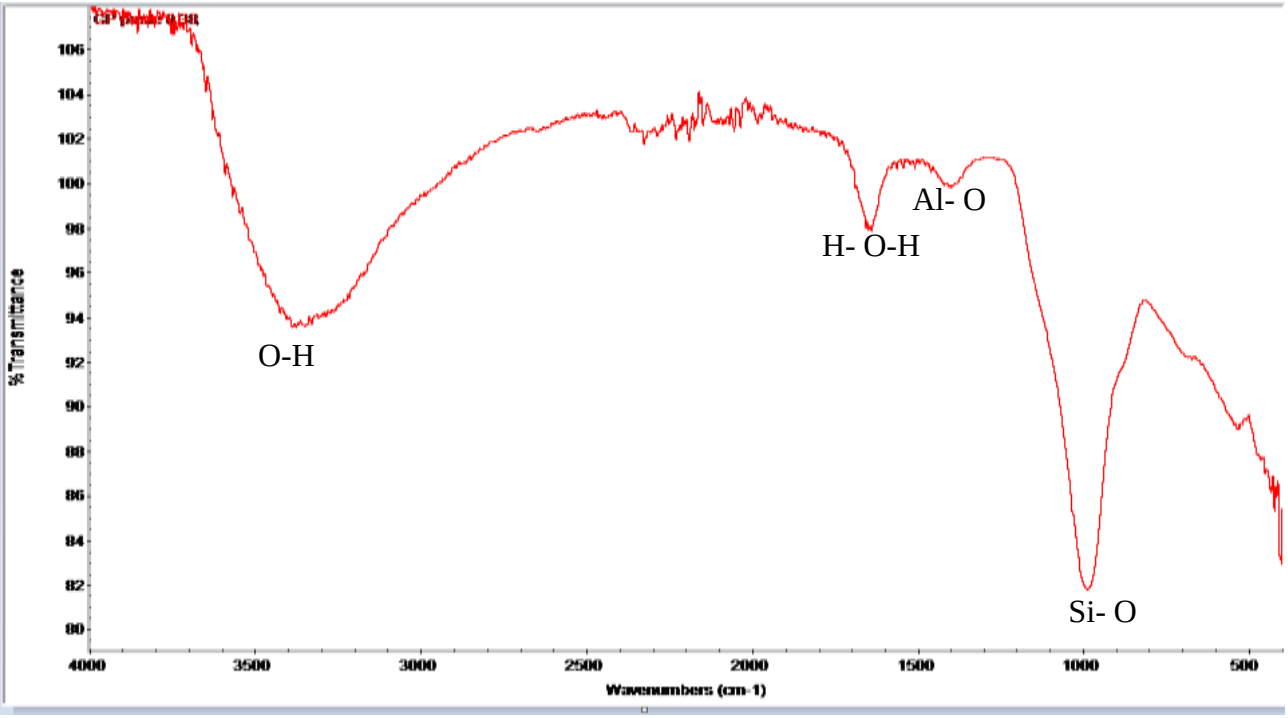

Fig 5.39: IR curve for the calcined clay geopolymer paste

Fig 5.40 – 5.42 shows the IR curves of the group three mortar samples: mixes SSP 0.7, SH 0.7 and SS 0.7. For the SSP 0.7 system shown in Fig 5.40, the decrease in the broad peak in the region of 950 cm^{-1}, which is assigned to the Si–O stretching, can be attributed to the partial and weak nature of the geopolymerisation reaction. The Fe–O–Fe stretching was found at 2350 cm^{-1} in the IR curve. This indicates that the hematite remained in the hardened sample even after activating the calcined clay with the sodium silicate pentahydrate solution.

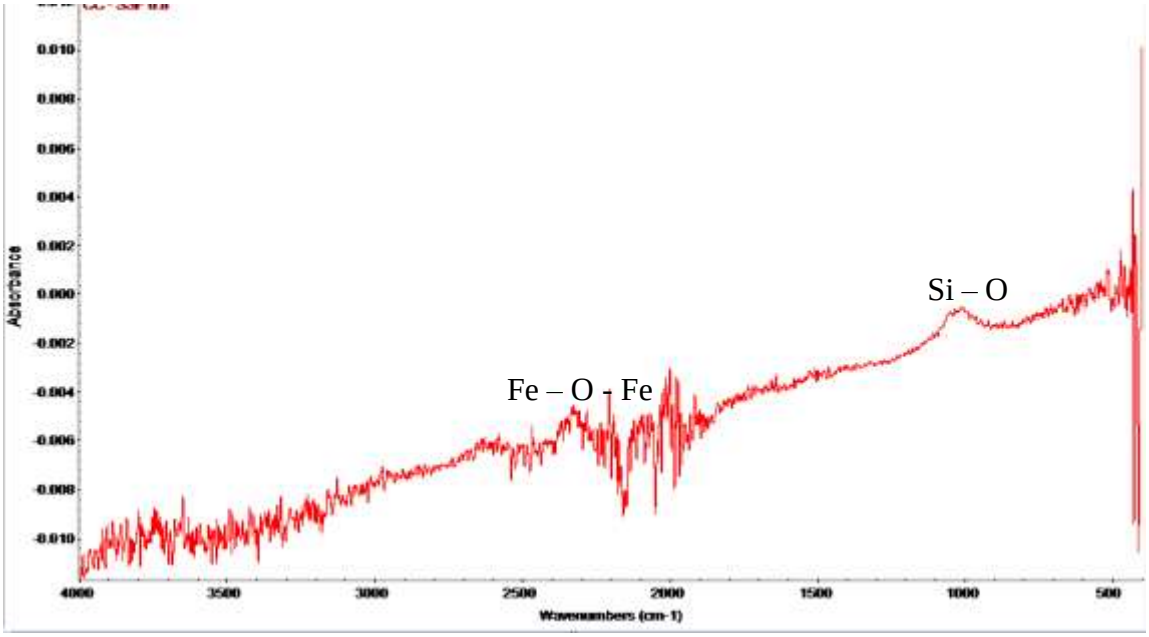

Fig 5.40 IR curve for the SSP 0.7 mortar

For the SH 0.7 synthesized mortar, both the broad band in the region of 3,250 cm^{-1} and the peak at 1,645 cm^{-1} can be attributed to the O-H bonding of water in the system, as shown in Fig 5.41. The narrowing of the Si-O symmetrical stretch is caused by the strong dissolution of the aluminosilicate in the calcined clay. This may be the reason for the weak binding phase characterized by the high Na:Si composition of the mix.

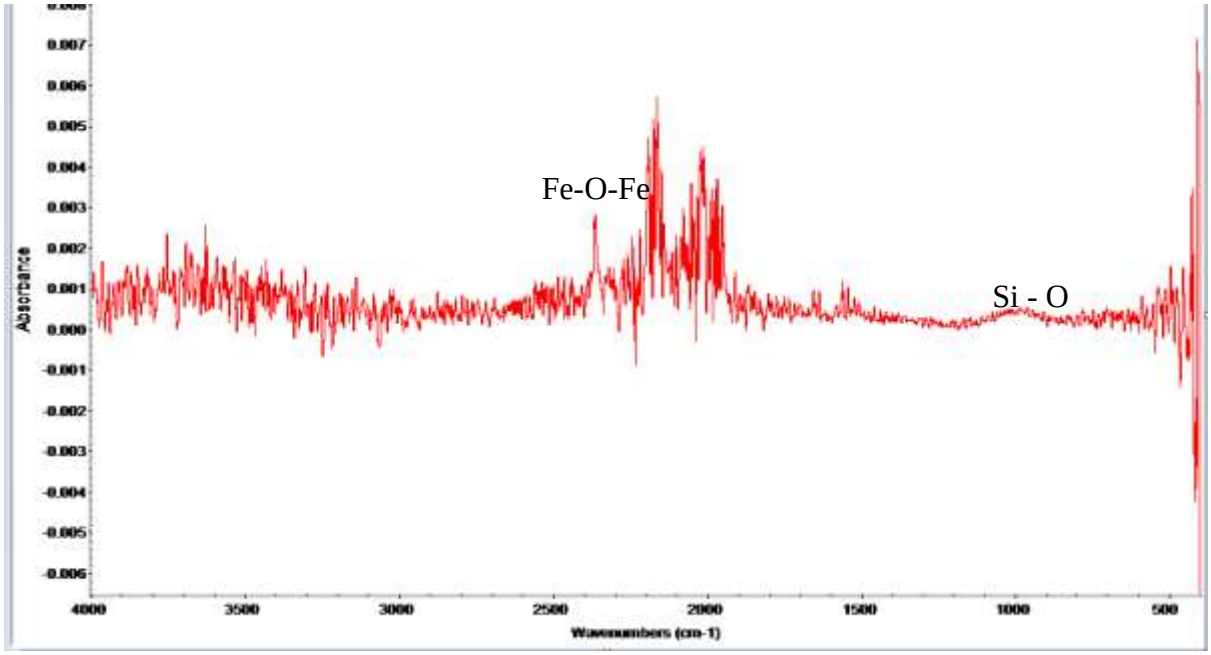

Fig 5.41: IR curve for the SH 0.7 mortar

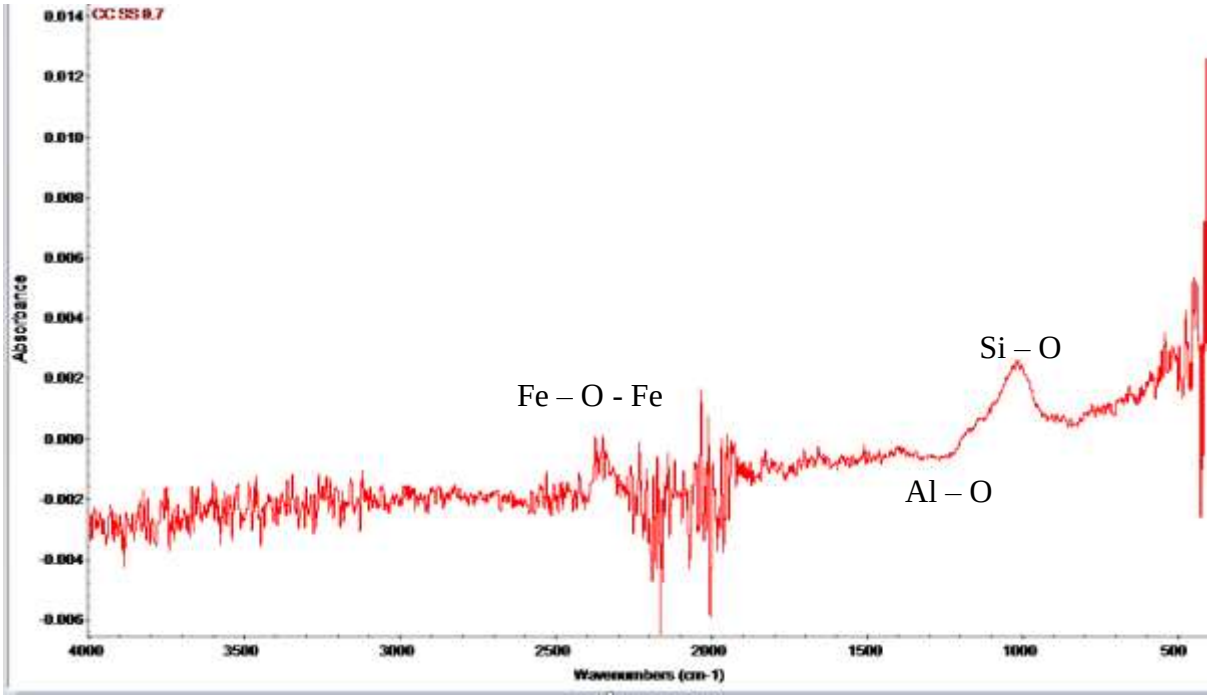

Fig 5.42: IR curve for the SS 0.7 mortar

The broad peaks in the region of 950 cm^{-1} and 1350 cm^{-1} of the SS 1.5 mix are Si–O and Al–O, respectively as shown in Fig 5.43. These bending and stretching peaks are indicative of the geopolymeric structure. This can be inferred from the findings of Puertas, Torres-Carrasco and Alonso (2015), who suggested that the bonding exhibited at the band around 966 cm^{-1} indicates the Si-O stretching vibration of SiO_4 and AlO_4 of geopolymer and N-A-S-H gel.

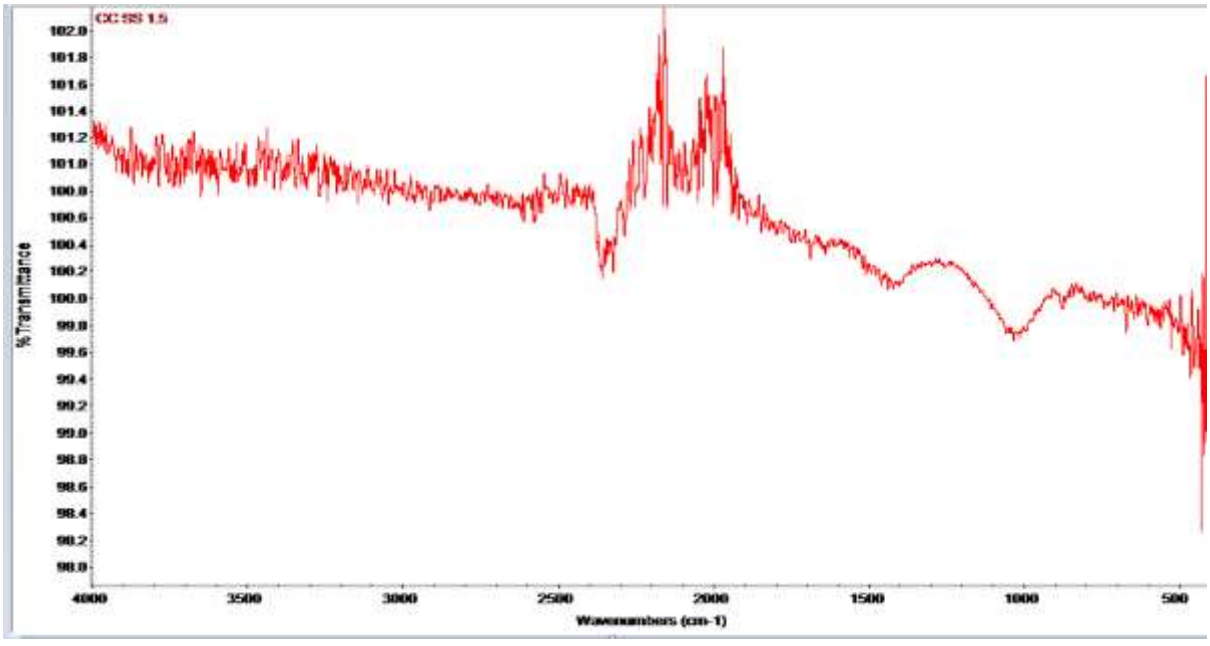

Fig 5.43: IR curve for the SS 1.5 Mortar

The FTIR spectra for the peak strength (SS1) mortar is shown in Fig 5.44. The Si-O vibration band generated by the SiO4 groups in this mortar can be seen at around 950 cm^{-1}, due to the formation of a sodium aluminosilicate type gel. The band at around 1350 cm^{-1} was attributed to the stretching vibrations generated by the Al-O bonds in the AlO4 groups. The bending vibrations generated by the OH groups in the water caused the band at 1625 cm^{-1}.

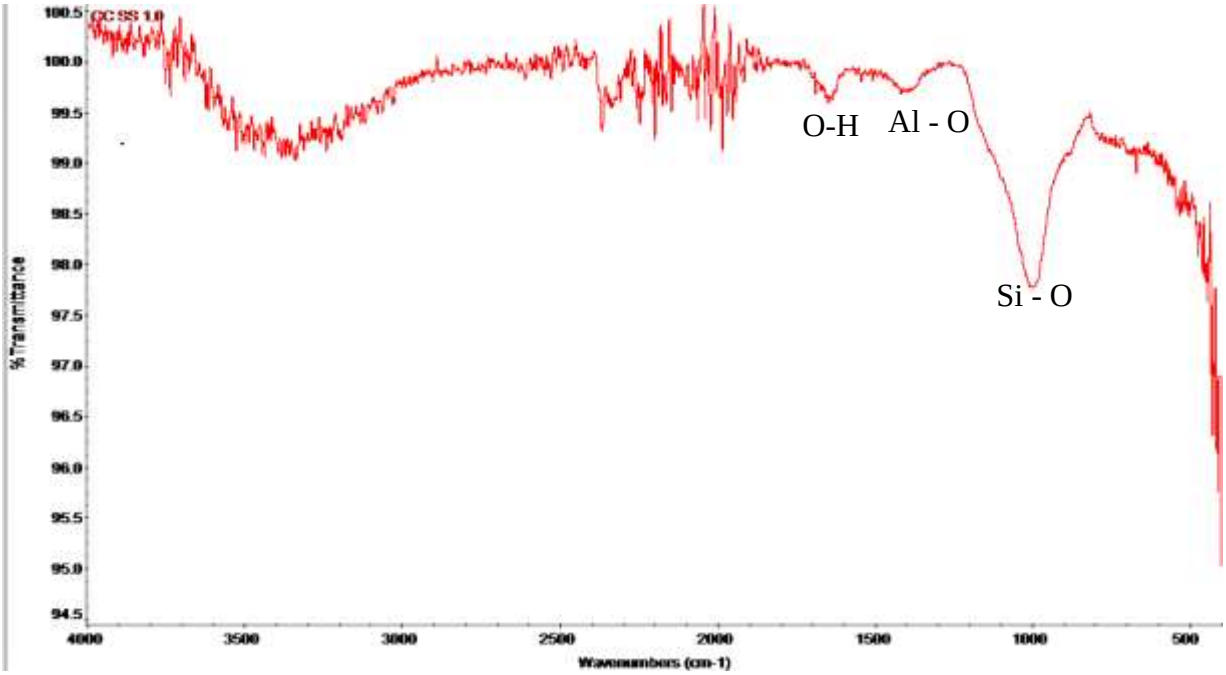

Fig 5.44: IR curve for the SS1 Mortar

5.8.2 Functional groups identification for the calcined clay geopolymer concrete

The IR curves shown in Fig 5.45 of the geopolymer concrete mixes shows that the symmetrical vibration at 1010 cm^{-1} has the lowest broad peak for the mix with the lowest binder content (GC/Na-R). The Si-OH bending vibration at 840 cm^{-1} can also be seen on the GC/Na-M-RM concrete resulting from the effect of the sodium hydroxide solution in the blended activator. Fig 5.46 shows the Si-O-Al-O vibration at 532 cm^{-1} in the potassium silicate activated geopolymer concrete. Meanwhile, the IR curves for the four concrete mixes is shown in Fig 5.47. This figure indicates that the FTIR spectra of the four geopolymer concrete mixes have similar bands with that of typical metakaolin geopolymer, thus confirming that occurrence of geopolymerizaton.

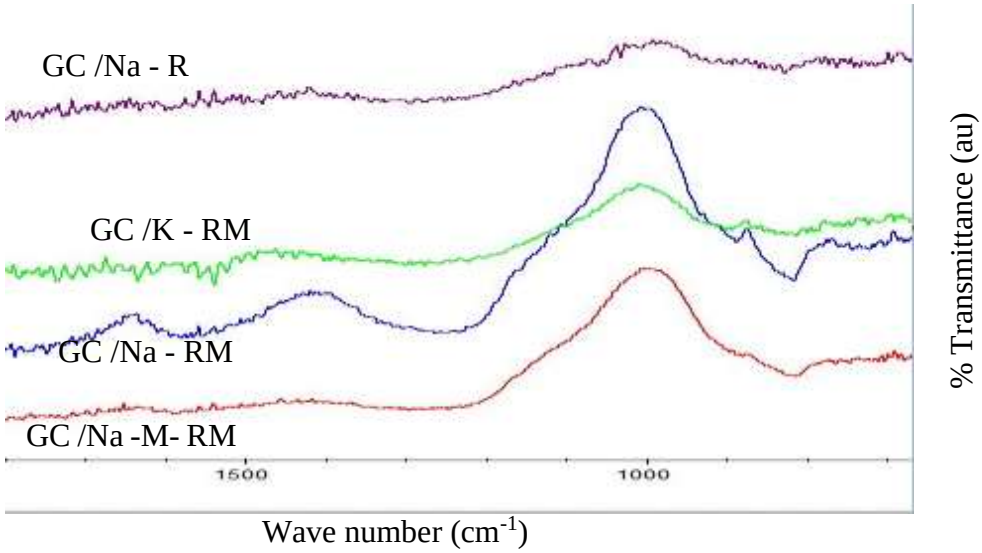

Fig 5.45: IR curve for the four geopolymer concrete mixes

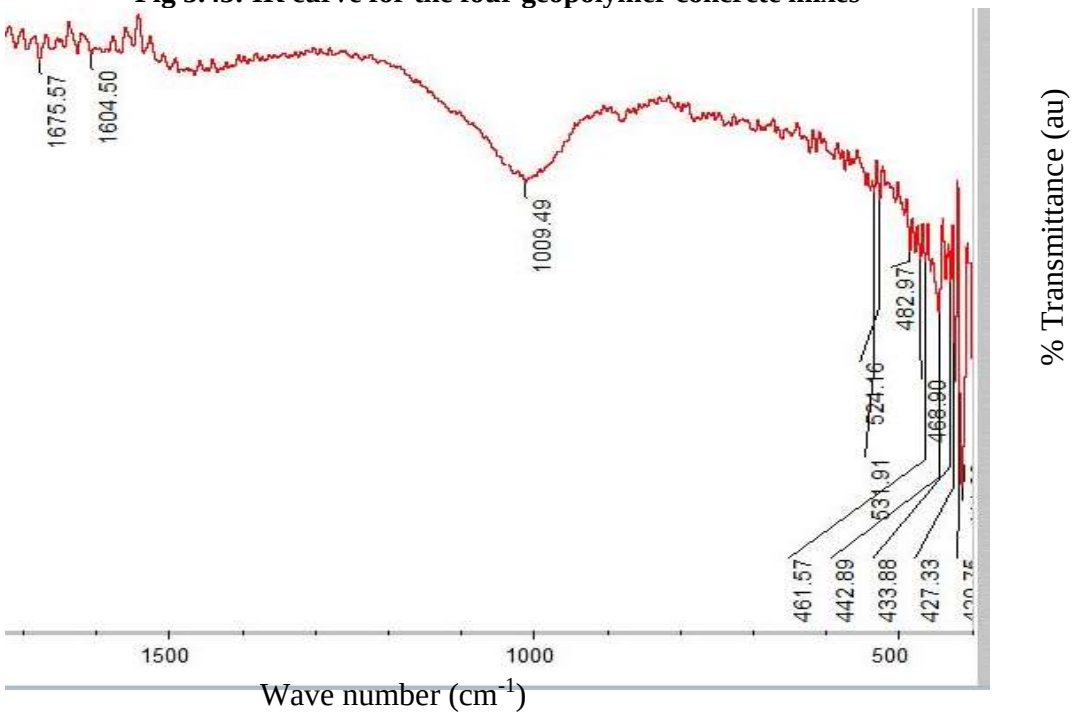

Fig 5.46: IR curve for the potassium silicate activated geopolymer concrete

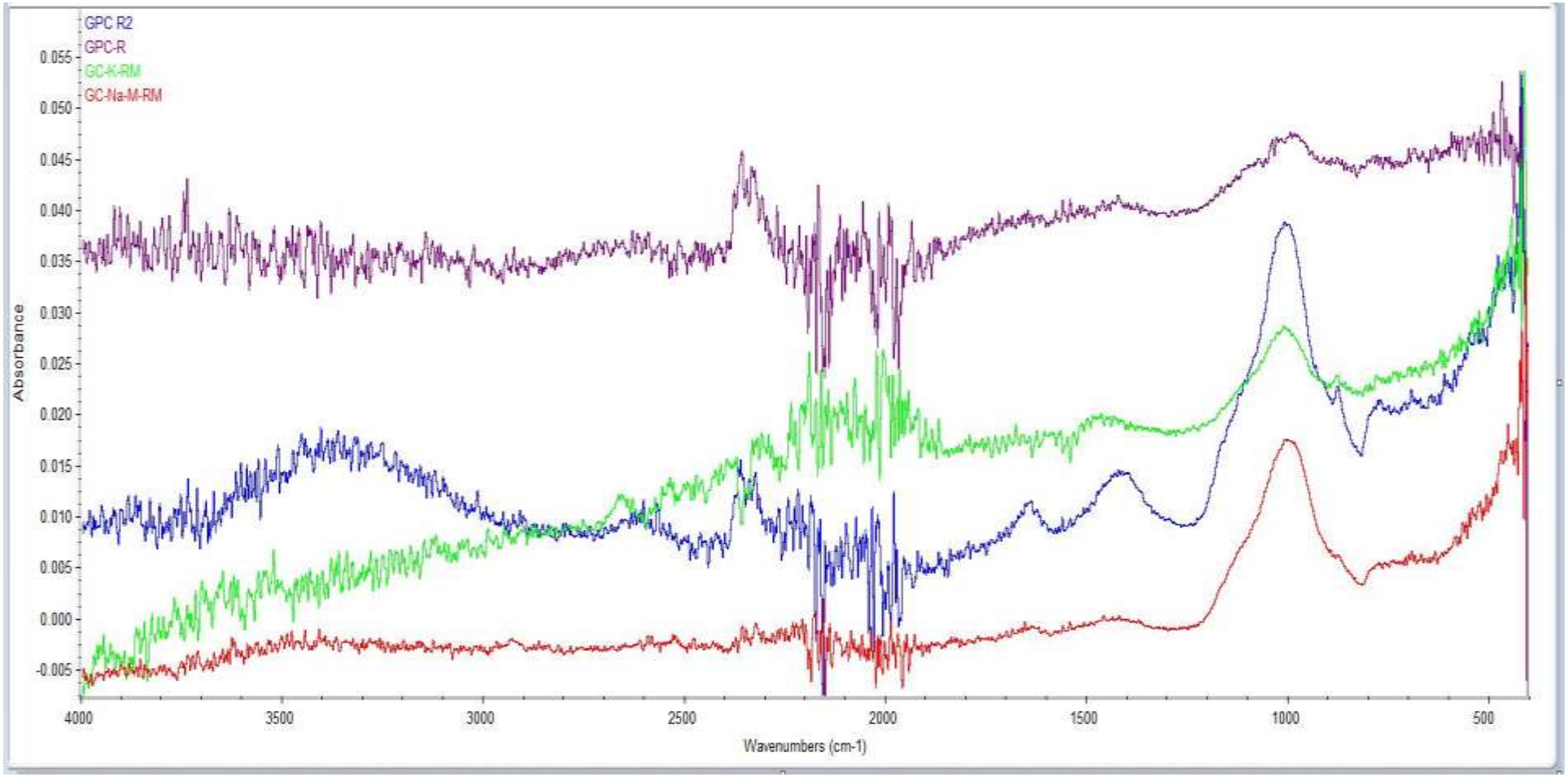

Fig 5.47: FTIR results of geopolymer concrete samples

All the FTIR spectra in Fig. 5.47 exhibit absorption bands generally found in metakaolin-based geopolymers. By comparing the data obtained from the FTIR with the reference database, it can be seen that, the absorption bands at 1050 and 750 cm^{-1} are respectively assigned to the asymmetric and symmetric vibrations of Si–O-Al and Si–O–Si bonding of AlO4 and SiO4 tetrahedrons of geopolymer as suggested by Elimbi, Tchakoute, and Njopwouo (2011). Puertas, Torres-Carrasco and Alonso (2015) also suggested that the bonding exhibited at the band around 966 cm^{-1} indicate the Si-O stretching vibration of SiO_4 and AlO_4 of geopolymer and N-A-S-H gel. Furthermore, the Fe – O – Fe stretching found at 2350 cm^{-1} in the FTIR spectra of Fig 5.47, indicated that the hematite remained in the hardened sample even after the geopolymer synthesis is completed.

CHAPTER 6 LIFE CYCLE ANALYSIS

6.1 Introduction

This chapter compares the life cycle and environmental impact of 1 m^3 of the geopolymer concrete mixes with that of Portland cement concrete produced in this study. The Life Cycle Analysis (LCA) was undertaken systematically in three stages:

Stage 1: Establishment of the system boundary and defining the functional unit.

Stage 2: Life Cycle Inventories (LCI) identification. This involved energy and materials consumption quantification, in addition to waste generation and associated emissions

Stage 3: Calculation of the various impact for every category identified in the LCI for each of the concrete mixes.

Details of these three stages are discussed below.

6.2 Functional unit and system boundaries

The system boundary for comparing the four geopolymer and control concrete mixes is from cradle to mixer. In other words, the studied system is limited to the production of the concrete constituents and therefore does not cover every stage of the concrete's life cycle (production to decommissioning). The boundary is set at intermediate level because the research cannot include all aspects of durability of the products. The system boundary used in this study terminates at an intermediate stage (cradle to gate), similar to previous work by Habert *et. al.* (2011), Heath *et. al.* (2014) and Passuello *et. al.* (2017). Specifically, the study excluded the common processes: mixing, placing, and curing of concrete (illustrated in Fig 6.1). This exclusion is because of the fact that the common processes have similar energy requirements in the studied mixes, as seen in the methodology chapter. The non-thermal (sealed) curing used for the geopolymer mixes in this study was therefore taken as similar to the water curing of traditional Portland cement concrete in terms of energy demand.

Fig 6.1 also reveals that the study excluded use and decommissioning of the concrete. This is because it was assumed that once concrete is placed into a structure the impact during the remainder of the life cycle will be the same for geopolymer concrete or Portland cement concrete.

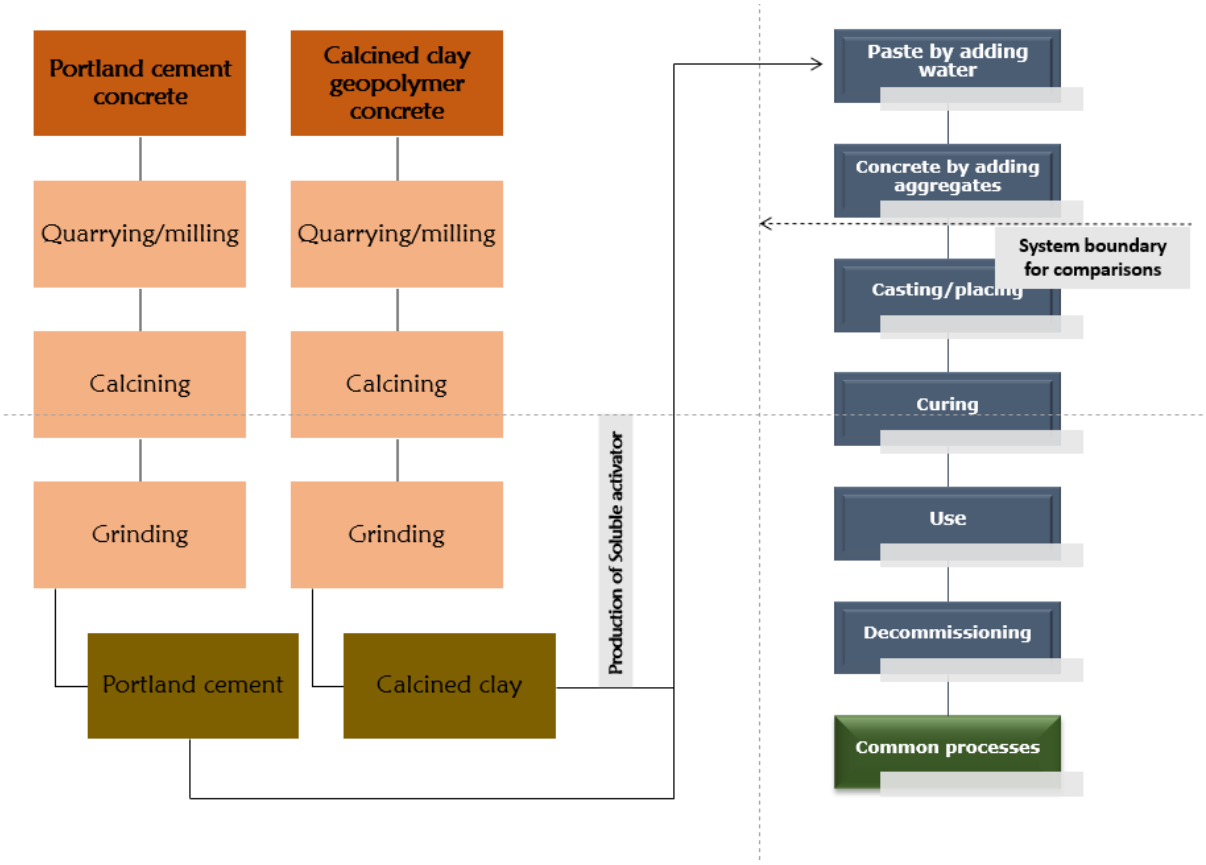

Fig 6.1: Schematic of the system boundary

The functional unit for this study is one cubic metre for the PC control and geopolymer concrete mixes, as presented in table 6.1. The reason for using 1 m^3 is because the mixes have a mechanical strength within the same range which makes the comparison meaningful, as presented in Chapter 5.

Table 6 1 Concrete mixing quantities (kg/m^3)

Mixes	Mix 1	Mix 2	Mix 3	Mix 4	Control
(Kg/m^3)	GC/Na-R	GC/Na-RM	GC/Na-M-RM	GC/K-RM	
CC	276	315	315	311	-
CEM I 54.5	-	-	-	-	404
54.5% Na_2SiO_3	276	315	-	-	-

37% Na_2SiO3	-	-	225	-	-
45% K_2SiO3	-	-	-	390	-
32% NaOH	-	-	90	-	-
FA	554	756	756	756	921
CA	1294	924	924	924	725
Free water	80	91	2	20	221

Key: GC = Geopolymer concrete; /Na= 54.5% sodium silicate solution; /Na-M = 37% sodium silicate solution blended with 32% sodium hydroxide solution; /K = 45% potassium silicate solution; -R = designed based on Rangan specification i.e. aggregate to binder ratio of 4.33; -RM = modified designed based on aggregate to binder ratio of 3.46; FA = fine aggregate; CA = coarse aggregate.

6.3 Technical data from various LCI

Maddalena, Roberts, and Hamilton (2018) in a recent LCA for novel green cements extracted Green House Gases (GHG) impact data from relevant data base in conformity with prior art. A similar approach is followed in this study. The LCI produced by Habert *et al.* (2011) for calcined kaolin clay is based on the data from the *Ecoinvent* database and estimates of production impacts from a plant feasibility study. This LCI is adopted in this study (Table 6.2) for the following reasons:

- The calcined lithomarge used in this study was extracted from an abandoned kaolin clay mining site in Northern Ireland and does not generate the massive waste associated with hydraulic mining of kaolin clay, for example extraction by water jet for the ceramic industries.
- The mass loss for the dehydroxylated lateritic clay as compiled by Mcintosh and Soutsos (2014) is similar to the values used by Habert *et. al* (2011).
- The global warming potential claimed by the Banah European Patent (2010) corresponds to the value recorded by Habert et. al (2011).

Table 6 2 LCI per kg of calcined clay (Habert *et. al* 2011) and CEM I (Chen *et. al.* 2010)

Impact category	Unit	Calcined clay	CEM I
Abiotic depletion	kg Sb eq	1.68E-4	1.59E-3
Acidification	kg SO_2 eq	3.24E-04	1.15E-3
Eutrophication	kg PO_4 eq	4.89E-05	1.73E-4
Global warming	kg CO_2 eq	9.24E-2	8.44E-1
Ozone layer depletion	kg CFC-11 eq	1.52E-9	2.28E-8
Human toxicity	kg 1,4-DB eq	2.36E-02	4.02E-2
Freshwater aquatic ecotoxicity	kg 1,4-DB eq	3.28E-03	4.14E-3
Marine aquatic ecotoxicity	kg 1,4-DB eq	4.59	1.94E-1
Terrestrial ecotoxicity	kg 1,4-DB eq	3.23E-04	1.17E-3
Photochemical oxidation	Kg C_2H_4	1.09E-05	4.26E-5

Code: kg Sb eq refer to kilograms of antimony equivalent; kg SO_2 eq refer to kilogram of sulphur oxides (acid in air) equivalent; kg PO_4 eq refer to kilogram phosphate equivalent of NH^{4+}; kg CO_2 eq refer to kilogram of carbondioxide fossil equivalent; kg CFC-11 eq refer to to kilogram of chloroflouro carbon equivalent; kg 1,4-DB eq refer to kilogram of 1,4-dichlorobenzene equivalent; kg C_2H_4 refer to kilogram ethylene equivalent into air.

The environmental data for 1 kg of binder component of PC control concrete and precursor component of the geopolymer concrete mixes are presented in Table 6.3. The life cycle inventory (LCI) adopted for each component in this study is as follows:

- CEM I Portland cement, Chen *et al.* (2010)

- Calcined clay, Habert, *et al.* (2011)
- Sand and gravel, Kellenberger *et al.* (2007)
- Soluble sodium silicate solution, Fawer, Concannon, and Rieber (1999)
- Sodium hydroxide, Habert *et. al.* (2011)
- Water, Kellenberger *et al.* (2007)

The input values from the *Ecoinvent* data are limited to the ten environmental categories and evaluated according to the CML01 method developed by the Centre of Environmental Science of Leiden University. This is a problem-oriented LCA method that focus on series of environmental impact categories as a function of emission to the environment or resource use. This method suggests equivalence factors that are generally applied for LCA. For example, in marine and terrestrial ecosystems, nitrogen is the most decisive factor, but the degree of eutrophic activity is determined by the phosphorous in the limbic area. Equivalence factors are then applied to convert the ammonium to phosphate as a measure of eutrophication.

6.4 Environmental impact calculation using CML 01

The output (environmental impact) presented in Table 6.4 was calculated by multiplying the values presented in Table 6.3 and the corresponding mixing quantity in Table 6.1. The details of the calculation for each concrete mix is presented in Appendix 3. In the case of the geopolymer concrete mixes, the soluble alkali solution was calculated based on the active substance, as recommended by the ecoinvent code of practice (Weidema *et al.*, 2009). For example:

- The sodium hydroxide solution used in the geopolymer mix (GC/Na-M-RM) has 32% of active substance. Therefore, 0.32 was multiplied by the quantity of the sodium hydroxide solution in the mix. The product was then multiplied by the corresponding impact value.
- The sodium silicate solution used for the GC/Na-R is 276 kg/m3, of which 54.5% is the active substance. The impact value from the LCI for GWP of sodium silicate is 1.066 CO_2 kg “Sodium silicate, WR furnace lumps, 100%”. The computed output value for this impact category for this mix will be 0.545 x 276 = 150.42 x 1.066 = 160.34 kg CO_2 eq.
- The *Ecoinvent* code of practice according to Weidema *et. al* (2009) also recommends that the amount of dilution water should not be included in the calculation because it

has already been added to the LCI of the dissolved chemicals. Therefore, the 45.5% Na_2SiO_3 solution (dilution water) is not included in the impact of water calculation.

Table 6 3: Technical data compiled by the various *Ecoinvent* data base

Impact category	Unit	Calcined clay	37% Na2SiO3	54.5% Na2SiO3	45% K2SiO3	32% NaOH	sand	Gravel	Tap water	CEM I
Abiotic depletion	kg Sb eq	1.68E-4	2.67E-3	3.93E-3	3.25E-3	0.52E-2	1.64E-5	2.95E-5	1.93E-6	1.59E-3
Acidification	kg SO_2 eq	3.24E-04	1.93E-3	2.84E-3	2.35E-3	0.34E-2	1.49E-3	2.34E-5	1.47E-6	1.15E-3
Eutrophication	kg PO_4 eq	4.89E-05	1.83E-4	2.7E-4	2.23E-4	2.59E-4	2.9E-6	4.15E-6	1.01E-7	1.73E-4
Global warming	kg CO_2 eq	9.24E-2	0.4218	0.6213	0.513	0.7168	2.4E-3	4.29E-3	1.55E-4	8.44E-1
Ozone layer depletion	kg CFC-11 eq	1.52E-9	3.26E-8	4.81E-08	3.97E-08	0.44E-7	2.63E-10	4.08E-10	1.36E-11	2.28E-8
Human toxicity	kg 1,4-DB eq	2.36E-02	2.97E-1	4.38E-1	3.61E-1	3.06E-1	1.61E-3	2.9E-3	9.87E-5	4.02E-2
Fresh water aquatic ecotoxicity	kg 1,4-DB eq	3.28E-03	0.78E-1	1.16E-1	0.95E-1	0.77E-1	3.15E-4	6.83E-4	4.95E-5	4.14E-3
Marine aquatic ecotoxicity	kg 1,4-DB eq	4.59	1.23E-2	1.81E-2	1.49E-2	1.52E-2	7.2E-1	1.85	1.84E-1	1.94E-1
Terrestrial ecotoxicity	kg 1,4-DB eq	3.23E-04	3.32E-3	4.88E-3	4.03E-3	1.49E-2	1.02E-3	2.85E-5	1.73E-6	1.17E-3
Photochemical oxidation	kg C_2H_4	1.09E-05	0.9E-4	1.32E-4	1.09E-4	1.48E-4	5.26E-7	1.01E-6	9.98E-8	4.26E-5

Table 6.4: Environmental impact of the concrete mixes

	Control	GC/Na-R	GC/Na-RM	GC/Na-M-RM	GC/K-RM
Abiotic depletion	6.79E-01	1.18E+00	1.33E+00	1.16E+00	1.36E+00
Acidification	1.85E+00	1.73E+00	2.14E+00	1.99E+00	2.17E+00
Eutrophication	7.56E-02	9.50E-02	1.06E-01	8.59E-02	1.08E-01
Global warming	3.46E+02	2.04E+02	2.31E+02	1.94E+02	2.35E+02
Ozone layer depletion	9.75E-06	1.44E-05	1.62E-05	1.23E-05	1.65E-05
Human toxicity	1.98E+01	1.32E+02	1.49E+02	1.06E+02	1.52E+02
Fresh water aquatic ecotoxicity	2.47E+00	3.40E+01	3.84E+01	2.64E+01	3.89E+01
Marine aquatic ecotoxicity	2.12E+03	4.08E+03	3.72E+03	3.70E+03	3.69E+03
Terrestrial ecotoxicity	1.43E+00	2.04E+00	2.44E+00	2.99E+00	2.47E+00
Photochemical oxidation	1.84E-02	4.10E-02	4.64E-02	3.83E-02	4.72E-02

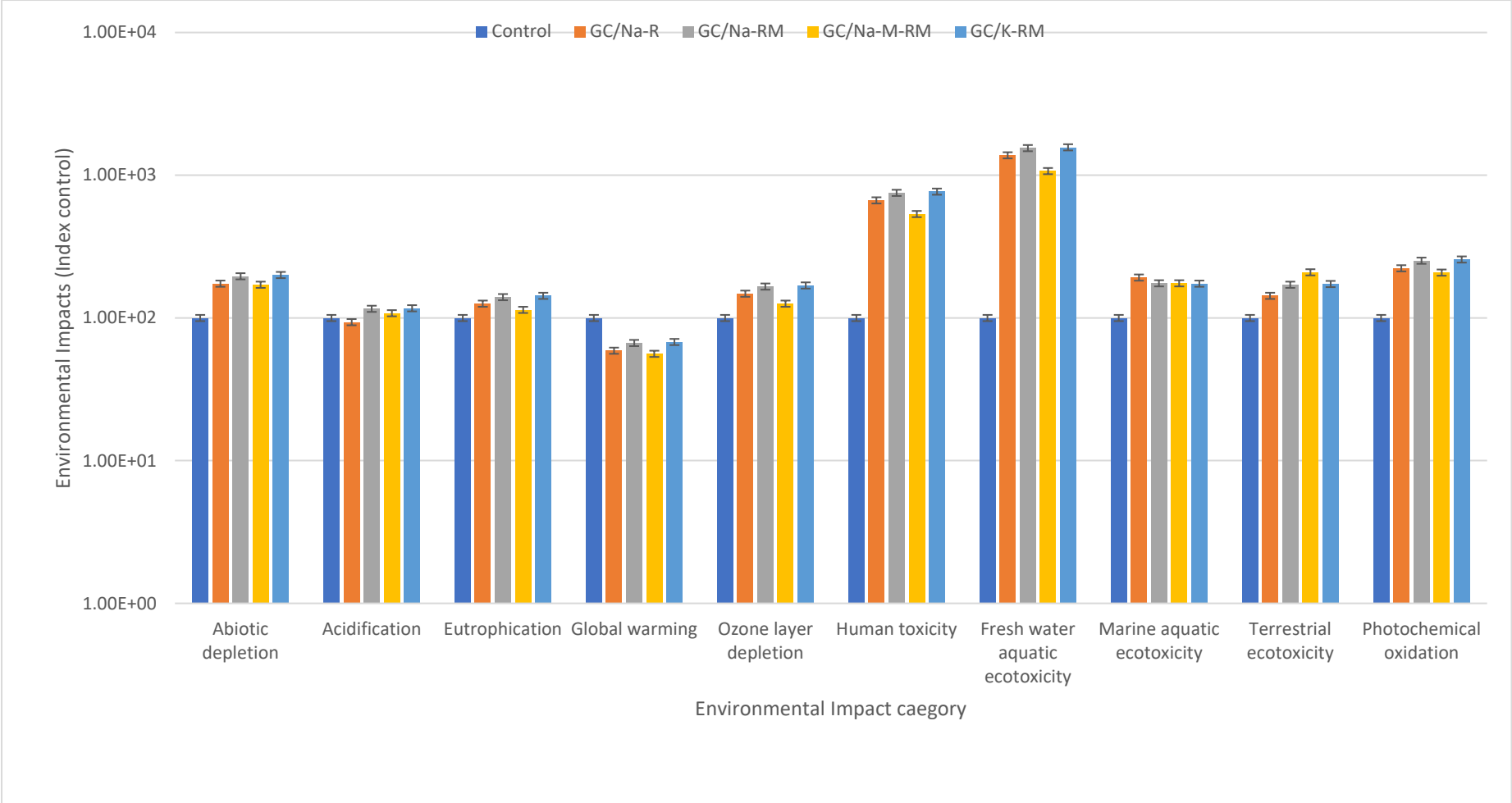

Fig 6.2: Comparison of the environmental impacts of the concrete mixes with the PC control concrete as the base case

6.5 Environmental analysis of the calcined clay geopolymer concretes compared to the PC concrete

Fig 6.2 shows the environmental impact related to the production of 1 m^3 of geopolymer concrete when compared with a Portland cement-based concrete, with similar mechanical strength characteristics. For example, the GWP for the GC/K-RM relative to that of the PC control concrete is computed as follows:

The estimated GWP of the PC control and GC/K-RM concretes are the sum of their constituents' GWP as shown in table 6.5. Meanwhile, the GWP for each constituent is the product of the mixing quantity (table 6.1) and the impact for that category (table 6.3). The LCI for the ten environmental impact categories for each mix are provided in Appendix 3.

Table 6 5: GWP of PC and GC/K-RM concrete

	PC	CC	K_2SiO_3	Sand	Gravel	Water	**GWP (table 5.4)**
GWP of PC concrete (kg CO_2 eq)	404 x 0.844 = 341	-	-	921 x 0.0024 = 2.21	725 x 0.00429 = 3.11	221 x 0.000155 = 0.0343	**346.4**
GWP of GC/K-RM concrete (kg CO_2 eq)	-	311 x 0.0924 =28.7	390 x 0.513 =200	756 x 0.0024=1.81	924 x 0.00429=3.96	20 x 0.000155 =0.0031	**234.5**

From table 6.5, taking the PC concrete as the base case: the GWP values in Fig 6.2 are computed as follows:

GWP of PC concrete = $\frac{346.4}{346.4} x\ 100 = 100\%$

GWP of GC/K-RM concrete = $\frac{234.5}{346.4} x\ 100 = 67.7\%$

It can be seen from Fig 6.2 that the results shows different trends for the various concrete mixes according to the impact category. Some of these trends are discussed in the next sub-sections.

6.5.1 Global warming potential

All the geopolymer concrete mixes have significantly lower GWP in comparison to the PC control mix as shown in Fig 6.2. It can be seen that a carbon dioxide saving of 32.1% and 43.9% was estimated for the GC/K-RM and GC/Na-M-RM mixes, respectively, in comparison to the PC concrete. The results obtained in this study also indicate a lower GWP of the calcined lithomarge compared to the metakaolin based geopolymers reported by other authors (Heath, *et.al*, 2014; Habert *et. al.* 2011). This enhanced carbon footprint saving is due to the extraction of the calcined clay from abandoned kaolin clay mining sites and the relatively low mass-loss during its dehydroxylation when compared to high purity kaolin clay.

6.5.2 Other environmental impacts

The geopolymer concretes showed increased environmental impacts compared to the Portland cement control concrete, which varied from slight to significant (Fig 6.2). For instance, the GC/K-RM have acidification impact of 117% and eutrophication impact of 143% of the PC concrete. Moreover, the blended activator mix (GC/Na-M-RM) have the least impact among the geopolymer concrete mixes for the other nine environmental impact categories. The reason for its enhanced environmental impact savings was because part of the silicate solution was substituted with sodium hydroxide solution.

It can also be seen in Fig 6.2 that the impact on freshwater aquatic toxicity and human toxicity of the blended geopolymer concrete was 535% and 1070 % respectively, when compared to the Portland cement concrete. These high environmental impacts were largely caused by the activator and not the calcined clay as previously established by Zografou (2015) and Habert, *et al.* (2011). However, considering the significant progress been made in developing waste-derived activators for geopolymers, these unfavourable impact values are already been addressed.

CHAPTER 7 RESULTS SUMMARY, CONCLUSIONS AND RECOMMENDATIONS FOR FURTHER WORKS

7.1 Results summary

This research studied the viability of producing geopolymer based on flash calcined lateritic clay sourced from Northern Ireland as the precursor. The effect of mix design parameters such as type, proportion and dosage of activators, curing conditions etc on the geopolymer mortar synthesis for this precursor has been evaluated. The molar oxide and mass ratio compositions for the peak strength geopolymer mortar has been determined. These variables have then been used for the formulation of geopolymer concrete based on four kind of activators. The fresh behaviour, mechanical properties and internal mechanisms of the produced geopolymer concretes has been characterized. The performance of the calcined lateritic clay as a replacement of scarce GGBS for a ternary hydraulically road binder mixture was also studied.

The results obtained and discussed in this thesis can be summarized as follows:

1. Low strength mortar is achieved by activating calcined clay with a sodium silicate solution derived from the dissolution of granular sodium silicate pentahydrate under normal atmospheric conditions. This decrease in strength results from the reduced alkalination potential of the silicate solution due to the dilution caused by chemically bound water. Also, limited free silicate ions are incorporated into the solid during the geopolymerization process, caused by a partial dissolution of the hydrous sodium silicate. As such, a low strength non-geopolymer matrix is precipitated which has unreactive residual calcined clay that prevented complete development of the geopolymer network.
2. Geopolymer synthesis of calcined clay mortar shows high sensitivity to variations in molar oxide ratios. Whereas all the mixes produced with the 54.5% sodium silicate solution had molar ratios that fell within the range specified by different authors, the strength obtained reached a maximum and then decreased subsequently with the variations in the molar oxide composition. Accordingly, the mix that achieved peak strength at all ages had the following molar ratios: - SiO_2/Al_2O_3 of 4.12, Na_2O/Al_2O_3 of 1, Na_2O/SiO_2 of 0.24 and H_2O/Na_2O of 14.1.
3. The microstructure of the peak strength mortar (mix based on calcined clay to 54.5% Na_2SiO_3 solution mass ratio of 1) reveals a dense and compact geopolymer structure. Conversely, the 32% NaOH solution activated calcined clay mortar produces a sponge-like, globular morphology on the surface of the matrix resulting from the alkali activation.

4. The XRD result indicates the Na/K–Al–Si–O geopolymeric peak of the 54.5% Na_2SiO_3 solution can be attributed to the high strength achieved in the mix. The result further reveals zeolite phases in the 32% NaOH activated mix. This was caused by the rapid dissolution of the silicate and aluminate component of the calcined clay in the system.
5. The FTIR results reveal broader Al-O and Si-O peaks in the 54.5% Na_2SiO_3 solution activated mix when compared to the 54.5% $Na_2SiO_3.5H_2O$ solution mix. This indicates that the calcined clay based geopolymer system is best produced using a fully dissolved silicate solution.
6. The geopolymer concrete mixes have a collapsed slump. The highest peak torque of 27.06 Nm was obtained in the mix with higher aggregate content (GC/Na-R). This indicates that the geopolymer concretes do not require much energy for shearing (mixing) and pumping.
7. A potassium silicate solution produces the most workable mix in terms of measured rheology with a peak torque of 0.63 Nm, plastic viscosity of 68 Pas and dynamic yield stress of 146.4 Pa, compared to the sodium silicate solution activated geopolymer concrete. Moreover, the mixes with 70% aggregate content were adequately categorized by the Bingham model (except the blended mix).
8. Blending of the sodium silicate with a sodium hydroxide solution in order to obtain a formulation with molar oxide composition ratio that is required for geopolymer, results in a lower compressive strength (36 MPa at 28 days) in comparison to another two mixes that have a similar binder content. This decrease in strength can be associated with an increased Na:Si ratio in the system.
9. A potassium silicate synthesized mix also shows less sensitivity to molar oxide ratios optimization compared to the sodium-based activated mixes.
10. The morphology of geopolymer concrete samples formulated with an aggregate to binder ratio (A:B) of 3.46 is denser and more compact in comparison to that of concrete produced with an A:B of 4.33 (as recommended by the Rangan method). This increase in binder content can also be associated with the enhanced compressive strength at 7 and 28 days, irrespective of the type of chemical activator used.
11. Distinct broad peaks that correspond to the Si–O, Al–O, O–H and Fe–O–Fe has been identified in the geopolymer concretes. The non-smooth curve was due to the presence of high amounts of iron in the calcined clay that caused the noise even though the samples were dried.

12. A ternary binder composition of CC (40%) / BOS (50%) / BPD (10%), when activated with 15% water content, satisfies the strength requirements of HRB10 (the 28 days compressive strength of standardized mortars higher than 10 MPa).

7.2 Conclusion

The key conclusions drawn from this research are:

1. Geopolymer synthesis of the flash calcined lateritic clay is very sensitive to molar oxide composition range of the system. Fully dissolved silicate solutions are necessary for the production of two-part system for this precursor.
2. Hydrous silicate dissolved under atmospheric condition and sodium hydroxide are not effective activators for the geopolymerisation of the calcined lateritic clay. This is a limitation to the potential of the precursor to be synthesized in a one-part geopolymer system under non-thermal curing condition.
3. Sealed curing conditions enhance the strength of the calcined clay geopolymer mortars by limiting the effects of atmospheric carbonation, regardless of the proportion or type of chemical activator used.
4. The microstructure of the calcined clay geopolymer mortar is dense and compact with sponge-like, globular morphology on the surface of the matrix.
5. The calcined lateritic clay geopolymer is only partially crystalline, containing ordered domains with structures similar to the Na-feldspar, albite and the K-feldspar, sanidine. These are the geopolymeric frameworks that are similar to Na-Poly(sialate-disiloxo) and K-Poly(sialate-disiloxo) respectively. These geopolymeric frameworks have Si:Al of 3.
6. The potassium silicate activated calcined clay geopolymer concrete is self- compacting with rheological characteristics that fits the Bingham model. The fresh concrete has a peak torque of 0.63 Nm compared to 9.6 Nm for the PC concrete. This indicate that lower energy is required for shearing (mixing) and pumping of the geopolymer concrete.
7. The calcined lateritic clay geopolymer concrete has superior freeze-thaw resistance compared to PC concrete.
8. The geopolymer concretes have lower global warming potential of between 32 – 44% of the PC concrete, depending on the type of activator used. However, it has higher environmental impact in other categories analysed caused by the silicate production.

9. The calcined clay can adequately substitute the scarce GGBS in the optimized ternary binder composition of GGBS (40%) / BOS (50%) / BPD (10%) for hydraulically road binder.

7.3 Limitation of the study

This research has undertaken limited durability assessment of the calcined clay geopolymer concrete focusing essentially on the freeze-thaw resistance. The chloride permeability assessment was inconclusive because of the drawbacks associated with the method when used in highly alkaline systems, despite being deployed by many researchers.

The study is also limited to the mass and energy balance of the calcined lateritic clay geopolymer concrete. Cost analysis has not been carried out which is an important driver towards enhancing commercialization of a geopolymer binder.

7.4 Recommendation for further works

This research focused on fresh behaviour, mechanical properties, and the microstructural characterisation of the calcined clay geopolymer concrete. Mix design data has been generated based on water demand and molar oxide compositional range using various kinds of alkali solutions. This data should, therefore, provide the basis for the development of methodologies for the mix design of low purity kaolin geopolymer binder. The development of mix design guidelines similar to BRE design of normal concrete mixes is essential towards the popularisation and industrial acceptance of geopolymer binders. Such guidelines can be of interest to researchers, designers, concrete production companies, and contractors. The guidelines will provide better insight into key mix proportion parameters that affect fundamental properties of geopolymer concrete formulated using a lateritic based binder.

Although geopolymer binders are generally known for their excellent resistance to aggressive conditions, it is important to carry out detailed durability performance assessment of the calcined clay geopolymer concrete. Specifically, the depth of carbonation and chloride ion permeability needs to be studied for the calcined lateritic clay geopolymer.

A recent study reported that Mossbauer spectroscopy has the potential to adequately characterise the geopolymer synthesis of calcined lateritic clay (Davidovits and Davidovits 2020). (Třískova et al. 2005) applied the technique to confirm the incorporation of Fe^{3+} ions in aluminosilicate network of iron-rich kaolin clay. Also, Lemougna *et al*. (2013) used the technique to identify the ferrous sites in volcanic ash and the ferric sites in an amorphous X-

ray phase. Their finding suggested incorporation of ferric iron in the tetrahedral matrix of the geopolymer product that yielded a ferro-silico-aluminate sequence (-Fe-O-Si-O-Al-O-). Therefore, using this technique will bridge the gap caused by the inherent limitation of Al-NMR spectroscopy in characterising the internal mechanisms of iron-rich calcined clay based geopolymers. Mossbauer spectroscopy is therefore suggested to enable a deeper understanding of the calcined clay geopolymer synthesis because it may reveal the behaviour of Fe^{3+} during the geopolymerisation, which is the equivalent of Al^{3+} in the aluminosilicate matrix.

REFERENCES

Abdul Aleem, M. I. and Arumailraj, P. D. (2012) 'Optimum mix for the geopolymer concrete', *Indian Journal of Science and Technology*, 5(3). Available at: http://www.geopolymer.org/science/introduction. (Accessed: 17 February 2020).

Abora, K. Quillin, K., Paine, K. A. and Dunster, A. M. (2009) 'Effect of mix design on consistence and setting time of alkali activated concrete', in *11th International Conference on Non-conventional Materials and Technologies (NOCMAT 2009)*. Bath, UK United Kingdom: BRE Centre in Innovative Construction Materials (BRE CICM).

Abora, K., Belena, I., Bernal, S. A., Duster, A., Nixon, P. A., Provis, J. L., Tagnit-Hamou, A. and Winnefeld, F. (2014) 'Durability and testing – Chemical matrix degradation processes', *RILEM State-of-the-Art Reports*. Springer Netherlands, 13, pp. 177–221. doi: 10.1007/978-94-007-7672-2_8.

ACI Committee (2013) *229R-13 Report on Controlled Low-Strength Materials*.

Al-Otaibi, S. (2008) 'Durability of concrete incorporating GGBS activated by water-glass', *Construction and Building Materials*. Elsevier, 22(10), pp. 2059–2067. doi: 10.1016/j.conbuildmat.2007.07.023.

Alanazi, H., Yang, M., Zhang, D. and Gao, Z. (2017) 'Early strength and durability of metakaolin-based geopolymer concrete', *ice - Institution of Civil Engineers*, pp. 46–54. doi: 10.1680/jmacr.16.00118.

Alonso, M. M., Gismera, S., Blanco, M. T., Lanzon, M. and Puertas, F. (2017) 'Alkali-activated mortars: Workability and rheological behaviour', *Construction and Building Materials*. doi: 10.1016/j.conbuildmat.2017.04.020.

Andrew, D., Quillin, K. and Kofi, A. (2011) *Alkali-activated binder concretes in construction-An introduction to their benefits and properties and barriers to their use*. Bre press. Available at: https://www.brebookshop.com/details.jsp?id=326684 (Accessed: 17 February 2020).

Arham, A. A. (2009) *Strength and Durability Properties of Alkali Activated Slag and Fly Ash-Based Geopolymer Concrete*.

Arjun, N. (2017) *Rheology of Concrete -Rheological Parameters of Fresh Concrete, the constructor*. Available at: https://theconstructor.org/concrete/rheology-of-concrete/15319/ (Accessed: 18 February 2020).

ASTM International (2019) *ASTM C618-19, Standard Specification for Coal Fly Ash and Raw or Calcined Natural Pozzolans for Use in Concrete*.

ASTM International (2004) *ASTM C496/C496M-11,Standard test method for splitting tensile strength of cylindrical concrete specimens*.

ASTM International (2018) *Standard Test Method for Electrical Indication of Concrete's Ability to Resist Chloride Ion Penetration 1*. doi: 10.1520/C1202-18.

ASTM International (2019) *ASTM C191-19, Standard Test Methods for Time of Setting of*

Hydraulic Cement by Vicat Needle.

Bai Kamara, K., Ganjian, E. and Khorami, M. (2019) 'optimisation of secondary waste gypsum for mechanical stability in road (base) and foundation', in *Fifth International Conference on Sustainable Construction Materials and Technologies*. Available at: http://www.claisse.info/2019 papers/5100.pdf.

Banfill, P. F. G. and Kitching, D. R. (1990) 'Use of a controlled stress rheometer to study the yield stress of oil well cement slurries', in *Rheology of Fresh Cement*, pp. 125–136.

Bature, A. S., Khorami, M., Ganjian, E. and Tyrer, M. (2019) 'Effects of Sodium Silicate Proportion on Strength Development of Calcined Clay Geopolymer Mortar'. in Ball, R, Dams, B, Ferrandiz-Mas, V, Ke, X, Paine, K, Tyrer, M & Walker, P. (ed.) *39th Cement and Concrete Science Conference 2019*. [online] held 2019. University of Bath, UK, 148–152. available from <https://purehost.bath.ac.uk/ws/portalfiles/portal/197842011/39th_Cement_and_Concrete_Science_Conference_2019.pdf>

Bature, A. S., Khorami, M., Ganjian, E. and Tyrer, M. (2018) 'Influence of Alkali Solution on Compressive Strength of Calcined Clay and GGBS Alkali Activated Mortar'. in Tyrer, M., Ganjian, E. and West, A. (ed.) *38th Cement and Concrete Science Conference*. held 2018. Paper No. 16

Bernal, S. A., Merjia de Gutierrez, R., Pedraza, A. L., Provis, J. L., Rodriguez, E. D. and Delvato, S. (2011) 'Effect of binder content on the performance of alkali-activated slag concretes', *Cement and Concrete Research*. Pergamon, 41(1), pp. 1–8. doi: 10.1016/J.CEMCONRES.2010.08.017.

Bernal, S. A. *et al.* (2014) 'Binder chemistry - High-calcium alkali-activated materials', *RILEM State-of-the-Art Reports*. Springer Netherlands, 13, pp. 59–91. doi: 10.1007/978-94-007-7672-2_3.

Bernal, S. A., Mejía De Gutiérrez, R. and Provis, J. L. (2012) 'Engineering and durability properties of concretes based on alkali-activated granulated blast furnace slag/metakaolin blends', *Construction and Building Materials*. Elsevier, 33, pp. 99–108. doi: 10.1016/j.conbuildmat.2012.01.017.

Blackstock, J. M., Neill, J. and McIntosh, J.A. (2017) *Geopolymeric Concrete and Methods of Forming It from a Basaltic Precursor*. EP 2 451 758 B1, 2017. Eurpoean Patent

Blessing, L., & Chakrabarti, Amaresh. author. (2009) DRM, a Design Research Methodology.

Brigatti, M. F., Galan, E. and Theng, B. K. G. (2006) 'Chapter 2 Structures and Mineralogy of Clay Minerals', *Developments in Clay Science*. Elsevier, pp. 19–86. doi: 10.1016/S1572-4352(05)01002-0.

British standard institution (2019) *BS EN 12390-3:2019 Testing hardened concrete. Compressive strength of test specimens*.

British Standards Institution. (2000) *Testing fresh concrete. Part 2, Slump test.* BSI.

British Standards Institution. (2005) *Methods of testing cement : part 1 : determination of*

strength. British Standard.

Brough, A. R. and Atkinson, A. (2002) 'Sodium silicate-based, alkali-activated slag mortars: Part I. Strength, hydration and microstructure', *Cement and Concrete Research*, 32(6), pp. 865–879. doi: https://doi.org/10.1016/S0008-8846(02)00717-2.

Casarez, R., Soberón, J. G. and Sánchez, J. A. (2014) 'Experimental study of XRD, FTIR and TGA techniques in geopolymeric materials'. Available at: https://www.recercat.cat/handle/2072/240186 (Accessed: 3 March 2020).

Cement Sustainability Initiative (2014) *Getting the Numbers Right*. Available at: http://www.wbcsdcement.org/index.php/key-issues/climate-protection/gnr-database.

Chen, C., Habert, G., Bouzidi, Y., and Jullien, A. (2010) 'Environmental Impact of Cement Production: Detail of the Different Processes and Cement Plant Variability Evaluation'. *Journal of Cleaner Production* 18 (5), 478–485

Chen, W. and Brouwers, H. J. H. (2007) 'The hydration of slag, part 1: Reaction models for alkali-activated slag', *Journal of Materials Science*. Springer, 42(2), pp. 428–443. doi: 10.1007/s10853-006-0873-2.

Chi, M. (2012) 'Effects of dosage of alkali-activated solution and curing conditions on the properties and durability of alkali-activated slag concrete', *Construction and Building Materials*. Elsevier, 35, pp. 240–245. doi: 10.1016/j.conbuildmat.2012.04.005.

Chi, M. (2016) 'Mechanical strength and durability of alkali-activated fly ash/slag concrete'. *Journal of Marine Science and Technology* [online] 24 (5), 958–967. available from <https://www.researchgate.net/publication/310620432> [8 April 2020]

Claisse, P. A. (2016) *Civil Engineering Materials*. Butterworth-Heinemann Ltd. Available at: https://www.bookdepository.com/Civil-Engineering-Materials-Peter-Claisse/9780081002759 (Accessed: 17 February 2020).

Claisse, P A., Lorimer, J. P. and Omari, M. H. (2001) 'Workability of cement pastes', *ACI Materials Journal*, 98(6). Available at: https://www.researchgate.net/publication/228887319_Workability_of_cement_pastes (Accessed: 18 February 2020).

Claisse, P. Tyrer, M. and Coupe, S (2010) Briefing: How to research and publish new concrete ingredients. Proceedings of the Institute of Civil Engineers – Construction Materials 163:2, 57 – 60.

Collins, H. (2010) "Creative Research: The Theory and Practice of Research for the Creative Industries" AVA Publications, p.38

Collis, J. and Hussey, R. (2013) Business research: A practical guide for undergraduate and postgraduate students. 4th edn. Basingstoke: Palgrave Macmillan

Crossrail (2017) *beneficially re-using material excavated during crossrail's construction*. Available at: http://www.crossrail.co.uk/construction/tunnelling/excavated-material# (Accessed: 17 February 2020).

Davidovits, J. (1994) 'Global Warming Impact on the Cement and Aggregates Industries', *World Resource Review*, 6(2), pp. 263–278. Available at: www.geopolymer.org (Accessed: 17 February 2020).

Davidovits, J. (2011) 'Application of Ca-based geopolymer with blast furnace slag, a review', in Jones, P. T.; Pontikes, Y.; Elsen, J.; Cizer, O.; Boehme, L.; Gerven, T.; Geysen, D.; Guo, M. and Blanpain, B. (ed.) *Second international slag valorization symposium* . Leuven, Belgium, pp. 1–18.

Davidovits, J. (2012) *Red geopolymer cement could become the standard*. Saint Quentin, France.

Davidovits, J. (2015) *Environmental implications of Geopolymers, Materials Today*. Available at: https://www.materialstoday.com/polymers-soft-materials/features/environmental-implications-of-geopolymers/ (Accessed: 5 March 2020).

Davidovits, J. (2015) *Geopolymer Chemistry and Applications*. 3rd edn. Geopolymer Institute.

Davidovits, J. (2019) *Ferro-sialate Geopolymers.* Geopolymer camp 2019. Available at: https://geopolymer.org/fichiers/gpcamp-2019/Davidovits%20-%20Ferro-sialate%20Geopolymer.pdf

Davidovits, J. and Davidovits, R. (2020) *Ferro-sialate Geopolymers (-Fe-O-Si-O-Al-O-)*. doi: 10.13140/RG.2.2.25792.89608/2.

Deb, P. S., Nath, P. and Sarker, P. K. (2014) 'The effects of ground granulated blast-furnace slag blending with fly ash and activator content on the workability and strength properties of geopolymer concrete cured at ambient temperature', *Materials and Design*. Elsevier Ltd, 62, pp. 32–39. doi: 10.1016/j.matdes.2014.05.001.

Donatello, S., Tyrer, M., and Cheeseman, C. R. (2010) 'Comparison of Test Methods to Assess Pozzolanic Activity'. *Cement and Concrete Composites* 32 (2), 121–127

Duxson, P.; Fernández-Jiménez, A.; Provis, J. L.; Lukey, G. C.; Palomo, A. and Van Deventer, J. S. J. and Provis, J. (2006) 'Geopolymer technology: The current state of the art', *Journal of Materials Science*, 42(9), pp. 2917–2933. doi: 10.1007/s10853-006-0637-z.

Duxson, P. *et al.* (2007) 'The role of inorganic polymer technology in the development of "green concrete"', *Cement and Concrete Research*, 37(12), pp. 1590–1597. Available at: https://www.sciencedirect.com/science/article/pii/S0008884607002001 (Accessed: 17 February 2020).

Elimbi, A., Tchakoute, H.K., and Njopwouo, D. (2011) 'Effects of Calcination Temperature of Kaolinite Clays on the Properties of Geopolymer Cements'. *Construction and Building Materials* [online] 25 (6), 2805–2812. available from <https://www.sciencedirect.com/science/article/pii/S0950061810007476> [4 May 2020]

Erdoğan, S. T. *et al.* (2008) 'Influence of the shape and roughness of inclusions on the rheological properties of a cementitious suspension', *Cement and Concrete Composites*. Elsevier, 30(5), pp. 393–402. doi: 10.1016/j.cemconcomp.2008.01.003.

Fawer, M., Concannon, M. and Rieber, W. (1999) 'Life cycle inventories for the production of sodium silicates', *International Journal of Life Cycle Assessment*. Springer Verlag, 4(4), pp. 207–212. doi: 10.1007/BF02979498.

Fernández-Jiménez, A. *et al.* (2017) 'Sustainable alkali activated materials: Precursor and activator derived from industrial wastes', *Journal of Cleaner Production*. Elsevier Ltd, 162, pp. 1200–1209. doi: 10.1016/j.jclepro.2017.06.151.

Fernández-Jiménez, A., Palomo, J. G. and Puertas, F. (1999) 'Alkali-activated slag mortars: Mechanical strength behaviour', *Cement and Concrete Research*. Elsevier Science Ltd, 29(8), pp. 1313–1321. doi: 10.1016/S0008-8846(99)00154-4.

Fletcher, R. A. *et al.* (2005) 'The composition range of aluminosilicate geopolymers', *Journal of the European Ceramic Society*. Elsevier, 25(9), pp. 1471–1477. doi: 10.1016/j.jeurceramsoc.2004.06.001.

Flick, U. (2015) Introducing research methodology: A beginner's guide to doing a research project. Sage.

Fu, Y., Cai, L. and Yonggen, W. (2011) 'Freeze-thaw cycle test and damage mechanics models of alkali-activated slag concrete', *Construction and Building Materials*. Elsevier, 25(7), pp. 3144–3148. doi: 10.1016/j.conbuildmat.2010.12.006.

Ganjian, E. *et al.* (2008) *Plasterboard and Gypsum Waste in a Novel Cementitious Binder for Road Construction*.

Geddes, D., Provis, J. L., Bernal, S. A. and Hayes, M. (2018) 'Effect of Calcination Method and Clay Purity on the Performance of Metakaolin-Based Geopolymers'. in *International Conference on Alkali Activated Materials and Geopolymers: Versatile Materials Offering High Performance and Low Emissions*. held 27 May 2018

Greenwood, N. N. and Earnshaw, A. (1997) *Chemistry of the Elements*. Second Edi. Butterworth-Heinemann.

Guggenheim, S. and Martin, R. T. (1995) R*eport definition of clay and clay mineral: joint report of the aipea nomenclature and cms nomenclature committees, Clays and Clay Minerals*.

Habert, G., D'Espinose De Lacaillerie, J. B. and Roussel, N. (2011) 'An environmental evaluation of geopolymer based concrete production: Reviewing current research trends', *Journal of Cleaner Production*. doi: 10.1016/j.jclepro.2011.03.012.

Heath, A., Paine, K. and McManus, M. (2014) 'Minimising the global warming potential of clay based geopolymers', *Journal of Cleaner Production*, 78. doi: 10.1016/j.jclepro.2014.04.046.

IEA WBCSD - World Business Council for Sustainable Development (2009) *Cement technology roadmap 2009: Carbon emissions reductions up to 2050*.

Imbabi, M., Carrigan, C. and McKenna, S. (2012) 'Trends and developments in green cement and concrete technology', *International Journal of Sustainable Built Environment*, 1(2), pp. 194–216. Available at:

https://www.sciencedirect.com/science/article/pii/S2212609013000071 (Accessed: 17 February 2020).

Karami, S. (2008) *Using By-product Industrial Materials to Replace All Cement in Construction Products*. Coventry. Available at: http://curve.coventry.ac.uk/open.

Kellenberger, D., Althaus, H.-J., Künniger, T., Lehmann EMPA, M., Niels Jungbluth, D., and Thalmann Bau-und Umweltchemie, P. (2007) *Swiss Centre for Life Cycle Inventories A Joint Initiative of the ETH Domain and Swiss Federal Offices Life Cycle Inventories of Building Products Data v2.0 (2007)* [online] available from <www.ecoinvent.org.> [6 April 2020]

Ketchen, D. and Bergh, D. (2004). Research methodology in strategy and management. Amsterdam: Elsevier.

Khatib, J. M. (2008) 'Performance of Self-Compacting Concrete Containing Fly Ash'. *Construction and Building Materials* 22 (9), 1963–1971

Khayat, K. H., Meng, W., Vallurupalli, K., and Teng, L. (2019) 'Rheological Properties of Ultra-High-Performance Concrete — An Overview'. in *Cement and Concrete Research*. vol. 124. Elsevier Ltd, 105828

Koehler, E. P. and Fowler, D. W. (2003) *Summary of Concrete Workability Test Methods*.

Koehler, E. P. and Fowler, D. W. (2004) 'Development of a Portable Rheometer for Fresh Portland Cement Concrete'.

Kothari, C.R., (2004) *Research methodology: Methods and techniques*. New Age International.

Kouassi, S. S. *et al.* (2010) D*issolution of waste glasses in high alkaline solutions*, *Original papers Ceramics-Silikáty*.

Kwasny, J. *et al.* (2016) 'banahCEM-comparison of properties of a laterite-based geopolymer with conventional concrete.', in *Proceedings of 9th International Concrete Conference 2016: Environment, Efficiency and Economic Challenges for Concrete*. Queen's University Belfast, pp. 383–394.

Kwasny, J., Soutsos, M. N., McIntosh, J. A., and Cleland, D. J. (2018) 'Comparison of the Effect of Mix Proportion Parameters on Behaviour of Geopolymer and Portland Cement Mortars'. *Construction and Building Materials* 187, 635–651

Lachemi, M. *et al.* (2008) 'Controlled low strength materials incorporating cement kiln dust from various sources', *Cement and Concrete Composites*. Elsevier, 30(5), pp. 381–392. doi: 10.1016/J.CEMCONCOMP.2007.12.002.

Lachemi, M. *et al.* (2010) 'Properties of controlled low-strength materials incorporating cement kiln dust and slag', *Cement and Concrete Composites*. Elsevier, 32(8), pp. 623–629. doi: 10.1016/J.CEMCONCOMP.2010.07.011.

Laskar, A. and Bhattacharjee, R. (2013) 'Effect of Plasticizer and Superplasticizer on Rheology of Fly-Ash-Based Geopolymer Concrete', *ACI Materials Journal*. Available at:

https://www.researchgate.net/publication/286320725 (Accessed: 18 February 2020).

Laskar, A. I. and Bhattacharjee, R. (2011) 'Rheology of fly-ash-based geopolymer concrete', *ACI Materials Journal*, 108(5), pp. 536–542. doi: 10.14359/51683263.

Lawan, A., Kaura, J. M. and Bature, A. S. (2016) 'CHARACTERIZATION OF CEMENT PASTE MODIFIED WITH NANOSILICA', *Nigerian journal of scientific research*, 15(2), pp. 228–233.

Lawther, S. E. M., Mcintosh, A., Nanukuttan, S. V, and Provis, J. (2016) 'Understanding the Microstructure of Alternative Binder Systems-BanahCEM, a Metakaolin Based Geopolymer'. in *Civil Engineering Research in Ireland.* [online] held 2016. available from <https://www.researchgate.net/publication/309032394> [9 March 2020]

LC3 project (2017) *The Material - Limestone Calcined Clay Cement*. Available at: https://www.lc3.ch/the-material/ (Accessed: 17 February 2020).

Le, D.-H. and Nguyen, K.-H. (2016) 'An Assessment of Eco-Friendly Controlled Low-Strength Material', *Procedia Engineering*. Elsevier, 142, pp. 260–267. doi: 10.1016/J.PROENG.2016.02.040.

Leavy, P. (2017) Research design : Quantitative, qualitative, mixed methods, arts-based, and community-based participatory research approaches.

Lemougna, P.N., MacKenzie, K.J.D., Jameson, G.N.L., Rahier, H., and Chinje Melo, U.F. (2013) 'The Role of Iron in the Formation of Inorganic Polymers (Geopolymers) from Volcanic Ash: A 57Fe Mössbauer Spectroscopy Study'. *Journal of Materials Science* 48 (15), 5280–5286

Liew, Y. M., Kamarudin, H., Mustafa Al Bakri, A. M., Bnhussain, M., Luqman, M., Khairul Nizar, I., Ruzaidi, C. M., and Heah, C. Y. (2012) 'Optimization of Solids-to-Liquid and Alkali Activator Ratios of Calcined Kaolin Geopolymeric Powder'. *Construction and Building Materials* 37, 440–451

Liew, Y. M. *et al.* (2016) 'Structure and properties of clay-based geopolymer cements: A review', *Progress in Materials Science*. Elsevier Ltd, pp. 595–629. doi: 10.1016/j.pmatsci.2016.08.002.

Lopez, R. F. (2009) *Calcined Clayey Soils as a Potential Replacement for Cement in Developing Countries*. Lausanne, EPFL. doi: http://dx.doi.org/10.5075/epfl-thesis-4302.

Lukowski, P. and Salih, A. (2015) 'Durability of mortars containing ground granulated blast-furnace slag in acid and sulphate environment.', in *Procedia Engineering*. 7th Scientific-Technical Conference Material Problems in Civil Engineering (MATBUD'2015), pp. 47–54.

Luukkonen, T. *et al.* (2018) 'One-part alkali-activated materials: A review', *Cement and Concrete Research*, 103, pp. 21–34. Available at: https://www.sciencedirect.com/science/article/pii/S0008884617306877 (Accessed: 4 March 2020).

Maddalena, R., Roberts, J.J., and Hamilton, A. (2018) 'Can Portland Cement Be Replaced by

Low-Carbon Alternative Materials? A Study on the Thermal Properties and Carbon Emissions of Innovative Cements'. *Journal of Cleaner Production* 186, 933–942

Mahieux, P.-Y., Aubert, J.-E. and Escadeillas, G. (2009) 'Utilization of weathered basic oxygen furnace slag in the production of hydraulic road binders', *Construction and Building Materials*. Elsevier, 23(2), pp. 742–747. doi: 10.1016/J.CONBUILDMAT.2008.02.015.

McIntosh, A., Lawther, S. E. M., Kwasny, J., Soutsos, M.N., Cleland, D., and Nanukuttan, S. (2015) 'Selection and Characterisation of Geological Materials for Use as Geopolymer Precursors'. in *Advances in Applied Ceramics*. held 1 October 2015. Maney Publishing, 378–385

Mcintosh, A. and Soutsos, M. (2014) 'Development of a Geopolymer Binder from the Interbasaltic Laterites of Northern Ireland'. in *Civil Engineering Research in Ireland*. held 2014. Queen's University Belfast

Messina, F. *et al.* (2017) 'Synergistic recycling of calcined clayey sediments and water potabilization sludge as geopolymer precursors: Upscaling from binders to precast paving cement-free bricks', *Construction and Building Materials*. Elsevier Ltd, 133, pp. 14–26. doi: 10.1016/j.conbuildmat.2016.12.039.

Müller, N. and Harnisch - Gland, J. (2008) *A Blueprint for a Climate-Friendly Cement Industry: How to Turn Around the Trend of Cement Related Emissions in the Developing World*.

Nataraja, M. C. and Nalanda, Y. (2008) 'Performance of industrial by-products in controlled low-strength materials (CLSM)', *Waste Management*. Pergamon, 28(7), pp. 1168–1181. doi: 10.1016/J.WASMAN.2007.03.030.

Neville, A. M. (2011) *Properties of concrete*. Pearson.

Ober, J. (2017) *Mineral commodity summaries 2017. Mineral commodity summaries*.

Pacheco-Torgal, F. *et al.* (2012) 'Durability of alkali-activated binders: A clear advantage over Portland cement or an unproven issue?', *Construction and Building Materials*, 30, pp. 400–405. doi: 10.1016/j.conbuildmat.2011.12.017.

Passuello, A. *et al.* (2017) 'Evaluation of the potential improvement in the environmental footprint of geopolymers using waste-derived activators', *Journal of Cleaner Production*. Elsevier, 166, pp. 680–689. doi: 10.1016/J.JCLEPRO.2017.08.007.

Provis, J. L., Fernández-Jiménez, A., *et al.* (2014a) 'Binder chemistry – Low-calcium alkali-activated materials', *RILEM State-of-the-Art Reports*. Springer Netherlands, 13, pp. 93–123. doi: 10.1007/978-94-007-7672-2_4.

Provis, J. L., Fernández-Jiménez, A., *et al.* (2014b) 'Binder chemistry – Low-calcium alkali-activated materials', *RILEM State-of-the-Art Reports*. Edited by Provis J. and van Deventer J. Springer, 13, pp. 93–123. doi: 10.1007/978-94-007-7672-2_4.

Provis, J. L., Duxson, P., *et al.* (2014) 'Historical aspects and overview', *RILEM State-of-the-Art Reports*. Springer Netherlands, 13, pp. 11–57. doi: 10.1007/978-94-007-7672-2_2.

Provis, J. L. (2014) *Introduction and Scope BT - Alkali Activated Materials: State-of-the-Art Report, RILEM TC 224-AAM, RILEM State-of-the-Art Reports*. Springer Netherlands. doi: 10.1007/978-94-007-7672-2_1.

Provis, J. L. (2018) 'Alkali-activated materials', *Cement and Concrete Research*. Elsevier Ltd, 114, pp. 40–48. doi: 10.1016/j.cemconres.2017.02.009.

Puertas, F., Palacios, M. and Provis, J. L. (2014) 'Admixtures', in *RILEM State-of-the-Art Reports*. Springer Netherlands, pp. 145–156. doi: 10.1007/978-94-007-7672-2_6.

Puertas, F., Torres-Carrasco, M. and Alonso, M. M. (2015) 'Reuse of Urban and Industrial Waste Glass as a Novel Activator for Alkali-Activated Slag Cement Pastes: A Case Study'. in *Handbook of Alkali Activated Cement, Mortars and Concrete*. Woodhead, 75–109

Rafeet, A. *et al.* (2017) 'Guidelines for mix proportioning of fly ash/GGBS based alkali activated concretes', *Construction and Building Materials*. Elsevier Ltd, 147, pp. 130–142. doi: 10.1016/j.conbuildmat.2017.04.036.

Rangan, B. V. (2008) 'Mix design and production of flyash based geopolymer concrete', *Indian concrete journal*, 82(5), pp. 7–15.

Reddy, A. S., Pradhan, R. K. and Chandra, S. (2006) 'Utilization of Basic Oxygen Furnace (BOF) slag in the production of a hydraulic cement binder', *International Journal of Mineral Processing*. Elsevier, 79(2), pp. 98–105. doi: 10.1016/j.minpro.2006.01.001.

Richey, R.C. and Klein, J.D., (2014) Design and development research: Methods, strategies, and issues. Routledge.

Ruiz-Santaquiteria, C. *et al.* (2013) 'Clay reactivity: Production of alkali activated cements', *Applied Clay Science*. Elsevier, 73(1), pp. 11–16. doi: 10.1016/j.clay.2012.10.012.

Sabir, B., Wild, S. and Bai, J. (2001) 'Metakaolin and calcined clays as pozzolans for concrete: A review', *Cement and Concrete Composites*. Elsevier Ltd, 23(6), pp. 441–454. doi: 10.1016/S0958-9465(00)00092-5.

Saunders, M. L. and Lewis, P. (2009) Research Methods for Business Students 4th edtn. Edinburg Gate: Pearson Education Limited

Saunders, M., Lewis, P. and Thornhill, A. (2016) Research Methods for Business Students. 7th edn. Edinburg Gate: Pearson Education Limited

Scrivener, K. L., John, V. M. and Gartner, E. M. (2018) 'Eco-efficient cements: Potential economically viable solutions for a low-CO 2 cement-based materials industry', *Cement and Concrete Research*. Elsevier Ltd, 114, pp. 2–26. doi: 10.1016/j.cemconres.2018.03.015.

Secondaryscience4all (2014) *Extracting iron | Secondary Science 4 All*. Available at: https://secondaryscience4all.wordpress.com/2014/07/21/iron-extraction-blast-furnace/ (Accessed: 17 February 2020).

Shi, C., Krivenko, P. V. and Roy, D. M. (2006) *Alkali-activated cements and concretes*. Taylor & Francis.

Shi, C., Qu, B. and Provis, J. L. (2019) 'Recent progress in low-carbon binders', *Cement and Concrete Research*, 122, pp. 227–250. Available at: https://www.sciencedirect.com/science/article/pii/S0008884619301838 (Accessed: 20 November 2019).

Siddique, R. and Klaus, J. (2009) 'Influence of metakaolin on the properties of mortar and concrete: A review', *Applied Clay Science*. Elsevier, 43(3–4), pp. 392–400. doi: 10.1016/j.clay.2008.11.007.

Şimşek, B., Uygunoğlu, T., Korucu, H., and Kocakerim, M. M. (2019) 'Performance of Dioctyl Terephthalate Concrete'. in *Use of Recycled Plastics in Eco-Efficient Concrete*. Woodhead Elsevier, 249–267

Singh, B., Ishwarya, G., Gupta, M., and Bhattacharyya, S.K. (2015) 'Geopolymer Concrete: A Review of Some Recent Developments'. in *Construction and Building Materials*. vol. 85. Elsevier Ltd, 78–90

Škvára, F., Jílek, T. and Kopecký, L. (2005) 'Geopolymer materials based on fly ash', *Ceram - silk*, 49(3), pp. 195–204. Available at: http://www.geopolymery.eu/aitom/upload/documents/publikace/2005/ceramics2005_03_195.pdf (Accessed: 3 March 2020).

Soleil-Raynaut, V. (2019) *An Introduction to Metakaolins*.

Song, S. *et al.* (2000) 'Hydration of alkali-activated ground granulated blast furnace slag', *Journal of Materials Science*. Kluwer Academic Publishers, 35(1), pp. 249–257. doi: 10.1023/A:1004742027117.

Steveson, M. and Sagoe-Crentsil, K. (2005) 'Relationships between composition, structure and strength of inorganic polymers', *Journal of Materials Science*. Springer, 40(8), pp. 2023–2036. doi: 10.1007/s10853-005-1226-2.

Stoops, G. and Marcelino, V. (2018) *Interpretation of Micromorphological Features of Soils and Regoliths* [online] Elsevier. available from <https://linkinghub.elsevier.com/retrieve/pii/C20140017285> [21 November 2019

Taha, R. A. *et al.* (2007) 'Evaluation of controlled low strength materials containing industrial by-products', *Building and Environment*. Pergamon, 42(9), pp. 3366–3372. doi: 10.1016/J.BUILDENV.2006.07.028.

Taylor, H. F. W. (1997) *Cement chemistry*. 2nd editio.

Teo, T. (2013). Handbook of Quantitative Methods for Educational Research.

Thomas, M. (2013) *Supplementary cementing materials in concrete*, *Supplementary Cementing Materials in Concrete*. CRC Press. doi: 10.1201/b14493.

Thomas, M. D. A. (1996) *Review of the effect of fly ash and slag on alkali-aggregate reaction in concrete*. Bre press. Available at: https://www.brebookshop.com/details.jsp?id=608 (Accessed: 17 February 2020).

Torres-Carrasco, M. and Puertas, F. (2017) 'Waste glass as a precursor in alkaline activation:

Chemical process and hydration products', *Construction and Building Materials*. doi: 10.1016/j.conbuildmat.2017.02.071.

Třískova, J., Nižňanský, D., Hanzlicek, T., Straka, P., and Steinerova, M. (2005) *Mössbauer's Spectroscopy Applied on Kaolinitic Clays*.

Van Jaarsveld, J. G. S., Van Deventer, J. S. J. and Lukey, G. C. (2002) 'The effect of composition and temperature on the properties of fly ash- and kaolinite-based geopolymers', *Chemical Engineering Journal*. Elsevier, 89(1–3), pp. 63–73. doi: 10.1016/S1385-8947(02)00025-6.

Vinai, R. and Soutsos, M. (2019) 'Production of sodium silicate powder from waste glass cullet for alkali activation of alternative binders', *Cement and Concrete Research*. Elsevier Ltd, 116, pp. 45–56. doi: 10.1016/j.cemconres.2018.11.008.

Wang, H., Li, H. and Yan, F. (2005) 'Synthesis and mechanical properties of metakaolinite-based geopolymer', *Colloids and Surfaces A: Physicochemical and Engineering Aspects*. Elsevier, 268(1–3), pp. 1–6. doi: 10.1016/j.colsurfa.2005.01.016.

Weidema, B., Hischier, R., Althaus, H., and Bauer, C. (2009) 'Code of Practice'. in *Final Report Ecoinvent Dat*a'. *v2. 1 No. 2*.

Wöllner (2020) *hydrothermal production of silicate solution*. Available at: https://www.woellner.de/en/home.html (Accessed: 29 February 2020).

Xu, H. and Van Deventer, J. S. J. (2000) 'The geopolymerisation of alumino-silicate minerals', *International Journal of Mineral Processing*. Elsevier, 59(3), pp. 247–266. doi: 10.1016/S0301-7516(99)00074-5.

Yip, C. K., Lukey, G. C. and Van Deventer, J. S. J. (2005) 'The coexistence of geopolymeric gel and calcium silicate hydrate at the early stage of alkaline activation', *Cement and Concrete Research*. Pergamon, 35(9), pp. 1688–1697. doi: 10.1016/j.cemconres.2004.10.042.

Yunsheng, Z. *et al.* (2007) 'Synthesis and heavy metal immobilization behaviors of slag based geopolymer', *Journal of Hazardous Materials*. Elsevier, 143(1–2), pp. 206–213. doi: 10.1016/j.jhazmat.2006.09.033.

Zhou, D.; Wang, R.; Tyrer, M.; Wong, H. and Cheeseman, C. (2017) 'Sustainable infrastructure development through use of calcined excavated waste clay as a supplementary cementitious material', *Journal of Cleaner Production*, 168, pp. 1180–1192. doi: 10.1016/j.jclepro.2017.09.098.

Zhou, D. (2016) 'DEVELOPING SUPPLEMENTARY CEMENTITIOUS MATERIALS FROM WASTE LONDON CLAY'.

Zografou, A.-I. (2015) *THE USE OF CHINA CLAY WASTE AS A CONSTRUCTION MATERIAL USING ALKALI-ACTIVATED CEMENT TECHNOLOGY*.

APPENDIX 1

Molar oxide composition calculations for Group 3 mixes of table 3.5

The molar oxides ratios obtained for the SSP:CC = 0.7; SS:CC = 0.7 and SH:CC = 0.7 are shown by column I.

F. Oxide molecular mass		A. Chemical compound of CC (% by mass)				B. sodium silicate composition (% by mass)				C. Sodium hydroxide composition (% by mass)			
Oxide	g	SiO_2	Al_2O_3	Na_2O		SiO_2	Na_2O	H_2O	**concentration**	Molarity 8 M	SH solid		32
SiO_2	60.07	35.18	29.6	0.13		36.6	17.9	45.5	**54.5**		water		68
Al_2O_3	101.93												
Na_2O	61.97												
H_2O	18.01	G. Mixture proportion of Group 3 (mass, g)								D. $Na_2SiO_3.5H_2O$ solution composition (% by mass)			
		Mix	sand	CC	32% SH	54.5% SS	54.5% SSP	free water		SiO_2	Na_2O	H_2O	**Concentration**
I. Molar Oxide ratios		SSP: CC = 0.7	1482	484	0	0	344	64		27.3	27.3	45.5	**54.5**
SSP:CC=0.7		SS:CC = 0.7	1482	484	0	344	0	64					
$SiO_2:Al_2O_3 = 2.4$		SH:CC = 0.7	1482	484	246	98	0	64		D. $Na_2SiO_3.5H_2O$ solid composition (% by mass)			
$Na_2O:Al_2O_3 = 0.4$										SiO_2	Na_2O	H_2O	**Concentration**
$H_2O:Na_2O = 33$										18.5	18.5	63	**37**
SS:CC = 0.7													
$SiO_2:Al_2O_3 = 3.5$		H. Molar oxide composition of the mixes											
$Na_2O:Al_2O_3 = 0.7$			**CC (1*5/4)**			**Sodium silicate**			**Sodiuum hydroxide**	**Free water**	**Total**		
$H_2O:Na_2O = 12.2$			SiO_2	Al_2O_3	Na_2O	SiO_2	Na_2O	H_2O	Na_2O	H_2O	H_2O	**SiO_2**	**Al_2O_3**	**Na_2O**	**H_2O**
SH:CC = 0.7		SSP:CC=0.7	2.83	1.41	0.01	0.58	0.56	15.25	-	-	3.55	3.41	1.41	0.57	18.8
$SiO_2:Al_2O_3 = 2.4$		SS:CC=0.7	2.83	1.41	0.01	2.1	0.99	8.69	-	-	3.55	4.93	1.41	1	12.24
$Na_2O:Al_2O_3 = 1.1$		SH:CC=0.7	2.83	1.41	0.01	0.6	0.28	2.48	1.27	9.29	3.55	3.43	1.41	1.56	15.32
$H_2O:Na_2O = 9.8$															

APPENDIX 2

XRD analysis for the calcined clay geopolymer grout showing hematite

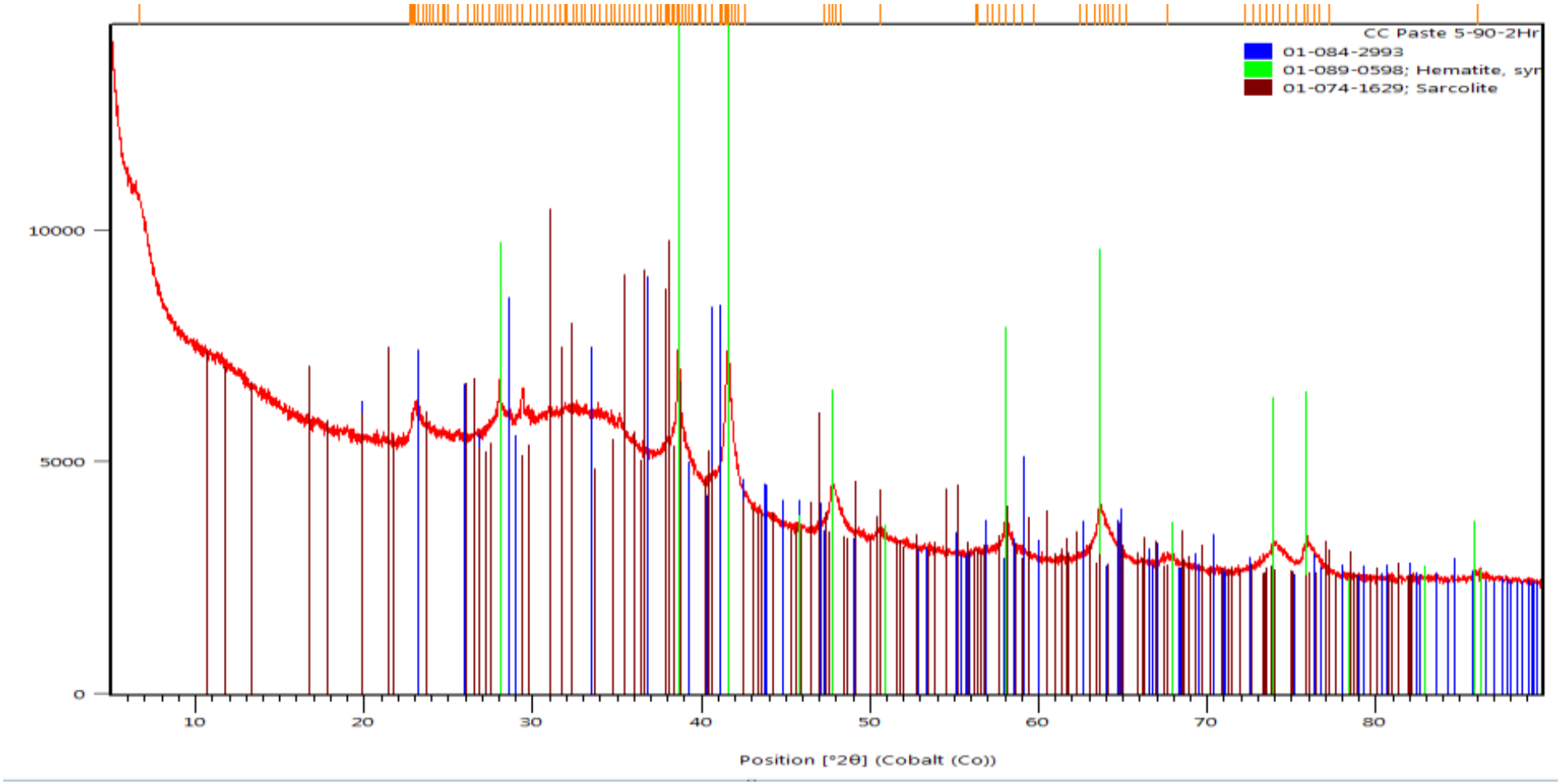

XRD spectra for the calcined clay geopolymer grout identifying muscovites

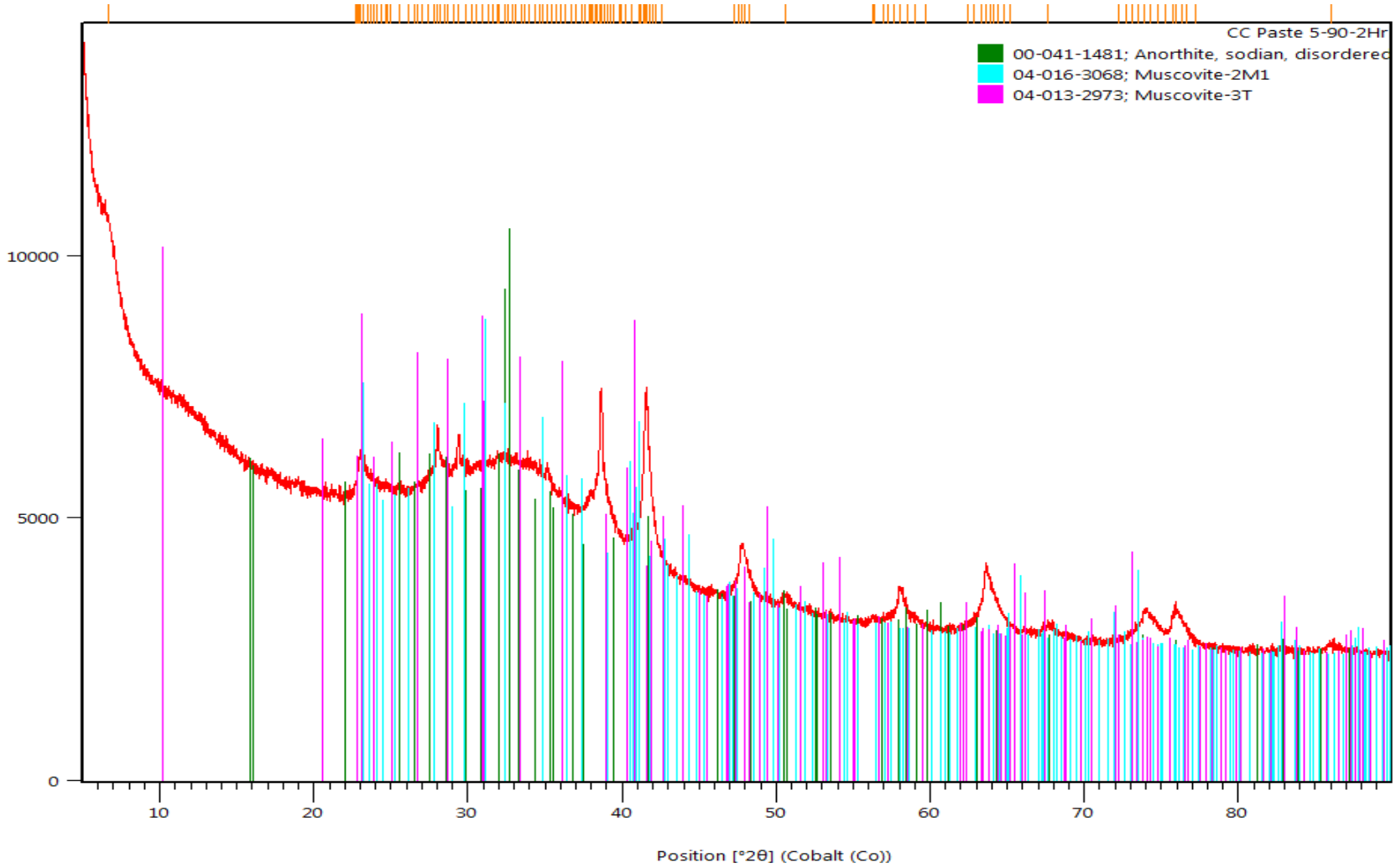

XRD spectra showing Kaolinite and sanidine minerals.

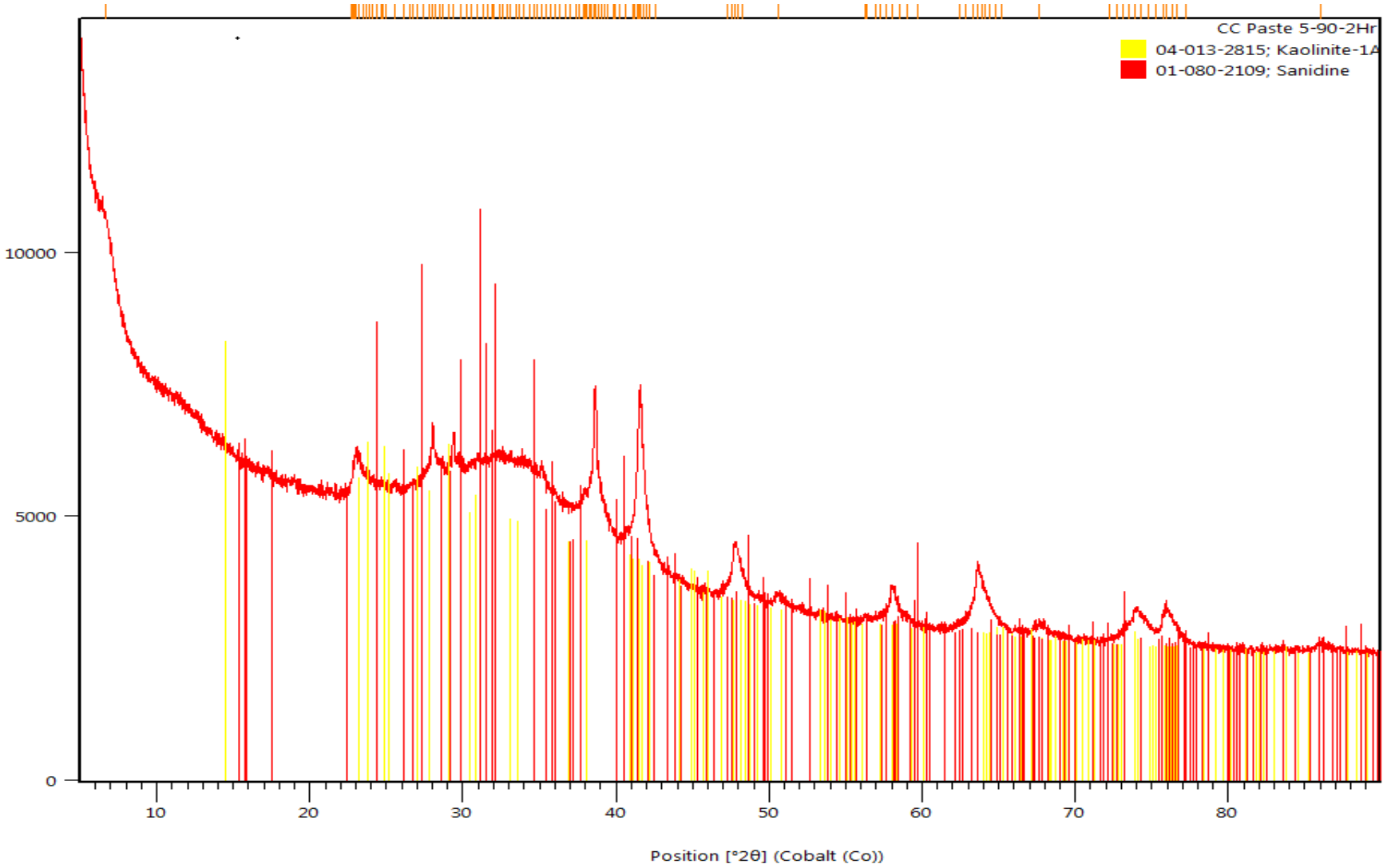

Semi-quantitative analysis of the calcined clay geopolymer paste

Compound Name	Chemical Formula	Score	Scale Factor	Display Color	Quality	Crystal System	SemiQuant...
Sodium Iron Phosphate	Na Fe P O4	43	0.274	Blue	S;ALT	Orthorhombic	6
Iron Oxide	Fe2 O3	35	1.096	Lime	S;ALT	Rhombohed...	7
Calcium Sodium Aluminum Silicate Hydroxide Phosphate Carbonate	Ca6.235 Na1.594 (Al4 Si6 O23) (O H)1.528 (P O4)0.5 (C O3)0.5	35	0.334	Maroon	S	Tetragonal	17
Sodium Calcium Aluminum Silicate	(Ca , Na) (Si , Al)4 O8	35	0.345	Green	I	Anorthic	10
Potassium Aluminum Silicate Hydroxide	K Al3 Si3 O10 (O H)2	30	0.232	Aqua	B;ALT	Monoclinic	12
Potassium Magnesium Aluminum Iron Silicate Hydroxide	K Mg0.18 Fe0.16 Al2.35 Si3.3 O10 (O H)2	38	0.287	Fuchsia	I	Hexagonal	9
Aluminum Silicate Hydroxide	Al2 Si2 O5 (O H)4	8	0.125	Yellow	I;ALT	Anorthic	2
Potassium Aluminum Silicate	K (Al Si3 O8)	34	0.357	Red	S;ALT	Monoclinic	10
Magnesium Silicon Oxide	Mg Si O3	38	0.274	Fuchsia	B;ALT	Orthorhombic	10
Potassium Aluminum Hydrogen Phosphate	K Al (H P O4)2	38	0.292	Teal	S	Anorthic	15

Semi quantitative analysis of the raw calcined clay

Compound Name	Chemical Formula	Score	Scale Factor	Display Color	Quality	Crystal System	SemiQuant [%]
Iron Oxide	Fe2 O3	47	0.992	Red	S;ALT	Rhombohedral	7
Aluminum Silicate Hydroxide	Al2 Si2 O5 (O H)4	Unmatc...	0.452	Lime	S	Anorthic	12
Iron Oxide	Fe3 O4	34	0.674	Aqua	I;ALT	Cubic	3
Potassium Sodium Magnesium Aluminum Iron Fluoride Aluminum Silicate Hydroxide	(K0.865 Na0.135) (Al1.886 Fe0.07 Mg0.036 Ti0.006) ((Si3.044 Al0.956) O10) (F0.054 (O H)1.946)	28	0.430	$000080FF	S	Monoclinic	26
Potassium Aluminum Iron Manganese Silicon Oxide Hydroxide Fluoride	K Al1.65 Fe0.35 Mn0.02 (Al0.7 Si3.3 O10) (O H)1.78 F0.22	23	0.406	Green	S	Monoclinic	22
Calcium Aluminum Silicate	Ca Al2 Si2 O8	22	0.324	Maroon	S	Anorthic	18
Potassium Sodium Calcium Aluminum Silicate	K0.42 Na0.58 Ca0.03 Al Si3 O8	18	0.315	Blue	I	Monoclinic	12

XRD spectra of the raw calcined clay identifying hematite, kaolinite, sanidine.

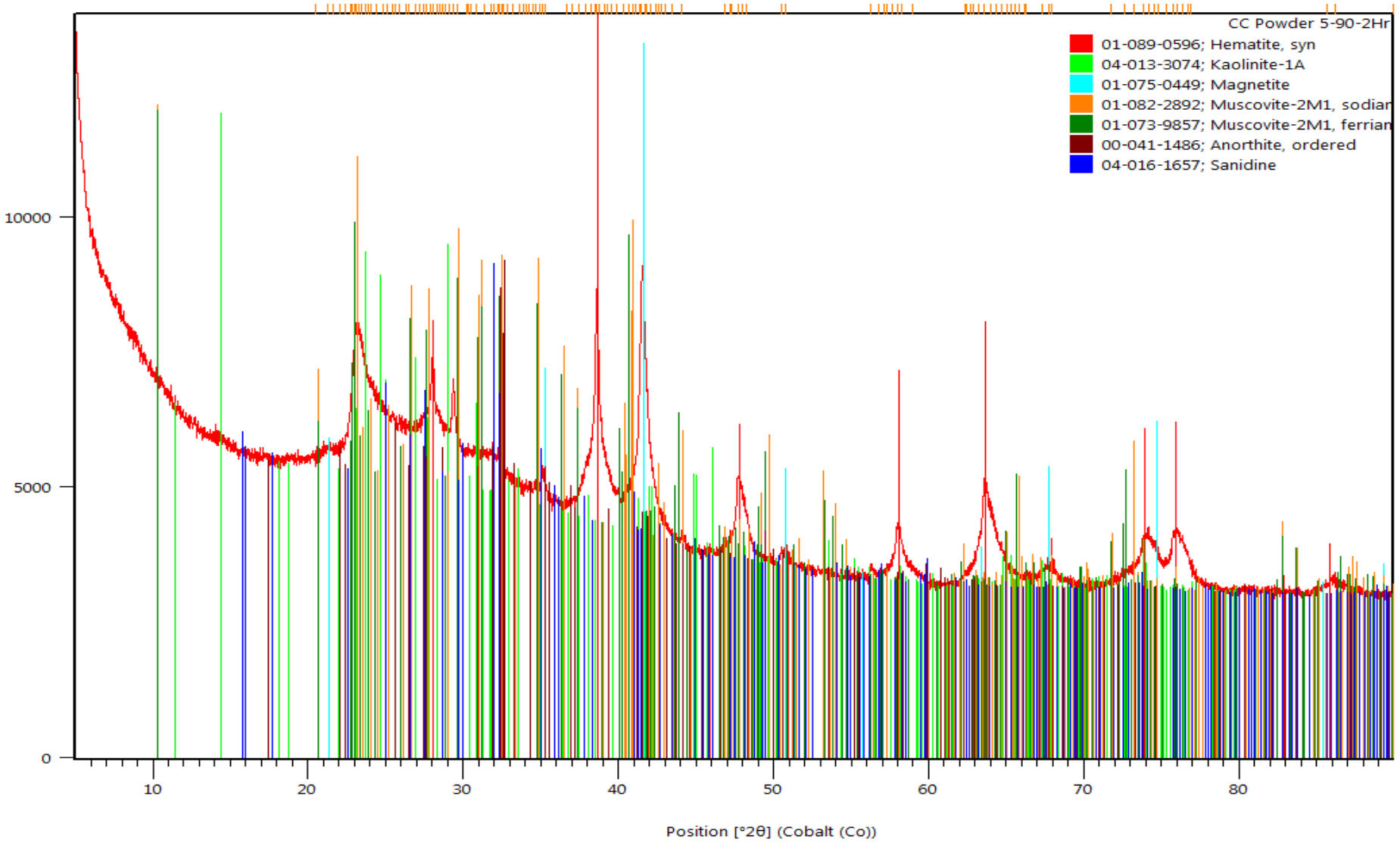

XRD spectra for the blended sodium hydroxide mortar identifying hematite and muscovite

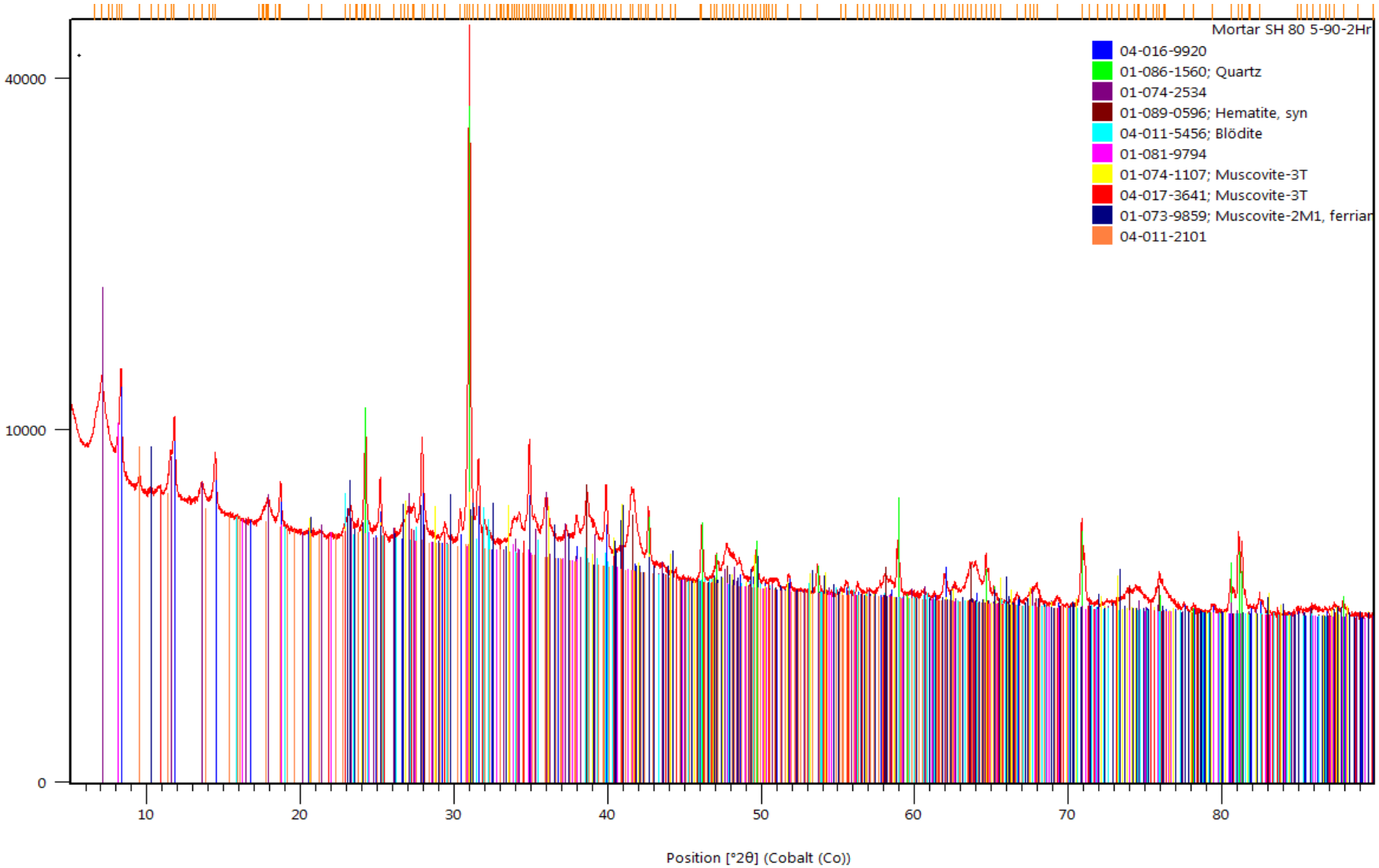

Semi-quantitative analysis of sodium hydroxide activated calcined clay mortar

Compound Name	Chemical Formula	Score	Scale F...	Display Color	Quality	Crystal System	SemiQuant [%]
Sodium Aluminum Silicate Hydrate	Na24 Al24 Si24 O96 (H2 O)64.8	42	0.110	Blue	B;ALT	Cubic	10
Silicon Oxide	Si O2	45	0.703	Lime	S;ALT	Hexagonal	30
Sodium Aluminum Silicate Hydrate	Na96 (Al96 Si96 O384) (H2 O)384.3	43	0.247	Purple	B	Cubic	13
Iron Oxide	Fe2 O3	39	0.072	Maroon	S;ALT	Rhombohedral	3
Sodium Magnesium Sulfate Hydrate	Na2 Mg (S O4)2 (H2 O)4	18	0.040	Aqua	I;ALT	Monoclinic	7
Calcium Silicate Hydroxide Hydrate	Ca3 (Si2 O6 (O H)2) (H2 O)	24	0.058	Fuchsia	I	Orthorhombic	1
Potassium Aluminum Iron Silicate Hydroxide	K (Al1.91 Fe0.09) (Si3 Al) O10 (O H)2	29	0.056	Yellow	S	Hexagonal	12
Potassium Sodium Magnesium Aluminum Iron Silicon Titanium Oxide Hydroxide	K0.90 Na0.05 Mg0.32 Ti0.03 Fe0.18 Al2.11 Si3.40 O10 (O H)2	30	0.019	Red	I;ALT	Hexagonal	4
Potassium Sodium Aluminum Iron Magnesium Silicon Oxide Hydroxide Fluoride	K0.92 Na0.08 Al1.88 Fe0.12 Mg0.04 (Al1.08 Si2.92 O10) (O H)1.89 F0.11	25	0.055	Navy	S	Monoclinic	19
Silicon Oxide	Si O2	16	0.048	$004080...	S	Monoclinic	1

Semi quantitative analysis of sodium silicate activated calcined clay geopolymer mortar

Compound Name	Chemical Formula	Score	Scale Fac...	Display Color	Quality	Crystal System	SemiQuant [%]
Silicon Oxide	Si O2	46	1.048	Blue	S;ALT	Hexagonal	34
Iron Oxide	Fe2 O3	43	0.020	Lime	S;ALT	Rhombohedral	1
Calcium Carbonate	Ca (C O3)	29	0.027	Maroon	S;ALT	Rhombohedral	1
Sodium Aluminum Silicate	Na Al Si3 O8	31	0.026	Aqua	S	Anorthic	1
Potassium Aluminum Silicate	K (Al Si3 O8)	25	0.020	Fuchsia	S;ALT	Monoclinic	3
Potassium Sodium Iron Aluminum Silicon Oxide Hydroxide	K0.8 Na0.2 Fe0.05 Al2.95 Si3.1 O10 (O H)2	24	0.023	$000080FF	S	Monoclinic	6
Potassium Sodium Aluminum Silicate	K0.22 Na0.78 Al Si3 O8	30	0.026	Yellow	I	Anorthic	4
Potassium Aluminum Iron Silicon Oxide	K0.98 Fe0.51 Al0.48 Si3.03 O8	24	0.076	Red	S	Monoclinic	9
Potassium Aluminum Silicate Hydroxide	K (Al4 Si2 O9 (O H)3)	20	0.200	Navy	I	Monoclinic	43

XRD spectra for the sodium silicate (SS1.5) activated geopolymer mortar identifying albite and sanidine minerals.

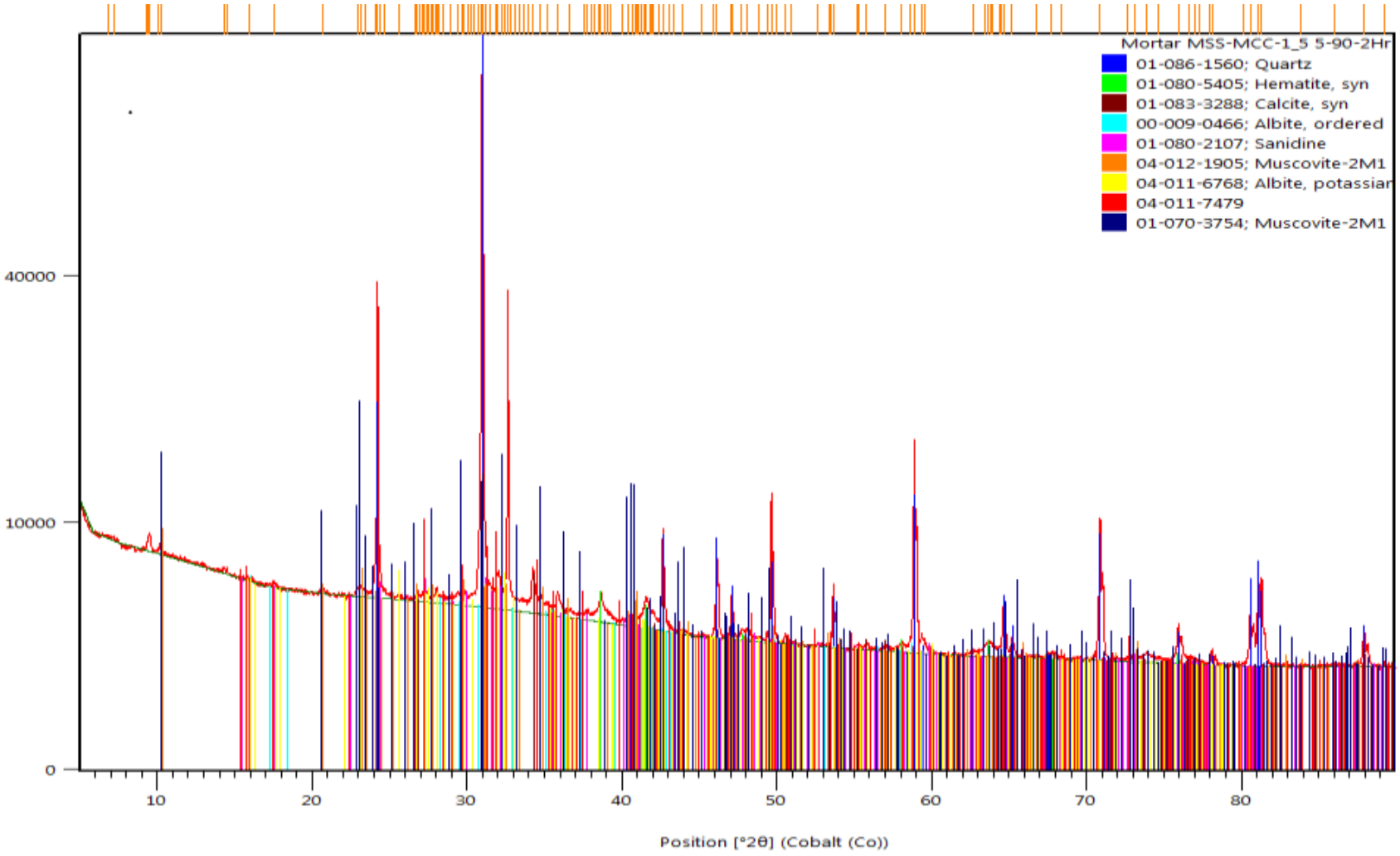

XRD spectra for the GC/Na-RM concrete identifying recrystalized geothite

APPENDIX 3

Environmental Impact for the control concrete:

	Abiotic depletion	Acidification	Eutrophication	Global warming	Ozone layer depletion	Human toxicity	Fresh water aquatic ecotoxicity	Marine aquatic ecotoxicity	Terrestrial ecotoxicity	Photochemical oxidation
sand	1.51E-02	1.37E+00	2.67E-03	2.21E+00	2.42E-07	1.48E+00	2.90E-01	6.63E+02	9.39E-01	4.84E-04
Gravel	2.14E-02	1.70E-02	3.01E-03	3.11E+00	2.96E-07	2.10E+00	4.95E-01	1341.25	2.07E-02	7.32E-04
PC	6.42E-01	4.65E-01	6.99E-02	3.41E+02	9.21E-06	1.62E+01	1.67E+00	7.84E+01	4.73E-01	1.72E-02
water	4.27E-04	3.25E-04	2.23E-05	3.43E-02	3.01E-09	2.18E-02	1.09E-02	4.07E+01	3.82E-04	2.21E-05
OPC concrete	6.79E-01	1.85E+00	7.56E-02	3.46E+02	9.75E-06	1.98E+01	2.47E+00	2.12E+03	1.43E+00	1.84E-02

Environmental Impact of the GC/Na-R mix

	Calcined clay	54.5% Na2SiO3	sand	Gravel	Tap water	GC/Na-R
Abiotic depletion	4.64E-02	1.08E+00	9.09E-03	3.82E-02	1.54E-04	1.18E+00
Acidification	8.94E-02	7.84E-01	8.25E-01	3.03E-02	1.18E-04	1.73E+00
Eutrophication	1.35E-02	7.45E-02	1.61E-03	5.37E-03	8.08E-06	9.50E-02
Global warming	2.55E+01	1.71E+02	1.33E+00	5.55E+00	1.24E-02	2.04E+02
Ozone layer depletion	4.20E-07	1.33E-05	1.46E-07	5.28E-07	1.09E-09	1.44E-05
Human toxicity	6.51E+00	1.21E+02	8.92E-01	3.75E+00	7.90E-03	1.32E+02
Fresh water aquatic ecotoxicity	9.05E-01	3.20E+01	1.75E-01	8.84E-01	3.96E-03	3.40E+01
Marine aquatic ecotoxicity	1.27E+03	5.00E+00	3.99E+02	2.39E+03	1.47E+01	4.08E+03
Terrestrial ecotoxicity	8.91E-02	1.35E+00	5.65E-01	3.69E-02	1.38E-04	2.04E+00
Photochemical oxidation	3.01E-03	3.64E-02	2.91E-04	1.31E-03	7.98E-06	4.10E-02

Environmental impact of GC/Na-RM mix

	Calcined clay	54.5% Na2SiO3	sand	Gravel	Tap water	GC/Na-R
Abiotic depletion	4.64E-02	1.08E+00	9.09E-03	3.82E-02	1.54E-04	1.18E+00
Acidification	8.94E-02	7.84E-01	8.25E-01	3.03E-02	1.18E-04	1.73E+00
Eutrophication	1.35E-02	7.45E-02	1.61E-03	5.37E-03	8.08E-06	9.50E-02
Global warming	2.55E+01	1.71E+02	1.33E+00	5.55E+00	1.24E-02	2.04E+02
Ozone layer depletion	4.20E-07	1.33E-05	1.46E-07	5.28E-07	1.09E-09	1.44E-05
Human toxicity	6.51E+00	1.21E+02	8.92E-01	3.75E+00	7.90E-03	1.32E+02
Fresh water aquatic ecotoxicity	9.05E-01	3.20E+01	1.75E-01	8.84E-01	3.96E-03	3.40E+01
Marine aquatic ecotoxicity	1.27E+03	5.00E+00	3.99E+02	2.39E+03	1.47E+01	4.08E+03
Terrestrial ecotoxicity	8.91E-02	1.35E+00	5.65E-01	3.69E-02	1.38E-04	2.04E+00
Photochemical oxidation	3.01E-03	3.64E-02	2.91E-04	1.31E-03	7.98E-06	4.10E-02

Environmental Impact: GC/Na-M-RM

	Calcined clay	37% Na2SiO3	32% NaOH	Sand	Gravel	Tap water	GC/Na-M-RM
Abiotic depletion	5.29E-02	6.01E-01	4.68E-01	1.24E-02	2.73E-02	3.86E-06	1.16E+00
Acidification	1.02E-01	4.34E-01	3.06E-01	1.13E+00	2.16E-02	2.94E-06	1.99E+00
Eutrophication	1.54E-02	4.12E-02	2.33E-02	2.19E-03	3.83E-03	2.02E-07	8.59E-02
Global warming	2.91E+01	9.49E+01	6.45E+01	1.81E+00	3.96E+00	3.10E-04	1.94E+02
Ozone layer depletion	4.79E-07	7.34E-06	3.96E-06	1.99E-07	3.77E-07	2.72E-11	1.23E-05
Human toxicity	7.43E+00	6.68E+01	2.75E+01	1.22E+00	2.68E+00	1.97E-04	1.06E+02
Fresh water aquatic ecotoxicity	1.03E+00	1.76E+01	6.93E+00	2.38E-01	6.31E-01	9.90E-05	2.64E+01
Marine aquatic ecotoxicity	1.45E+03	2.77E+00	1.37E+00	5.44E+02	1.71E+03	3.68E-01	3.70E+03
Terrestrial ecotoxicity	1.02E-01	7.47E-01	1.34E+00	7.71E-01	2.63E-02	3.46E-06	2.99E+00
Photochemical oxidation	3.43E-03	2.03E-02	1.33E-02	3.98E-04	9.33E-04	2.00E-07	3.83E-02

Environmental Impact of GC/K-RM

	Calcined clay	45% K2SiO3	sand	Gravel	Tap water	GC/K-RM
Abiotic depletion	5.22E-02	1.27E+00	1.24E-02	2.73E-02	3.86E-05	1.36E+00
Acidification	1.01E-01	9.17E-01	1.13E+00	2.16E-02	2.94E-05	2.17E+00
Eutrophication	1.52E-02	8.70E-02	2.19E-03	3.83E-03	2.02E-06	1.08E-01
Global warming	2.87E+01	2.00E+02	1.81E+00	3.96E+00	3.10E-03	2.35E+02
Ozone layer depletion	4.73E-07	1.55E-05	1.99E-07	3.77E-07	2.72E-10	1.65E-05
Human toxicity	7.34E+00	1.41E+02	1.22E+00	2.68E+00	1.97E-03	1.52E+02
Fresh water aquatic ecotoxicity	1.02E+00	3.71E+01	2.38E-01	6.31E-01	9.90E-04	3.89E+01
Marine aquatic ecotoxicity	1.43E+03	5.81E+00	5.44E+02	1.71E+03	3.68E+00	3.69E+03
Terrestrial ecotoxicity	1.00E-01	1.57E+00	7.71E-01	2.63E-02	3.46E-05	2.47E+00

Photochemical oxidation	3.39E-03	4.25E-02	3.98E-04	9.33E-04	2.00E-06	4.72E-02